Advancement in FRP composites using three-dimensional stitched fabrics and enhancement in FRP bridge deck component properties.

Vimala Shekar
West Virginia University

ADVANCEMENT IN FRP COMPOSITES USING 3-D STITCHED FABRICS AND ENHANCEMENT IN FRP BRIDGE DECK COMPONENT PROPERTIES

Vimala Shekar

Thesis submitted to the
College of Engineering and Mineral Resources
at West Virginia University
in partial fulfillment of the requirements
for the degree of

Master of Science
In
Civil Engineering

Hota V.S. GangaRao, Ph.D., Chair
Hemanth Thippeswamy, Ph.D.
Udaya B. Halabe, Ph.D

Department of Civil and Environmental Engineering

Morgantown, West Virginia

2000

Keywords: 3-D stitched fabrics, laminates, Composites, FRP bridge deck.

UMI Number: 1408460

UMI®

ProQuest Information and Learning Company
300 North Zeeb Road
P.O. Box 1346
Ann Arbor, MI 48106-1346

ABSTRACT

ADVANCEMENT IN FRP COMPOSITES USING 3-D STITCHED FABRICS AND ENHANCEMENT IN FRP BRIDGE DECK COMPONENT PROPERTIES

Vimala Shekar

Use of FRP composites in construction industry has been growing rapidly. However, currently all composite products are manufactured with one and/or two dimensional fibers and fabrics (1-D or 2-D). A shortcoming thick composite ($\geq$ 0.75 in.) made of 1-D or 2-D fabrics is its dramatic reduction in strength, i.e., up to 50% of thin ($\leq$0.5 in.) composites. This can be attributed to shear lag leading to ply-by-ply failure; in addition, premature failure of matrix and fibers or the interface failure is very common in thick composites. Therefore, the motivation of the present work is to fabricate and test composites with 3-D stitched fabrics, which overcome the limitations in composites made of 1-D or 2-D fabrics.

In this study, composites were fabricated using 3-D stitched fabrics with different: (1) fiber architecture; (2) stitch density; (3) stitch material; and (4) manufacturing process. Strength and stiffness of composites with 3-D stitched fabrics (at coupon level) under tension, bending and shear loads were experimentally established and theoretically evaluated. Structural properties of composites made of 3-D stitched fabrics were compared with the structural properties of composites made of unidirectional fibers and 2-D stitched fabrics. Composites made of 3-D stitched fabrics were found to have enhanced strength and stiffness (about 30%).

The existing FRP bridge deck component (first generation) was modified with respect to weight, fiber architecture and manufacturing process leading to the development of the second generation FRP bridge deck component. In the second generation FRP bridge deck component, the self-weight was reduced by about 11% without sacrificing strength and stiffness. The global stiffness of second generation FRP bridge deck component was evaluated experimentally (3 point bending test) and theoretically by Approximate Classical Lamination Theory. The ultimate stress of second generation FRP bridge deck component (30.8 ksi) was three times more than that of first generation FRP bridge deck component (10.3 ksi). The stiffness of second generation FRP bridge deck component was found to be 8.28E+08 lbs-in^2/foot width while the stiffness of first generation FRP bridge deck component was found to be 8.44E+08 lbs-in^2/foot. Trail second generation FRP bridge deck module has to be tested under fatigue loads.

Dedicated to

"omsakthi"

ACKNOWLEDGEMENTS

I was very fortunate to have Dr. Hota GangaRao as my advisor, a person whom I genuinely like, admire and respect as an academician. I learned a great deal from his approach to the solution of problems, from his profound insights into relevant points of issues and from his philosophical views. His advice and guidance were of a great value to me while conducting this research. For this I will be indebted.

Special thanks to Dr. Hemanth Thippeswamy for his help by way of ingenious suggestions and endeavor. I would like to express my special thanks to Dr. Udaya Halabe for the knowledge I gained through his teaching, which was helpful in advancing my research objectives and understanding. My special regards to Dr. Vijay for his valuable guidance and encouragement during the course of this research.

My special thanks to Mr. David Turner for preparing my test specimens. Thanks to Mr. Dana Humberson, for the help he provided in the laboratory.

I also would like to thank Mr. Rajesh, Mr. Srinivas, Mr. Sanjay, Mr. Ganesh, Ms. Lakshmi, Mr. John and other friends for the invaluable help while conducting my experiments.

I would like to acknowledge the West Virginia Department of Transportation-Division of Highways and the United States Department of Transportation-Fedral Highway Administration for provding the financial support. Thanks to Johnston Industries Inc., for providing the stitched composite fabrics, and Creative Pultrusions Inc., PPG Industries Inc., Richhold Chemicals Inc., and Anchor Reinforcements Inc., for manufacturing the sample.

Finally, I wish to express my sincere and heartfelt thanks to Mr. Shekar Chittibabu and Niveda Shekar whose understanding and encouragement were a constant consolation during the long arduous process of completing this thesis.

TABLE OF CONTENTS

LIST OF TABLES

LIST OF FIGURES

CHAPTER 1

INTRODUCTION

1.1 General Remarks

Fiber reinforced polymer (FRP) composite materials and structural components with continuous fibers and fabrics are gaining importance for civil infrastructure applications. These composite materials have shown their superiority over metals in applications requiring high strength to weight ratio, excellent fatigue and corrosion resistance, as well as energy absorption. The first generation of composite materials consisted mainly of unidirectional fibers. However, a major concern of unidirectional fiber composites is the development of premature cracking due to low stiffness and strength properties in a direction perpendicular to the main reinforcement. To overcome this problem, two-dimensional (2-D) fabrics were developed to manufacture composite structural components (Sotiropoulos 1995). Composites made of 2-D fabrics have good mechanical properties in the plane of reinforcement but possess low through-thickness strength and stiffness.

To improve through-thickness properties of composites, multi-axial woven, braided, stitched fabrics were developed. Kim (1983) and Chung (1987) showed that through-thickness (third direction) fibers improve interlaminar shear strength and reduce delamination. Although multi-axial woven and braided composites offer excellent mechanical properties, multi-axial weaving and braiding process are time consuming, and require specially designed weaving and braiding machines (Adanur and Tsao, 1994). Machine stitching saves time and also eliminates kinks developed during weaving or braiding. Therefore, the motivation of the present work is to fabricate composites with 3-D stitched fabrics and study the effects of third directional fibers on mechanical properties such as strength and stiffness. The main purpose of stitching is to avoid crimping of fibers; thus realizing better mechanical properties. In addition, this operation can produce uni-, bi-, tri- and quadra - axial fabrics tailored to incorporate the reinforcement in mass-produced structural components. Hence one can take full advantage of mechanical and physical properties of structural composites with 3-D stitched fabrics.

1.2 Objectives

The main objective was to develop 3-D stitched fabrics that could be utilized to mass-produce structural composite components that could provide better strength and stiffness per unit weight of composite components.

The sub-objectives of this research were to:

- Experimentally determine strength and stiffness properties of composites made of 3-D stitched fabrics at coupon level, from two different manufacturing processes, (SCRIMP and Pultrusion) under tensile, bending and shear loads;
- Verify experimental results with analytical results in terms of strength, stiffness and failure criteria of composites with 3-D stitched fabrics;
- Optimize the existing FRP bridge deck component (first generation FRP bridge deck component) with respect to weight, shape and fiber architecture to develop a new FRP bridge deck component (Second generation FRP bridge deck component); and

- Compute global stiffness of the optimized FRP bridge deck component (second generation FRP bridge deck component) both experimentally (3-point bending test) and theoretically (Approximate Classical Lamination Theory).

1.3 Report Organization

A study of published literature has been carried out and reported in Chapter 2, with emphasis on development of composites with 3-D stitched fabrics for infrastructure applications. Specifically, a compilation of past research on FRP structural shapes at the Constructed Facilities Center-West Virginia University (CFC-WVU) is presented. Additionally, literature survey on composites with 3-D stitched fabrics, conducted by various researchers is presented in the same chapter.

A general description of materials used in composites with 3-D stitched fabrics, and their different manufacturing process (SCRIMP and Pultrusion) are described in Chapter 3. In addition, test specimens, test set-up and test procedure used for various tests conducted (tension, bending and shear) throughout the experimental part of this research are presented.

Stiffness and strength results and evaluation of coupons are presented in Chapter 4. Comparison between theoretical and experimental results at coupon level is provided in the same chapter. Appendix A presents Classical Lamination Theory (CLT) approach to predict the stiffness of composites with 3-D stitched fabrics.

In chapter 5, the following issues are presented: (i) Optimization and modeling of FRP bridge deck component (second generation FRP bridge deck); (ii) Alignment of fibers in flanges and webs to improve shear and bending performance; (iii) Comparison of stiffness value of existing FRP bridge deck component (first generation FRP bridge deck component) over optimized FRP bridge deck component (second generation FRP bridge deck component); and (iv) Experimental test results of 3-point bending test on second generation FRP bridge deck component. Appendix B presents Approximate Classical Lamination Theory (ACLT) to predict the global stiffness of optimized FRP bridge deck component (second generation FRP bridge deck component). The local stability of second generation FRP bridge deck component (buckling of web) is also checked. Appendix C presents the computation of stiffness of web by Approximate Classical Lamination Theory (ACLT).

Finally, Chapter 6 presents the summary and conclusions of the present work and recommendations for future research on composites with 3-D stitched fabrics for applications in civil infrastructures.

CHAPTER 2

LITERATURE REVIEW

2.1 Introduction

Two-dimensional composites (2-D composites) have been typically used in structural components (I beam, Box-beam, WF beam) for the past three decades. These composites emerged in such structural components because of their better mechanical properties (stiffness to weight ratio, strength to weight ratio) and good resistance to environmental degradation (e.g. corrosion). However, a shortcoming of 2-D composites is that their strength in the thickness direction is relatively low. As a result, under static and fatigue loading, these composites suffer cracking of matrix and fibers, together with delamination, and ply-by-ply failure (interlaminar shear failure) between plies. In the following section, a critical review of the following are given:

- Performance of composite with unidirectional fibers
- Performance of composites with bi-directional fabric
- Behavior of 3-D composites with respect to impact, stitch density, fabric process, fiber architecture and creep

2.2 Research at CFC-WVU

Several research studies have been conducted at the Constructed Facilities Center-West Virginia University (CFC-WVU) on structural components (I beam, Box-Beam, bridge deck module) at coupon and component level. Though the fiber architecture and matrix have been improved over years, these components failed at the web-flange junction when subjected to static loads. This type of failure occurs mainly due to lack of fibers in thickness directions resulting in inefficient load transfer. A compilation of past research at CFC-WVU on performance of FRP coupons and structural components with different fiber architecture is given in the following sub-sections.

2.2.1 Performance of Composite Coupons and Structural Components with Uni-Directional Fibers

Doyle (1991) tested four composite coupons to failure to predict their ultimate tensile strength. The coupons (0.5" thick) consisted mainly of unidirectional fibers with fiber volume content of about 35%. The ultimate failure was at 12 ksi and the failure mode, which was first ply failure, was observed to be uniform across the depth of the section. The specimen had a low tensile modulus of $2x10^6$ psi. The low strength and stiffness observed was due to poor fiber architecture.

Sonti and Barbero (1992) performed stress analysis on pultruded glass composite I-beams. I-beam was built with rovings and continuous strand mat (OC). Continuous strand mat was introduced mainly to improve transverse properties and to reduce delamination. Coupons were cut from the web of I-beams and were tested for tension. The average ultimate failure stress was about 21 ksi. During 3-point bending test, the component failed exhibited shear failure in the web. Shear failure occurred because there was no continuity in fiber lay-up at the web-flange junction and also because of inadequate amount of glass fabric to resist shear. Therefore, strength and stiffness of FRP components could be improved by incorporating bi-directional fabrics and also by having continuity of fabrics from the flange to web.

2.2.2 Performance of Composite Coupons and Structural Components with Bi-Directional Fabrics

Sonti (1997) conducted tensile tests on coupons cut from a multi-cellular deck panel. The deck panel had modified fiber architecture [compared to Sonti (1992) specimens] in the flanges and webs. The flanges and exterior webs were built with rovings and 0/90 fabrics while the interior webs were built with rovings and ± 45 fabrics. The coupons (0.18" thick) with fiber volume content of about 33% were cut from the flange of multi-cellular deck panel and subjected to tensile loading. The average ultimate failure stress increased to 55 ksi because of modifications in fiber architecture i.e., bi-directional fabrics. The tensile modulus of the specimen was also improved to 2.9×10^6 psi. In addition to coupon tests, failure tests were conducted on multi-cellular deck panels subjected to concentric patch load. A catastrophic failure occurred at 25 kips and delamination was observed in the web-flange interface of the exterior web. Shear failure was also observed in the interior webs. This may be attributed to improper transfer of shear between the fabrics.

Vedam (1997) evaluated the strength and stiffness of FRP bridge deck module (comprised of double-trapezoid component and hexagonal component) at coupon and component levels. Coupons were cut from flange and web of hexagonal deck and were subjected to tension and bending loads. The fiber volume content was increased to 44%. Coupons (0.75" thick) failed at about 42 ksi because of interlaminar shear failure (progressive ply-by-ply separation). Due to higher fiber volume content, tensile modulus of the specimen were increased to 3.5×10^6 psi. Failure tests were conducted on double-trapezoid component under static loading. Failure was observed (same as in multi-cellular deck panel) at the junction of web-flange under a static load of about 30 kips. The failure was initiated under the load due to web buckling.

From the above research information generated through experiments conducted at the CFC-WVU on composite coupons and structural components, we can conclude that failure at web-flange junction of composite structural components could be overcome by developing 3-D composites which may have better resistance to delamination of composite through the thickness, thus leading to better interlaminar shear resistance.

2.3 Research on Composites with 3-D Stitched Fabrics

Several researchers investigated the effect of through-thickness fibers (stitch in the third direction) on composite properties. Some of the advantages of 3-D composites over 2-D composites are:

- Higher stiffness and strength, specially interlaminar (through-thickness) shear strength
- More tolerance to damage (resistance to delamination and interlaminar shear stress)
- Better impact resistance

2.3.1 Effect of Impact

Cholakara et.al. (1989) have studied the effect of repeated impact on stitched composites, and observed that stitched Kevlar-fiber/epoxy composites were able to withstand more impact than the non-stitched composites before failing. But Mouritz et.al. (1996) found that there was accumulation of microstructural damage in stitched

GRP (Glass Reinforced Polymer) composites subjected to repeated impact. The author also focused on the study of flexural strength and interlaminar shear strength of stitched composites followed by repeated impact tests. The GRP laminate was made from E-glass fibers and vinyl ester resin. The glass preforms consisted of alternating stacking sequence of woven roving and chopped-strand mat to a total of 14 plies. The preforms were stitched with Kevlar-49 thread in a modified lock stitch. The Kevlar was sewn in parallel rows along the direction of the 0^0 fibers in the woven roving plies and the stitches were 5 mm apart. The composites were fabricated using Vacuum-Assisted Resin-Transfer Molding Process (VARTM). The authors observed that due to impact, the amount of delamination damage was higher in stitched composites. This was because, stitched composites reist higher interlaminar bending stresses. Also, under single-impact loading, the GRP composites suffered slight reduction in flexural strength but a large reduction in interlaminar shear strength. The shear strength reduced considerably because a single impact creates many types of damage leading to shear failure, i.e., shear-induced polymer cracking, debonding and/or delaminations. Under repeated impacts, the composites experienced a large detrioration in the flexural strength because of fracture of the glass fibers.

Wu and Wang (1994) studied the behavior of stitched laminates under in-plane and transverse impact loading. E-glass/epoxy composite had a stacking sequence of two $0^0/90^0$ plies. The laminates were fabricated by resin transfer molding process. Untwisted Kevlar 29 rovings were used to stitch the fabric. From the experimental results, the authors concluded that there was insignificant reduction of in-plane stiffness due to stitching. When the loading direction was parallel to the stitch threads, damage was away from the neighborhood of the stitch threads, and edge delamination was found to be suppressed by this stitching reinforcement. On the other hand, when the loading direction was perpendicular to that of the stitch threads, the stitched laminates always failed at these locations. Stitching was found to enhance the threshold load resistance of impact-induced delamination cracking of the laminate.

2.3.2 Effect of Stitch Density

Adanur and Tsao (1994) studied the effects of different stitch distance and distribution on the mechanical behavior of 3-D composites. The 3-D composite consisted of glass woven rovings and Kevlar yarns were introduced as the third-direction fibers through the fabric layers in the stack using an industrial sewing machine. The sewing needle was chosen as round tip to avoid fiber damage during stitching. Interlock type of stitch was used to bind the plies together. Two types of stitch patterns were used: parallel and bi-axial. The distance between sewing lines was 5, 10, 15 and 20 mm. In general, the authors reported that 3-D composites had higher flexural strength compared to 2-D composites. However, as the stitch density decreased, flexural strength increased. The higher the stitch density, the more damage occured to the composite. Also bi-axial stitching increased the flexural strength relative to parallel stitching. Dense stitching (5 mm) caused excessive fiber breakage because of stress concentrations developed at needle punch and on the other hand, low stitch density decreased the impact resistance of the specimen because the energy absorbed by the sample was low. The effect of stitch density on interlaminar shear was similar to the effect on flexural strength, i.e., as the stitch density increased, shear strength increased upto a point.

2.3.3 Effect of Fabric Process and Fiber architecture

Hinrichs et.al under a contract to NASA Langley Research Center, developed composite wing on a commercial transport aircraft. The program was focused on developing carbon fiber preforms that were stitched through the thickness. These preforms were impregnated with resin by a resin film infusion process (RFI). Hence these materials were referred to as Stitched/RFI composites. A variety of different carbon dry fabric forms were considered for use as the basic building block material for making the carbon preforms. The dry fabric forms were supplied by Saerbeck and Heinso Companies. Saerbeck process (fabrics developed at Saerbeck Company) automates the lay-up process by combining fibers in the four basic directions (0, 45, -45, 90) into one basic stack of fabric. AS4 and IM7H samples having fiber architecture of $(45, -45\ 0_2\ 90)_s$ were produced by Saerbeck process. Heinsco process (fabrics developed at Heinsco Company) used a fine tacky epoxy resin coated with E-glass fiber thread to hold fibers together to make the unidirectional ply. These unidirectional plies were then hand laid at different angles. Once the desired stack was obtained the material was heated and chilled. AS4 with fiber architecture of $(45,0_2,-45,90)_s$ was developed by Heinsco process. All the dry preforms from Saerbeck and Heinsco Companies were made as flat composite panels by resin film infusion (RFI) process. From the experimental test results at coupon level, the (Hinrichs et.al.) observed that the samples from Saerbeck process were found to be stiffer than the samples from Heinsco process. This may be due to the fact that Saerbeck process produced best alignment of fibers. The tensile stiffness of Saerbeck samples was about 10% higher than the Heinsco samples and the compressive stiffness of Saerbeck samples was about 14% higher than that of Heinsco samples. From the above results we can conclude that there is a significant effect of fiber architecture on mechanical properties of 3-D composites.

2.3.4 Effect of Creep

Stitched composite not only enhances damage tolerances such as delamination, but also improves creep deformation. Bathgate et.al. (1997) investigated tensile creep behavior of woven fabric composite stitched through the thickness with carbon threads along the loading direction. Creep tests were conducted at various temperatures. It was found that through-thickness stitching significantly improved resistance to creep deformation and creep rupture of stitched composites.

2.4 Conclusions

From the research work on 3-D composites, we can conclude that structural components with 2-D composite materials mostly failed in shear at the flange-web junctions. This failure criterion has instigated several researchers to innovate a new type of composite, known as 3-D composites. Although stitching in 3-D composites increases structural integrity, it also causes fiber damage. (Adanur and Tsao, 1994). Factors influencing the extent of fiber damage are:

- Alignment of fibers
- Manufacturing process
- Stitch density
- Type of thread used for stitching
- Type of needle tip used for stitching

There is an optimum level, beyond which stitching does more harm than good (Adanur and Tsao 1994). Hence, in the current work precautions in terms of stitch density, manufacturing process, alignment of fibers, etc. have been taken to minimize fiber damage while manufacturing 3-D stitched fabrics.

CHAPTER 3

MATERIALS, MANUFACTURING AND TEST PROCEDURES

3.1 Introduction

Properties of FRP composites depend on fiber orientation (parallel or normal to load), fiber arrangement (aligned or random) and quantity, and also on the type of resin. The fibers provide most of the stiffness and strength, while the resin binds the fibers together, thus, providing load transfer between fibers. Other constituents such as fillers, pigments, accelerators play their respective roles in enhancing the composite properties and performance.

The most commonly used fibers in FRP composite sections are glass fibers. Glass fibers are available in various forms like rovings, chopped strands, mats, woven fabrics, stitched fabrics, etc. The structural performance (strength, stiffness, thermal response, etc.) of FRP composites also depends on manufacturing aspects, curing process controls, etc.

The most commonly used resins in FRP composite sections are thermosets. The most common thermoset resins include epoxies, polyester, vinyl ester, phenolic, etc. The properties of a composite, such as transverse stiffness and strength depend mainly on the resin type. Resins protect fibers from environmental and mechanical abrasion. Resins have to be selected based on fiber type and manufacturing process. During manufacturing of composites, improper curing temperature and time for resin may lead to a resin dominated failure. Hence, one has to be careful in selecting a proper resin and manufacturing process to attain good composite strength. A designer should select constituent materials concurrent with the structure with a good understanding of composite part production.

3.2 MATERIALS

3.2.1 Stitched Fabrics

In the current work, composites with 3-D stitched fabrics were used to show the enhancement in strength and stiffness. The stitched fabrics were supplied by Johnston Industries Inc., in the trade name of VectorPly Non-Crimp Fabrics (NCF). In NCF, unidirectional fibers are organized into layers of variable weight and orientations. The layers are then continuously stitched together precisely at the desired orientations. Details of stitched fibers supplied by Johnston Industries Inc., are given in Table 3.1. Vector-Ply fabrics were manufactured via a single pass in-line process that requires less material handling and less stitching.

The product codes used for VectorPly NCF were designed to describe the fabric orientation and density. The presence of mat or veil was also included in the product code designation. This allows easy identification and specification of VectorPly NCF. A typical sample is represented as follows:

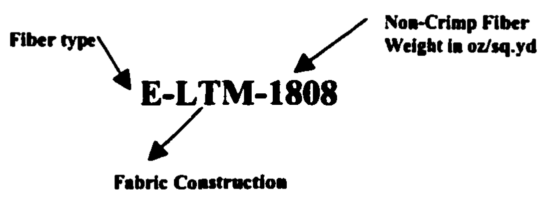

Details of stitched fabrics used in our experimental program are shown in Table 3.1. The fabrics were stitched at Johnston Industries Inc., using an industrial sewing machine. The stitch density varied from 1 to 7 as given in Table 3.1. Some of the samples were stitched only with glass while others were stitched with alternate glass and yarn.

Each of these samples was further stitched at the CFC-WVU using an ordinary sewing machine. The fabrics supplied by Johnston Industries Inc., were laid in two layers (to maintain symmetric laminate) and stitched with nylon thread as shown in Table 3.1.

Fabric Type	Number of Layers	Total Fabric Weight (oz/sq.yd)	Stitched At	Details of 3-D Stitch	
				Stitch Material	Stitch Density
E-LT-2400	2 layers of 24 oz	48	J	G-Y-G-Y	7
E-LT-2400	4 layers of 24 oz	96	J, WVU	G-Y-G-Y, Ny	7
E-LT-2400-14P	2 layers of 24 oz	48	J	G	3.5
E-LT-2400-14P	4 layers of 24 oz	96	J,WVU	G, Ny	3.5
E-QX-2600-5	2 layers of 26 oz	52	J	G	3.5
E-QX-2600-5	4 layers of 26 oz	104	J, WVU	G, Ny	3.5
E-QX-2600-5	4 layers of 26 oz	104	WVU	Ny	1
E-QX-5300	2 layers of 53 oz	106	J	G-Y-N-Y-G	7
E-QX-5300	4 layers of 53 oz	212	J, WVU	G-Y-N-Y-G, Ny	7

Table 3.1 Details of Stitched Fabrics

Notes:

- LT: Longitudinal/Transverse fibers at $0^0/90^0$
- QX: Quadraxial fibers at $0^0/45^0/90^0/-45^0$
- G: Glass
- Y: Yarn
- Ny: Nylon
- N: No stitch
- J: Fabric stitched at Johnston Industries Inc.,
- J, WVU: Fabric stitched at Johnston Industries Inc. and CFC-WVU

3.2.2 Resin

To bind the stitched fabrics together, vinyl ester was used. Formulation for the resin was given by Creative Pultrusions, Inc.

3.3 MANUFACTURING

The choice of manufacturing process depends mainly on the type of fibers and resin, temperature required to form the part and cure the resin, and the cost effectiveness of the process involved (Barbero, 1998). SCRIMP and pultrusion process were used in the experimental program. Description of SCRIMP and pultrusion process are given in the following sub-sections.

3.3.1 Seemann's Composite Resin Injection Molding Process (SCRIMP)

Stitched fabrics supplied by Johnston Industries Inc., were made into thin composite sheet by SCRIMP process at PPG Industries Inc. and Anchor Reinforcements Inc. The sheets were manufactured by SCRIMP (a hybrid of RTM) process which was developed and patented by Seeman's Composites. In the SCRIMP process, the E-glass fabrics are placed in a closed mold. Resin is drawn into the mold by vacuum, which is created at the outlet of the mold as shown in Figure 3.1. The resin passing through the mold wets out the fabrics. During this process, it also displaces the air, which escapes through special air vents. The resin is then cured at room temperature, and the cured part is cooled and cut to the required shape.

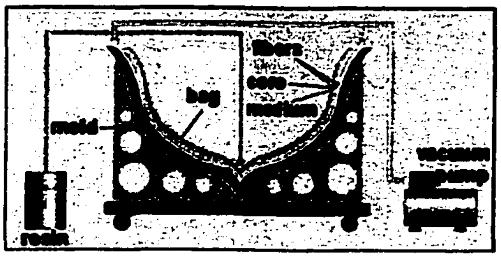

Figure 3.1 SCRIMP Process

Some of the advantage of SCRIMP Process are:

- Saves labor and time with dry lay-up
- Creates a healthier and cleaner environment
- Needs low capital investment
- Offers tooling flexibility
- Can mold large complex shapes

Some of the disadvantages are:

- Uses low curing temperature (can lead to improper curing)
- Leads to stress concentrations at kinks developed in fabrics

3.3.2 Pultrusion Process

Pultrusion is an automated process where composite materials are manufactured continuously with constant cross-sectional profiles. In this process, fiber reinforcement in the form of rovings, stitched fabric, mat, etc are pulled from a creel through strand-tensioning device into a resin impregnation bath. The fiber reinforcements placed in dry condition into the impregnation resin chamber where they are wetted by resin supplied under pressure (Barbero 1998). The wet reinforcement passes through the preformer into a die where curing takes place at prescribed temperature. Once the curing is done, the composite part is pulled continuously and cut by an appropriate saw to the required length as shown in Figure 3.3.

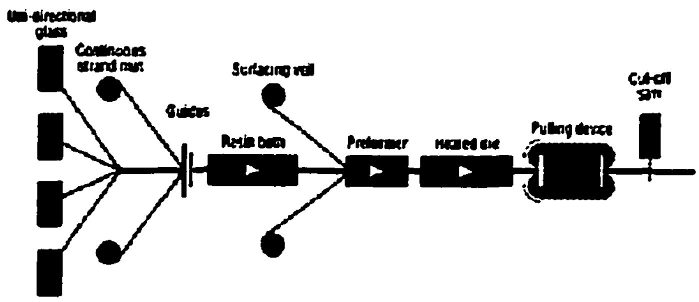

Figure 3.2 Pultrusion Process

Some of advantages of pultrusion process are:

- Convenient for mass-production
- No stress concentrations, as the fibers are always in tension
- Proper curing of resin
- Enhances structural properties of composite
- Good fiber alignment

Some of its disadvantages are:

- High manufacturing cost
- Improper wet-out of fibers at higher thickness

Four layers of quadraxial fabric of type E-QX-2600-5 were stitched by an ordinary sewing machine at CFC-WVU resulting in a 104 oz/yd^2 fabric. The fabric was stitched with nylon thread through its thickness and the distance between the stitch lines was 0.75 inch. The stitched fabric was then pultruded along with rovings (6.5 rovings per inch) and chopped strand mat (CSM) as per the specifications given by Creative Pultrusions, Inc. Fiber architecture for the specimen E-QX-2600-5 with rovings and CSM is as shown in Figure 3.2.

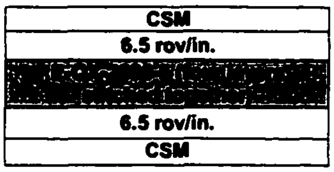

Figure 3.3 Fiber Architecture in Pultruded Composite

Pultrusion of 3-D composites was accomplished at Reichhold Industries Inc., and Creative Pultrusions, Inc. Some of the parameters such as resin formulation and cure temperature for the pultruded part were varied during manufacturing. The resin used by Reichhold Industries Inc., had more of bromine content than the resin used by Creative Pultrusions, Inc. With regard to cure temperature, Creative Pultrusions, Inc., used only one heater, which was maintained at 300^0F while Reichhold Industries Inc., used two heaters, one of which was maintained at 275^0F and the other was maintained at 300^0F. The pull speed for the pultruded part was mantained same (10 inch/minute) at Reichhold Industries Inc., and Creative Pultrusions, Inc.

Details of manufacturing process for the stitched fabrics are shown in Table3.2.

Specimen	Manufacturing Process	Manufacturing Place
E-LT-2400 (J)	SCRIMP	PPG
E-LT-2400 (J, WVU)	SCRIMP	PPG
E-LT-2400-14P (J)	SCRIMP	PPG
E-LT-2400-14P (J, WVU)	SCRIMP	PPG
E-QX-2600-5 (J)	SCRIMP	PPG
E-QX-2600-5 (J, WVU)	SCRIMP	PPG
E-QX-5300 (J)	SCRIMP	PPG
E-QX-5300 (J, WVU)	SCRIMP	PPG
E-QX-2600-5 with rovings and CSM (WVU)	SCRIMP	Anchor Industries Inc.
E-QX-2600-5 with rovings and CSM (WVU)	Pultrusion	Reichhold Industries Inc.
E-QX-2600-5 with rovings and CSM (WVU)	Pultrusion	Creative Pultrusions Inc.

Table 3.2 Details of Composite Manufacturing Process

Notes: **J:** Fabric is stitched at Johnston Industries Inc., only
J, WVU: Fabric is stitched at Johnston Industries Inc. and CFC-WVU
WVU: Fabric is stitched at CFC-WVU only

3.4 TESTING

Three types of tests (Tension, Bending and Short-beam shear) were performed on 3-D composite samples at coupon level to study the stiffness and strength properties. Tension test was performed as per ASTM D 3039; three point bending test was performed as per ASTM D 790; and short-beam shear test was performed as per ASTM D 2344. The test specimens, specimen preparation, test set-up and test procedure for all type of tests are described in the following sections.

3.4.1 Tension Test

3.4.1.1 Test Specimen

The SCRIMP and Pultruded samples were in the form of flat rectangular sheets. The samples were cut as per ASTM specifications and the dimensions are given in Table 3.3 and 3.4. Three specimens from each batch were tested under tension to failure. Totally 33 tests were conducted as per ASTM D 3039.

SCRIMP Specimens	Gage Length (in)	Width (in)	Thickness (in)
E-LT-2400 (J)	7	1	0.062
E-LT-2400 (J+WVU)	7	1	0.126
E-LT-2400-14P (J)	7	1	0.057
E-LT-2400-14P (J+WVU)	7	1	0.133
E-QX-2600 -5 (J)	7	1	0.071
E-QX-2600 - 5 (J+WVU)	7	1	0.139
E-QX-5300 (J)	7	1	0.112
E-QX-5300 (J+WVU)	7	1	0.216
E-QX-2600-5+Rovings (WVU)	6	1	0.19

Table 3.3 Dimensions of SCRIMP Tension Test Specimens

Pultruded Specimens	Gage Length (in)	Width (in)	Thickness (in)
E-QX-2600-5 +Rovings (WVU) (From Reichhold Industries Inc.)	6	1	0.25
E-QX-2600-5 +Rovings (WVU) (From Creative Pultrusions, Inc.)	6	1	0.25

Table 3.4 Dimensions of Pultruded Tension Test Specimens

3.4.1.2 Specimen Preparation

The ends of the specimens were sanded with a sand paper and degreased with Isopropyl alcohol to remove grease and dirt. FRP tabs (1/8" thick) and aluminum tabs (1/4" thick) were used for SCRIMP and Pultruded samples, respectively. The tabs were glued at the ends of specimens by pneumatic gun. The glue (Plexus adhesive) was applied with pressure and cured for 24 hours to ensure proper adhesion of the tabs to the specimen. Tabs are generally used to avoid the crushing of specimens between the grips and thus avoid grip failure of the specimen. Two strain gages were then mounted (one in the longitudinal direction and other in transverse direction) at the center of specimen as shown in Figure 3.4, to record longitudinal strain, transverse strains, and failure strains.

3.4.1.3 Test Set-up and Test Procedure

The specimens were tested using a universal testing machine (BALDWIN) as per ASTM D3039 as shown in Figure 3.5. The gages were connected to strain indicators to record the strain values at constant load intervals. The speed of the machine was adjusted to 260 lbs/min. Specimens were loaded to failure, to evaluate ultimate failure stress of the coupon.

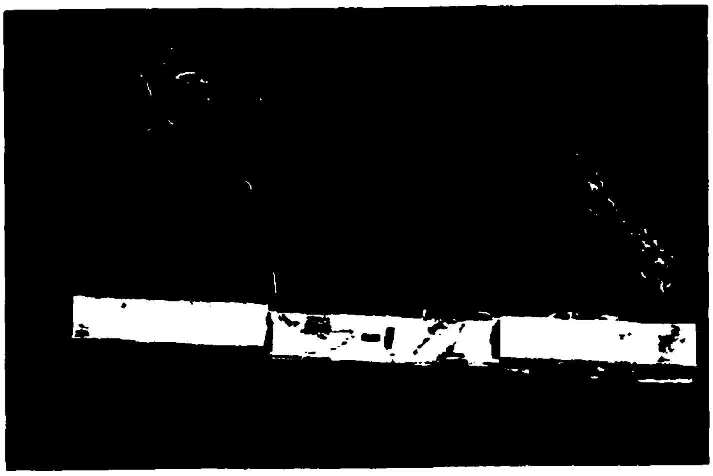

Figure 3.4 Specimen Preparation for Tensile Test

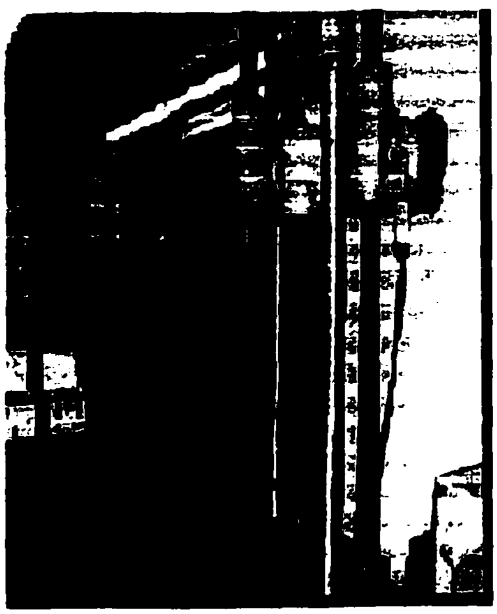

Figure 3.5 Test Set-Up for Tension Test

3.4.2 Bending Test

3.4.2.1 Test Specimen

The test specimens were cut as per dimensions recommended by ASTM D790 for a three point bending test with a span to depth ratio of 32:1. Dimensions of test specimens are shown in Table 3.5 and 3.6. Three specimens from each batch were tested for bending test, thus a total of 33 tests were conducted as per ASTM D790.

SCRIMP Specimens	Span Length (in)	Width (in)	Thickness (in)
E-LT-2400 (J)	2	1	0.062
E-LT-2400 (J,WVU)	4	1	0.126
E-LT-2400-14P (J)	2	1	0.057
E-LT-2400-14P (J,WVU)	4	1	0.133
E-QX-2600 -5 (J)	2	1	0.071
E-QX-2600 - 5 (J,WVU)	4	1	0.139
E-QX-5300 (J)	4	1	0.112
E-QX-5300 (J,WVU)	8	0.5	0.216
E-QX-2600-5 +Rovings (WVU)	8	0.5	0.19

Table 3.5 Dimensions of SCRIMP Bending Test Specimens

Pultruded Specimen	Span Length (in)	Width (in)	Thickness (in)
E-QX-2600-5 +Rovings (WVU) (Manufactured at Reichhold Industries inc.)	8	0.5	0.25
E-QX-2600-5 +Rovings (WVU) (Manufactured by Creative Pultrusions, Inc.)	8	0.5	0.25

Table 3.6 Dimensions of Pultruded Bending Test Specimens

3.4.2.2 Specimen Preparation

Once the test specimens were ready, strain gages were installed on the compression face of the bending coupons. The gages were protected with a rubber cushion on compression face, during the application of the load. For the specimens which had a span length of 8 inches there was difficulty in protecting the gages with the rubber cushion because of small width (0.5") in the specimen, hence the strain gage was placed at an eccentricity of 0.5 inch from the center of the bending specimens.

3.4.2.3 Test Set-Up and Test Procedure

The bending tests were conducted using an Instron Model 4411. The Instron cross speed was set (varied according to thickness of test specimen) as per ASTM D790. Three point bending, with simply supported conditions with knife edge load at center of the specimen was performed. Compressive strains were recorded at constant load intervals. Tensile strains were recorded by flipping the coupons and applying the knife edge load at center of the specimen. The specimens were tested to failure and the corresponding failure strains were noted. The test set-up is shown in Figure 3.6.

Figure 3.6 Test Set-Up for Bending Test

3.4.3 Short-Beam Shear Test

3.4.3.1 Test Specimen

The test specimens were cut as per dimensions recommended by ASTM D2344. The span to depth ratio was maintained at 7:1. The test specimens E-QX-2600-5 (stitched at WVU) were tested for shear. These specimens had a thickness in the range of 0.2" ~0.25" and the span was maintained at 1.75". The specimens other than E-QX-2600 -5 (ref Table 3.1) were not tested for shear because they exhibited slippage due to their smaller thickness. Details of short-beam shear test specimens are given in Table 3.7.

Test Specimen	Manufactured at	Length (in)	Width (in)	Thickness (in)
E-QX-2600 5	Anchor Reinforcements, Inc.	1.75	0.5	0.2
E-QX-2600 5	Reichhold Industries, Inc.	1.75	0.25	0.25
E-QX-2600 5	Creative Pultursions, Inc.	1.75	0.24	0.25

Table 3.7 Dimensions of Short-Beam Shear Test Specimens

3.4.3.2 Test Set-Up and Test Procedure

The specimens were tested to failure after preparing them as per ASTM standards. Since the dimensions of the specimens were too small, strain gages were not installed on the specimena. For the short-beam shear test, test specimens were mounted on Instron Model 4411 as shown is Figure 3.7. The cross speed of Instron machine was set to 0.05in/min. as per ASTM D2344 and test specimens were loaded with knife-edge load at center.

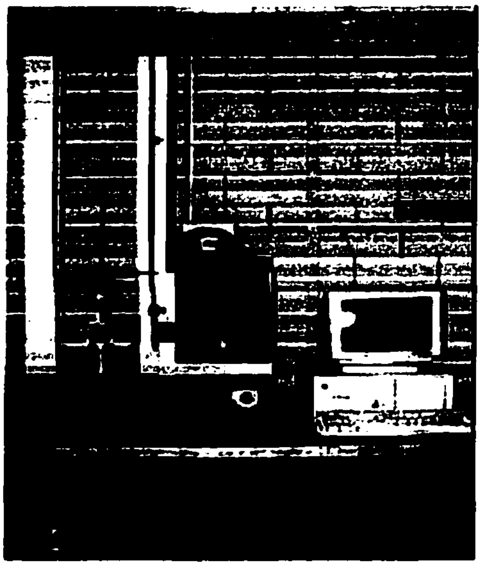

Figure 3.7 Test Set-Up for Short-Beam Shear Test

The specimens were simply supported.

In the following chapter, the experimental test results (tension, bending and shear) are tabulated and discussed in detail. The experimental stiffness and strength values of 3-D composite are correlated with that of theoretical stiffness and strength values. Also, structural properties of composites made of 3-D stitched fabrics are compared with structural properties of composites made of unidirectional fibers and 2-D stitched fabrics.

CHAPTER 4

ANALYSIS OF EXPERIMENTAL AND THEORETICAL RESULTS

4.1 Introduction

Experimental evaluation of strength and stiffness of composite structural shapes and analytical correlation's are of great importance for establishing sound design approaches. Elastic properties and performance of FRP composites are highly dependent on fiber content, orientation, distribution and manufacturing process and type of resin. In addition to experimental evaluations, analytical methods are also needed to predict material behavior based on the geometry and constituents of the composites.

Experimental and theoretical evaluations of Young's modulus and ultimate stress of FRP composites with 3-D stitched fabrics is presented in this chapter. The analytical results based on classical lamination theory (Appendix A) are then compared with those of experimental results to establish their validity.

Finally, the strength and stiffness of FRP composites with 3-D stitched fabrics (as predicted by experiment and theory) are compared with that of FRP composites with 2-D stitched fabrics.

4.2 Experimental Results

4.2.1 Tension Test Results

A total of 27 coupon tests were conducted on SCRIMP specimens, and 6 tests were conducted on pultruded specimens. After recording and plotting load versus longitudinal strain of coupons under tension, tensile modulus (slope of plot) was determined.

Tensile modulus, Poisson's ratio and failure stress of composites with 3-D stitched fabrics under tensile loading, along the fiber direction were computed as per equation 4.1 through 4.3.

Tensile Modulus: $$E_x^{Ten} = \frac{P}{\varepsilon_L \times b \times t} \quad (4.1)$$

Poisson's ratio: $$\nu = \frac{\varepsilon_T}{\varepsilon_L} \quad (4.2)$$

Ultimate Stress: $$\sigma_{ult} = \frac{P_{ult}}{b \times t} \quad (4.3)$$

Where,

E_x^{Ten} = Tensile modulus (psi)

(P/ε_L) = Slope of Load versus Longitudinal Strain (lbs/in/in)

b = width of the specimen (in)

t = thickness of the specimen (in)

ν = Poisson's ratio

ε_T = Transverse Strain (in/in)

ε_L = Longitudinal Strain (in/in)

σ_{ult} = Ultimate failure stress (psi)

P_{ult} = Ultimate load (lbs)

Stress versus longitudinal strain plots for SCRIMP and pultruded specimens are shown in Figure 4.1 through Figure 4.3. The tension test data for SCRIMP and pultruded specimens are shown in Table 4.1 and Table 4.2, respectively.

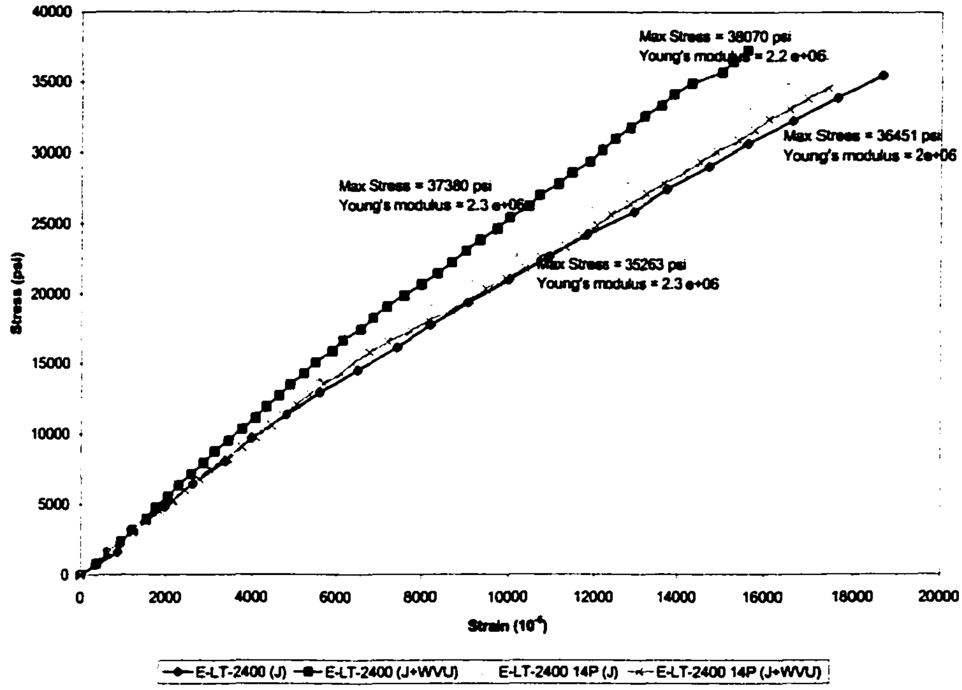

Figure 4.1 Stress Versus Longitudinal Strain for Composites with Biaxial Fabrics (0/90) - SCRIMP

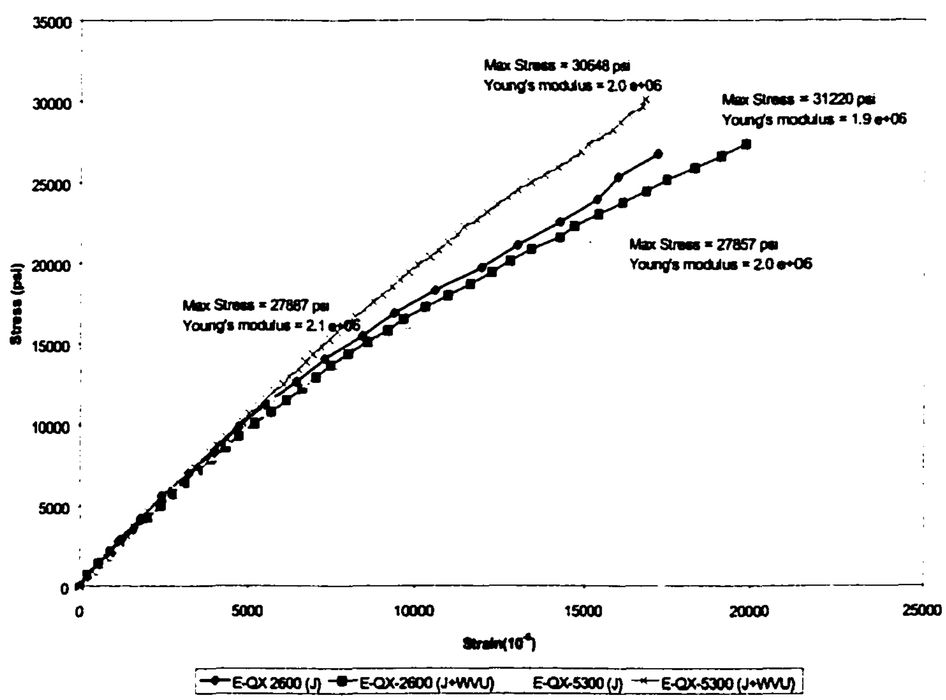

Figure 4.2 Stress Versus Longitudinal Strain for Composites with Quadraxial Fabrics (0/45/90/-45) – SCRIMP

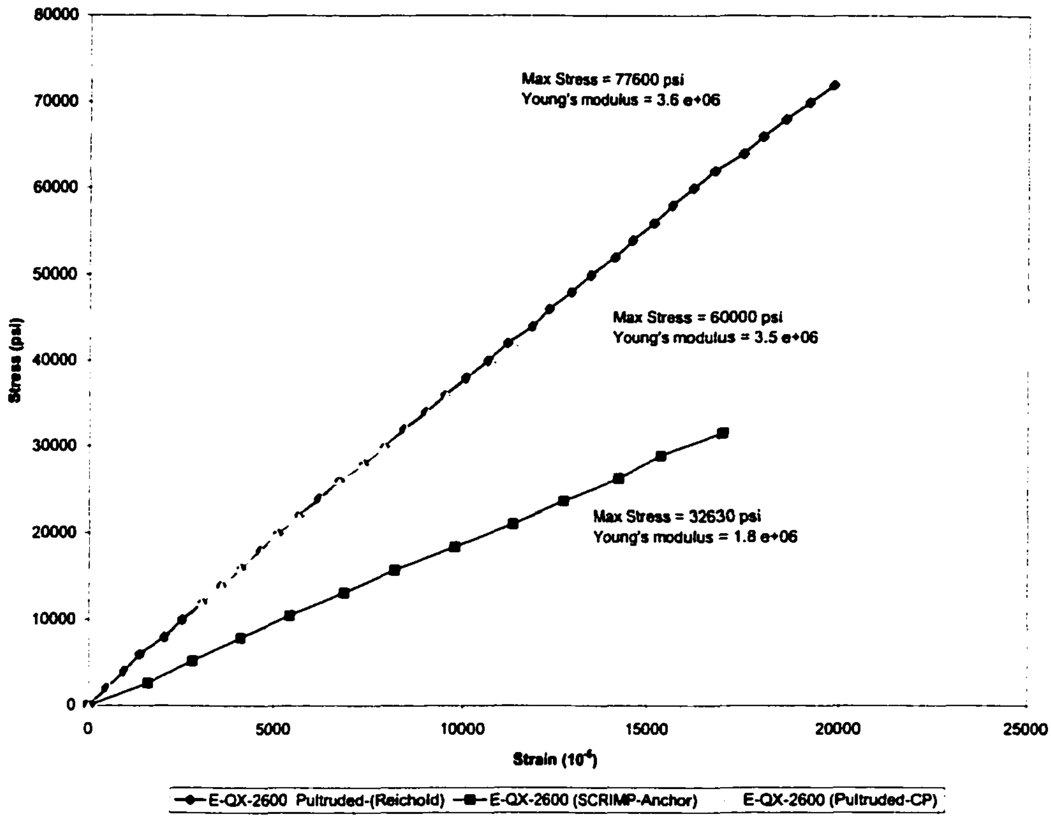

Figure 4.3 Stress Versus Longitudinal Strain for E-QX-2600 (5)

SCRIMP Specimens	Test No	Tensile Modulus (psi)	Average Tensile Modulus (psi)	Poisson's Ratio	Ultimate Load (lbs)	Ultimate Stress (psi)	Average Ultimate Stress (psi)
E-LT-2400 (J)	1	2.00E+06	2.06e+06	0.11	2260	36452	38870
	2	2.01E+06		0.13	2440	39355	
	3	2.19E+06		0.13	2530	40806	
E-LT-2400 (J+WVU)	1	2.28E+06	2.03e+06	0.15	4710	37381	36931
	2	1.99E+06		0.10	5000	39683	
	3	1.83E+06		0.14	4250	33730	
E-LT-2400-14P (J)	1	2.14E+06	2.08e+06	0.10	2470	43333	38889
	2	1.91E+06		0.09	2010	35263	
	3	2.20E+06		0.15	2170	38070	
E-LT-2400 14P (J+WVU)	1	2.30E+06	2.29e+06	0.15	3900	29323	30351
	2	2.27E+06		0.14	3520	26466	
	3	2.29E+06		0.11	4690	35263	
E-QX-2600 5 (J)	1	1.96E+06	1.98e+06	0.35	1780	25070	26479
	2	1.86E+06		0.35	1880	26479	
	3	2.12E+06		0.32	1980	27887	
E-QX-2600 5 (J+WVU)	1	1.67E+06	1.88e+06	0.23	4740	34101	32350
	2	1.93E+06		0.35	4340	31223	
	3	2.04E+06		0.36	4410	31727	
E-QX-5300 (J)	1	2.14E+06	2.01e+06	0.19	2720	24286	28125
	2	2.01E+06		0.24	3120	27857	
	3	1.88E+06		0.22	3610	32232	
E-QX-5300 (J+WVU)	1	2.40E+06	2.17e+06	0.18	7400	34259	29660
	2	2.13E+06		0.26	5200	24074	
	3	1.99E+06		0.26	6620	30648	
E-QX-2600 5 +Rovings (WVU)	1	1.80E+06	1.85e+06	0.30	6100	32105	34561
	2	1.88E+06		0.35	7400	38947	
	3	1.87E+06		0.31	6200	32631	

Table 4.1 Results of Tension Tests (SCRIMP Specimens)

PULTRUDED Specimens	Test No	Tensile Modulus (psi)	Average Tensile Modulus (psi)	Poisson's Ratio	Ultimate Load (lbs)	Ultimate Stress (psi)	Average Ultimate Stress (psi)
E-QX-2600 5 +Rovings (WVU) (Reichhold Industries, Inc.)	1	3.40E+06	3.33e+06	0.22	18750	72394	75611
	2	3.50E+06		0.27	20100	77606	
	3	3.11E+06		0.20	19900	76834	
E-QX-2600 5 +Rovings (WVU) (Creative Pultrusions, Inc.)	1	3.90e+06	3.74e+06	0.25	15500	62000	60667
	2	3.56e+06		0.27	15000	60000	
	3	3.75e+06		0.26	15000	60000	

Table 4.2 Results of Tension Tests (Pultruded Specimens)

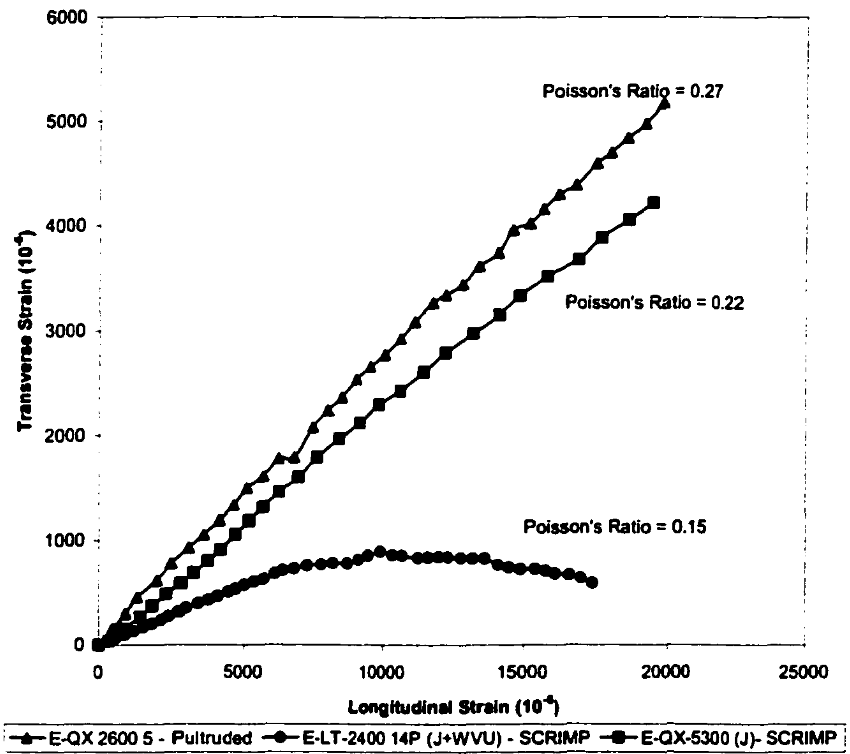

Figure 4.4 Poisson's effect on SCRIMP and Pultruded Test Specimens

4.2.2 Discussion of Tension Test Results

In the current section the behavior of SCRIMP and Pultruded specimens under tensile load are discussed.

- **SCRIMP Samples**

From Figures 4.1 and 4.2, no significant difference is found in strength and stiffness of composites with two layers of biaxial/quadraxial fabrics versus four layers of biaxial/quadraxial fabrics [between E-LT-2400 (J), E-LT-2400 (J+WVU)]. Lack of significant difference in properties has been attributed to 100% increase in thickness of four layers composite samples over two layers of samples. Also, the ultimate load resistance was twice that of composites with two layers of fabrics. On an average, composites with bi-axial fabrics were about 30 ~ 40% stronger than composites with quadraxial fabrics (Table 4.1). In the composites with quadraxial fabrics, contribution from the fibers oriented at $\pm 45^0$ is very limited, and also the specimens sheared of at 45^0 angle under tensile load.

- **Pultruded Samples**

The pulturded specimens supplied by Reichhold Industries Inc., and Creative Pultrusions, Inc. did not have significant difference in stiffness, but there was about 20% difference in ultimate stress. This is attributed to low curing temperature at Creative Pultrusions, Inc. In addition, the resin formulation used by Creative Pultrusions, Inc. was different from Reichhold Industries Inc., i.e., more of bromine content in the resin by Reichhold industries Inc.

- **SCRIMP Versus Pultruded Samples**

Figure 4.3 represents, stress versus strain of SCRIMP and pultruded specimens (same fiber architecture as shown in Figure 3.1) under tension load. SCRIMP specimens were only 50% of strength of pultruded specimens. Such variations may be attributed to manufacturing discrepancies in SCRIMP specimens. The major drawbacks in SCRIMP process are:

- Low curing temperature, which may lead to pre-mature failure in fibers
- Improper wet out of resin, which results in 20-25% reduction in thickness of the composite part (Table 4.1 and Table 4.2) which eventually lead to lower strength and stiffness.
- High stress concentration at kinks developed in fabrics

- **Poisson's Ratio for SCRIMP and Pultruded Samples**

Poisson's ratios of SCRIMP and pultruded specimens are shown in Figure 4.4. Composites with bi-axial fabrics have low Poisson's ratio compared to composites with quadraxial fabrics. For composites with bi-axial fabrics, the curve for logitudinal versus transverse strain is linear only upto 50% of ultimate load. Additional loading (beyond 50% of ultimate load) did not induce much of transverse strain (Figure 4.4). Hence composites with bi-axial fabrics have exhibited a bi-linear stress versus strain relationship. The bi-linear stress versus strain relationship was not observed in SCRIMP sample with quadraxial fabrics, because fabrics oriented at $\pm 45^0$ have contributed for a linear variation which is lacking in SCRIMP samples with bi-axial fabrics. However, Poisson's ratio for pultruded specimens was linear upto ultimate load.

4.2.3 Failure modes

Failure modes of SCRIMP and pultruded test specimens are shown in Figure 4.5 and Figure 4.6, respectively. The failure modes in SCRIMP specimens with bi-axial fabrics were different from those with quadraxial fabrics. In specimens with bi-axial fabrics, the longitudinal fibers in the outer ply pulled apart. The longitudinal strain versus transverse strain (Figure 4.4) was linear up to about 50% of ultimate load, beyond which it was non-linear up to failure. This indicates that 0^0 fibres have been strained to maximum extent which lead to fiber pull out. In specimens with quadraxial fabrics, shear failure was observed at fibers oriented at 45^0 because the fibers were able to take only 70% of ultimate load and since 45^0 fibers are next outermost to 0^0 (which can take 100% of load), the fibers sheared of leading to shear failure.

In pultruded specimens, outer fibers (rovings) pulled apart leaving the core (stitched fabric) intact. The strain measured at the core of test specimens was nearly thrice that of strain measured at outer layers. At 25% of ultimate stress, the strain at core was about 17,000 microstrains while the strain in outer fibers was only 5,700 microstrains. The differential strain between outer fibers and the core, reveals that stiffness mismatch between the core and outer fibers, lead to interlaminar shear in the matrix that binds outer fibers and the core. From the above failure mode, we can conclude that the above failure mechanism will be helpful in modifying fabric designs for optimal load transfer, i.e., the stiffness mismatch between the core and outer fibers could be avoided.

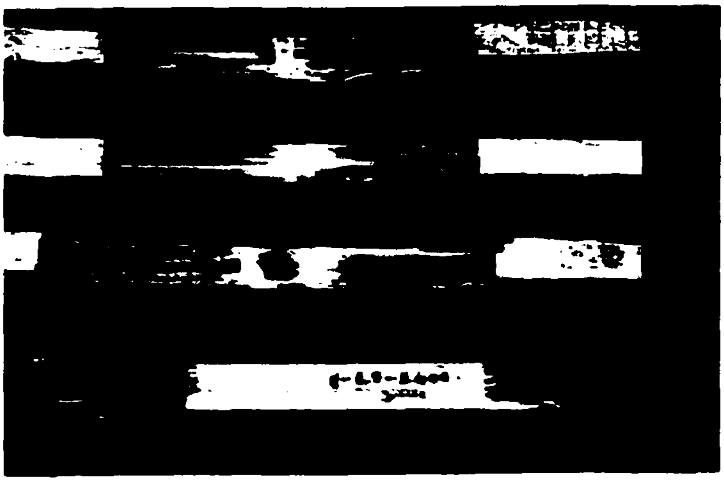

Figure 4.5 Failure Mode of SCRIMP Specimens under Tension

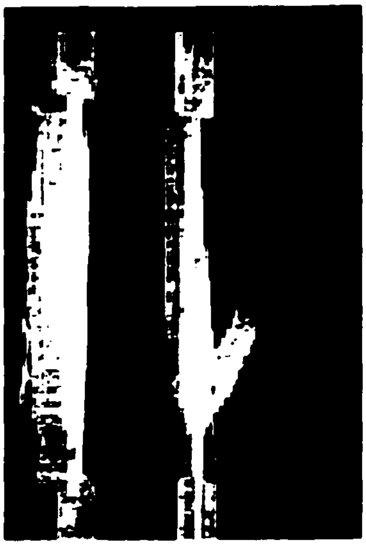

Figure 4.6 Failure Mode of Pultruded Specimens under Tension

4.3 Bending Test Results

A total of 33 tests were conducted under three point bending loads with simply supported boundary conditions. The load-deflection data was recorded by Instron machine (Model 4411) and strain was recorded using strain indicator. A load-deflection plot was used to obtain the slope of the elastic zone.

Bending modulus from deflection and failure stress of composites with 3-D stitched fabrics, along the fiber direction was computed as per equations 4.4 and 4.5.

Bending Modulus (from deflection): $$E_x^{Ben} = \frac{P \times L^3}{4 \times \delta \times b \times d^3} \quad (4.4)$$

Ultimate Stress: $$\sigma_{ult} = \frac{M \times c}{I} \quad (4.5)$$

E_x^{Ben} = Bending Modulus (psi)

(P/δ) = Slope of Elastic Zone of Load Versus Deflection Curve (lbs/in/in)

L = Span of the Specimen (in)

I = Moment of Inertia (in^4) = $bt^3/12$

b = Width of the Specimen (in)

t = Tthickness of the Specimen (in)

M = Bending Moment (lbs-in) = PL/4

c = Distance from Outer Compression/Tension Face to the Neutral Axis (in)

σ_{ult} = Ultimate Stress (psi)

Load versus deflection plots for SCRIMP and pultruded specimens are shown in Figure 4.7 and Figure 4.8, respectively. Results of bending test for SCRIMP and pultruded specimens are shown in Table 4.3 and Table 4.4, respectively.

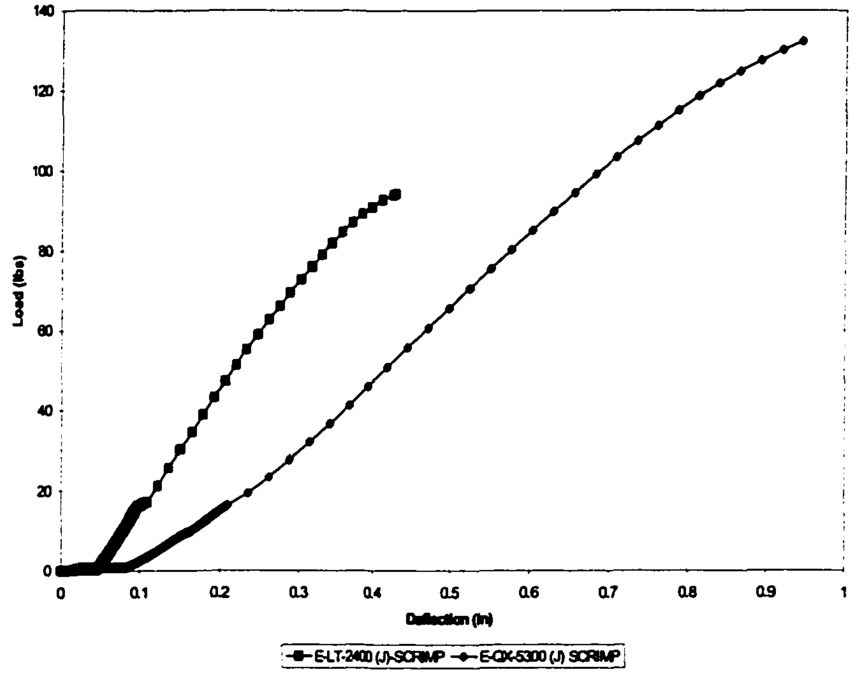

Figure 4.7 Load Versus Deflection for SCRIMP Specimens

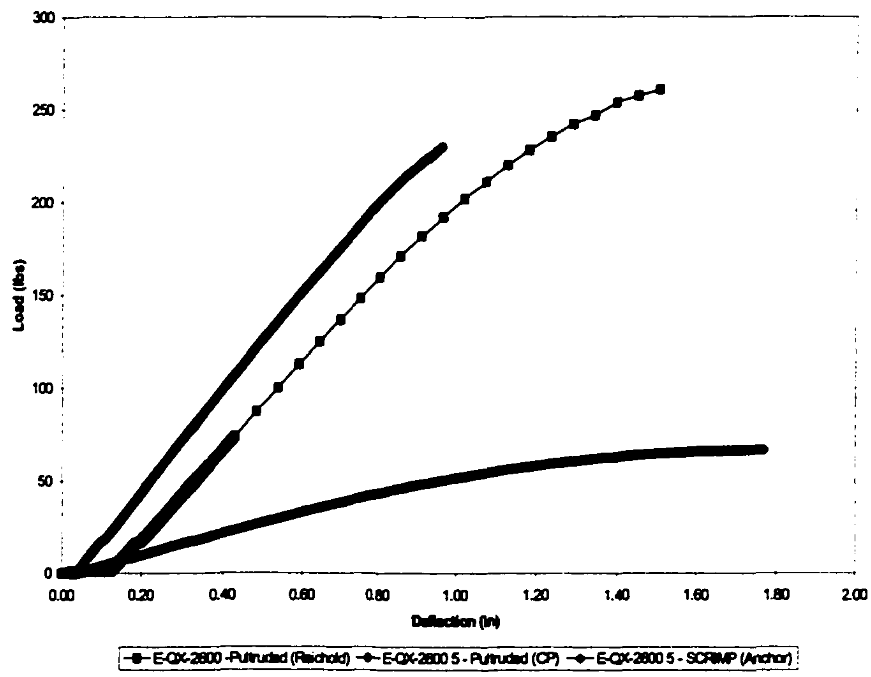

Figure 4.8 Load Versus Deflection for E-QX-2600 5 Specimens

4.3.1 Discussion on Bending Test Results

In the current section the behavior of SCRIMP and pultruded specimens under bending loads are discussed.

- **SCRIMP Samples**

The ultimate stress in SCRIMP specimens with bi-axial fabrics was about 40% higher than the ultimate stress in SCRIMP specimens with quadraxial fabrics. This may be attributed to 25% contribution from 0^0 fibers in the bi-axial fabrics and only about 15% contribution from 0^0 and $\pm 45^0$ fibers in the quadraxial fabrics with little of contribution from $\pm 45^0$ fibers.

- **SCRIMP Versus Pultruded Samples**

The Load versus deflection plot (Figure 4.8) indicates that pultruded specimens exhibit more ductility than the SCRIMP specimens. From Tables 4.3 and 4.4, the ultimate load and bending stiffness of SCRIMP specimens were found to be about 40 ~ 60% lesser than the ultimate load of pultruded specimens.

The strength and stiffness of SCRIMP specimen E-QX-2600 5 were only about 50% of pultruded specimen (Table 4.4). This may be due to non-uniformity of resin flow in SCRIMP specimens. The stiffness and ultimate stress of pultruded specimens is 3.4E+06 psi of 92,848 psi respectively while stiffness and strength of SCRIMP specimens is 2.09E+06 psi and 42,783 psi. This is attributed to major drawbacks in SCRIMP process as described in section 4.2.2.

4.3.2 Failure Modes

Failure modes of SCRIMP and pultruded specimens are shown in Figure 4.9 and Figure 4.10, respectively. Failure modes in pultruded specimens were less catastrophic compared to SCRIMP specimens. After the release of bending loads, pultruded specimens recovered most of the deflection unlike the SCRIMP specimens. SCRIMP specimens had delamination on both tension and compression faces under bending loads. Failure in SCRIMP specimens was more of delamination type rather than tension failure. In pultruded specimens, failure was initiated in tension face with rovings pulling apart leading to tension failure. Damage was less on the compression face of pultruded specimens.

SCRIMP Specimens	Test No	Bending Modulus (From Deflection) (psi)	Average Bending Moudulus (psi)	Ultimate Load (lbs)	Ultimate Stress (psi)	Average Ultimate Stress (psi)
E-LT-2400 (J)	1	2.43E+06	2.06e+06	94.252	73558	78300
	2	1.88E+06		105.61	82422	
	3	1.88E+06		101.124	78921	
E-LT-2400 (J+WVU)	1	1.56E+06	1.56e+06	131.87	49837	49531
	2	1.69E+06		145.69	55060	
	3	1.45E+06		115.62	43696	
E-LT-2400-14P (J)	1	2.66E+06	2.31e+06	79.78	73666	72348
	2	2.04E+06		76.73	70849	
	3	2.23E+06		78.55	72530	
E-LT-2400 14P (J+WVU)	1	1.32E+06	1.26e+06	149.8	50811	47497
	2	1.22E+06		142.31	48271	
	3	1.26E+06		127.98	43410	
E-QX-2600 5 (J)	1	1.29E+06	1.11e+06	98.34	58524	49222
	2	1.05E+06		75.92	45181	
	3	9.96E+05		73.87	43961	
E-QX-2600 5 (J+WVU)	1	1.07E+06	1.05e+06	123.25	38274	35434
	2	9.98E+05		106.9	33197	
	3	1.09E+06		112.16	34830	
E-QX-5300 (J)	1	1.83E+06	1.99e+06	93.18	44569	52312
	2	2.06E+06		132.37	63315	
	3	2.09E+06		102.55	49051	
E-QX-5300 (J+WVU)	1	2.21E+06	2.32e+06	84.86	43652	39479
	2	2.20E+06		80.45	41384	
	3	2.54E+06		64.93	33400	
E-QX-2600 5 +Rovings (WVU)	1	1.62e+06	2.09e+06	47.30	31446	42783
	2	2.12e+06		66.71	44343	
	3	2.55e+06		79.08	52561	

Table 4.3 Results of Bending Tests (SCRIMP Specimens)

PULTRUDED Specimens	Test No	Bending Modulus (From Deflection) (psi)	Average Bending Modulus (psi)	Ultimate load (lbs)	Ultimate Stress (psi)	Average Ultimate Stress (psi)
E-QX-2600 5 +Rovings (WVU) - Reichhold Industries, Inc.	1	3.54E+06	3.5E+06	254.23	90957	92849
	2	3.50E+06		263.59	94306	
	3	3.40E+06		260.73	93283	
E-QX-2600 5 +Rovings (WVU) - Creative Pultrusions, Inc.	1	4.50e+06	4.3E+06	229.77	86116	87508
	2	4.20e+06		224.26	88205	
	3	4.20e+06		224.26	88205	

Table 4.4 Results of Bending Tests (Pultruded Specimens)

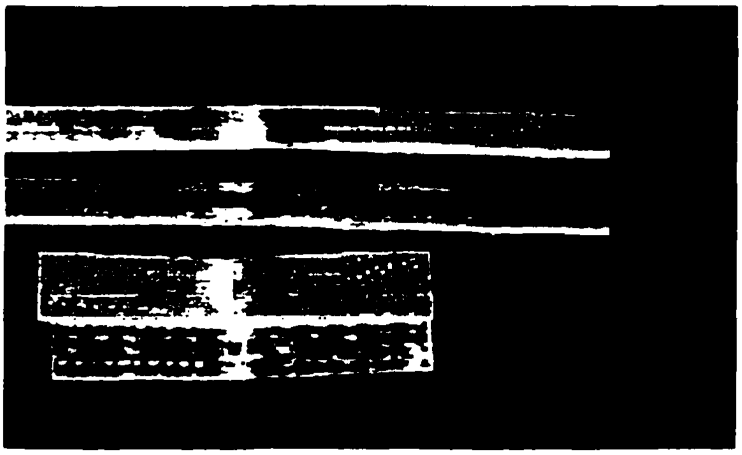

Figure 4.9 Failure Mode of SCRIMP Specimens Under Bending

Figure 4.10 Failure Mode of Pultruded Specimens Under Bending

4.4 Short-Beam Shear Test Results

Short-beam shear tests were conducted on specimen E-QX-2600 5. A total of 9 tests were conducted on test specimens and the shear strength was computed as follows:

Shear strength: $$\tau = \frac{3 \times P_{ult}}{4 \times b \times t} \qquad (4.6)$$

Where,

τ = Shear Strength (psi)

P_{ult} = Ultimate Load (lbs)

b = Width of Specimen (in)

t = Thickness of Specimen (in)

Results of short-beam shear tests are shown in Table 4.5 and Table 4.6.

SCRIMP Specimens	Test No	Shear Strength (psi)	Average Shear Strength (psi)	Ultimate load (lbs)
E-QX-2600 5 +Rovings (WVU)	1	5056	5353	674
	2	5939		792
	3	5064		675

Table 4.5 Results of Short-Beam Shear Tests (SCRIMP Specimens)

PULTRUDED Specimens	Test No	Shear Strength (psi)	Average Shear Strength (psi)	Ultimate load (lbs)
E-QX-2600 5 +Rovings (WVU) - Reichhold Industries, Inc.	1	5032.6	4806	419
	2	4780.6		398
	3	4605.3		384
E-QX-2600 5 +Rovings (WVU) - Creative Pultrusions, Inc.	1	3135.5	4044	251
	2	4323.9		332
	3	4671.2		344

Table 4.6 Results of Short-Beam Shear Tests (Pultruded Specimens)

4.4.1 Failure Modes

Test specimens under 3 point load (Short span or L/t less than 5 to 8) had a shear failure at the interface of the fabric and rovings. Shear failure of pultruded test specimens is shown in Figure 4.11. As the shear increased, cracks formed at the interface of laminates (rovings and fabric), i.e., the rovings split apart from the fabrics. From this we can conclude that the matrix (between rovings and fabric) first underwent cracking, leading to interlaminar shear failure. Higher shear stress could be obtained if the failure is driven to initiate in fiber rather than in the matrix.

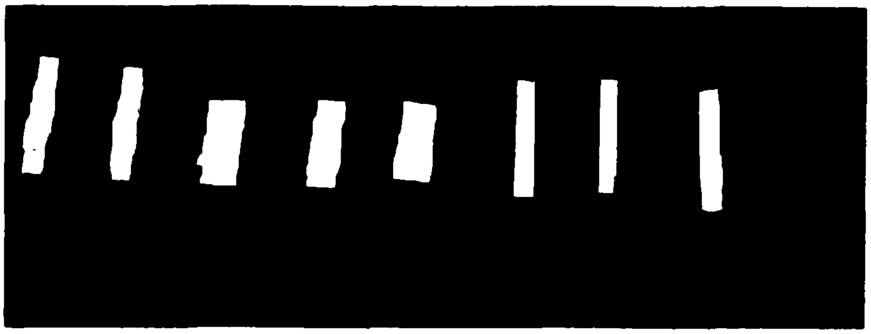

Figure 4.11 Failure Mode of Pultruded Specimen Under Shear Load

4.5 Theoretical Analysis

4.5.1 Prediction of Axial and Bending Stiffnesses

Theoretical predictions of mechanical properties such as stiffness and strength at coupon level were made based on the material properties of glass fibers and matrix. Laminate properties were computed based on the rule of mixtures (Barbero, 1998). Halpin-Tsai equations were also incorporated into Classical Lamination Theory (CLT) in computing the laminate properties. The analysis of composites with 3-D stitched fabrics is presented in Appendix A. The following steps are involved in the analysis. Each of these steps is described in detail in Appendix A.

- Compute material properties
- Compute fiber volume fraction
- Evaluate lamina properties
- Calculate in-plane reduced stiffness matrix (Q)
- Calculate transformed reduced stiffness matrix $[\bar{Q}]$
- Compute the final $[\bar{Q}]$ matrix

- Compute stiffness matrix
- Compute laminate moduli
- Compute axial stiffness and bending stiffness

4.5.2 Prediction of Failure Stresses

The fiber architecture in composites with 3-D stitched fabrics consists of fabrics and unidirectional fibers. The conventional failure stress theories like maximum stress theory, Tsai-Hill or Tsai-Wu theory will not be applicable because all these theories were developed based on unidirectional fibers. Hence, a new approach has been carried out for predicting the failure stress.

Assuming the outer ply (rovings) and core (stitched fabric) as two springs in parallel with different spring stiffness, the ultimate load taken by the two springs is calculated as:

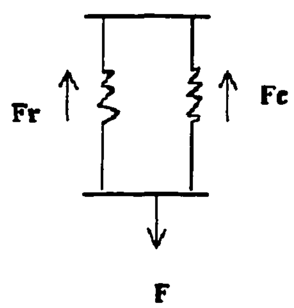

$$F = F_r + F_c \qquad (4.7)$$

Where,

F = Ultimate load (lbs)

F_r = Force in outer layers (Rovings)

F_c = Force in core (Fabric)

But $\Delta = F/k$ (4.8)

Where Δ= Deflection of the spring system

k = Equivalent spring stiffness

Substituting equation 4.8 in 4.7

$\Delta k = \Delta_r k_r + \Delta_c k_c$ (4.9)

The strain in core was measured with extensometer and was found to be 2.9 times that of strain in the outer plies (rovings) at the same load level

i.e., $2.9\Delta_r = \Delta_c$ (4.10)

Substituting equation 4.10 into equation 4.9

$\Delta k = \Delta_r k_r + 2.9\Delta_r k_c$ (4.11)

$\Delta k = \Delta_r (2E_r t_r b_r/L_r + 2.9E_c t_c b_c/L_c)$ (4.12)

E_r = Spring stiffness for rovings = 3.5E+06 psi

t_r = Thickness of outer ply = 0.069 in.

t_c = Thickness of core = 0.107 in.

b_r = Width of outer ply = 1 in.

b_c = Width of core = 1in.

L_r = Length of outer ply = 1in.

L_c = Length of core = 1 in.

$\Delta k = \Delta_r$ [{(2x 3.5E+06 x 0.069 x 1)/1} + {(2.9 x 2.4E+06 x 0.107 x 1)/1}]

$\Delta k = \Delta_r$ (1.23+06)

Δ_r = Failure strain in the outer ply ranges from 18000E-06 ~ 21000E-06

Therefore, Δk = 1.23E+06 x 18000E-06 = 22140 lbs

But Δk = F (from equation 4.8)

Therefore ultimate load = $F = \Delta k = 22140$ lbs

Ultimate stress = F/A = 22140/0.245 = 90,367 psi (where A is the cross section area of the composite sample)

Hence, the failure stress of the coupon = 90.3 ksi

The experimental results of strength and stiffness are correlated with theoretical results and tabulated in Table 4.7

Laminate Properties	Experimental Results (WVU)	Theoretical	Experimental Results (CP)
Tensile Modulus (psi)	3.33E+06	4.2E+06	4.1E+06
Bending Modulus (psi)	3.5E+06	4.4E+06	4.5E+06
Shear Strength (psi)	4806	6490	5852
Failure Stress (psi)	75611	90367	81769

Table 4.7 Correlation of Experimental and Analytical Results for E-QX-2600 5

4.6 Comparison of Strength and Stiffness of 3-D and 2-D Composites

A graphical representation of strength and stiffness of composites for unidirectional bi-directional fabric and new fabric (3-D stitched fabric) is given in Figure 4.12. Composites with unidirectional fibers (35% fiber volume content) exhibited a low strength of 12 ksi and stiffness of 2.0E+06 psi. Composite with bi-directional fabric (33% of fiber volume content) improved the strength to 55 ksi and stiffness to 2.9E+06 psi. Composite with 3-D stitched fabrics with 45% fiber volume content exhibited about 30% more strength and about 20% more stiffness than composites with 2-D stitched fabrics.

Compared to the conventional material (steel), 3-D composite attained an increase of 95% in strength, though steel is about ten times stiffer than 3-D composite.

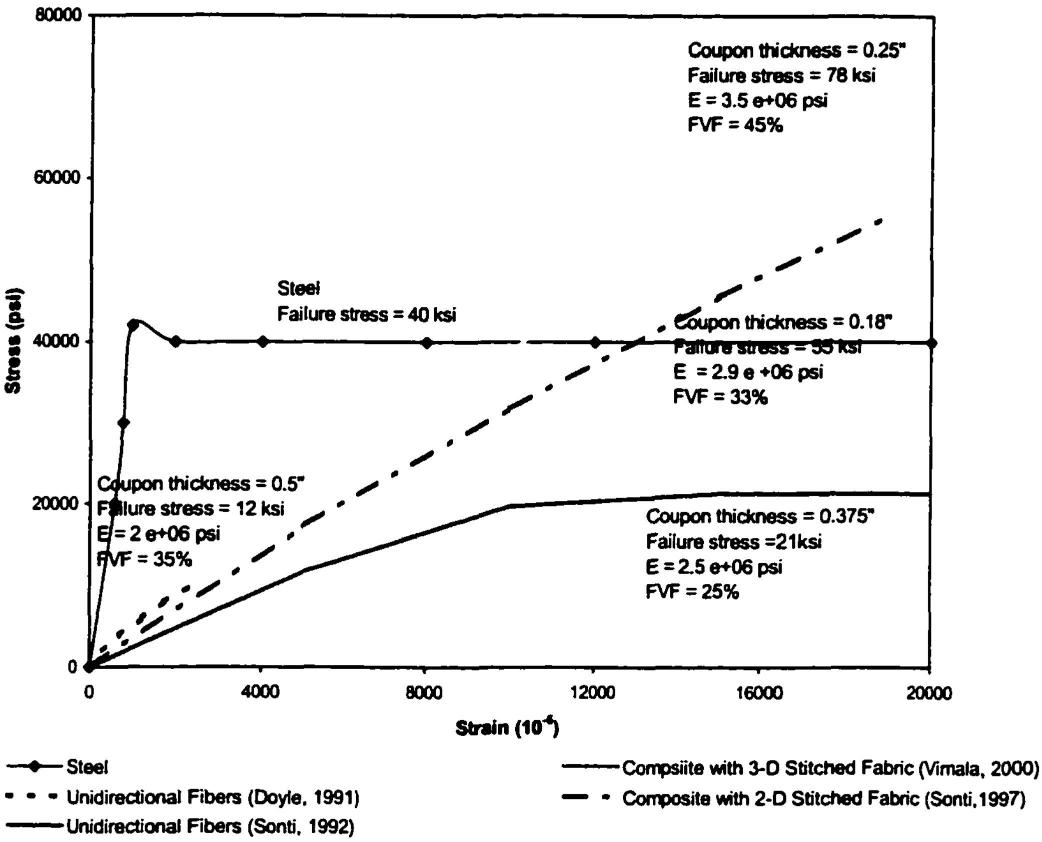

Figure 4.12 Strength and Stiffness of Composite with Different Type of Fabrics

4.7 Conclusions

The strength and stiffness of 3-D composite varies with respect to fiber architecture, stitch density, stitch material, and manufacturing process. Each item is dealt in detail in the following paragraphs.

Effect of fiber architecture

- SCRIMP specimens with bi-axial fabrics were stronger and stiffer than SCRIMP specimens with quadraxial fabrics.
- No significant change was observed in the strength between the SCRIMP specimens with two layers of fabric and SCRIMP specimens with four layers of fabric (double the density).
- Poisson's ratio for SCRIMP specimens with biaxial fabrics was about 50% of SCRIMP specimens with quadraxail fabrics.

Effect of Stitch Density and Stitch Material

- The ultimate bending stress of SCRIMP specimens stitched at Johnston Industries Inc., and WVU were only 60% of SCRIMP specimens were stitched at Johnston Industries Inc. This is attributed to the fact that a further stitch at WVU by nylon thread lead to the development of high stress concentration due to needle punch (Table 4.3).
- SCRIMP specimens with stitch density of 7 (Table 3.1) were only 5% ~7 % stronger than the SCRIMP specimens with stitch density of 3.5. This is because all the specimens with stitch density of 7 were stitched with alternate of glass and yarn (pitch

distance of glass thread was 0.25") and the specimens with stitch density of 3.5 were stitched only with glass (pitch distance of glass thread was 0.25") which indicates that there was not much contribution from the yarn thread.

Effect of Manufacturing Process

- Strength and stiffness of SCRIMP specimens were about 50% of pultruded specimens. This is attributed to the major drawbacks in SCRIMP process such as resin absorption, improper wet-out, low curing temperature
- Curing temperature in pultrusion greatly affects the strength of composite. Specimens pultruded at Creative Putrusion Inc, were about 20% lower in strength than specimens pultruded at Reichhold Industries Inc. This may be attributed to low curing temperature at Creative Pultursion Inc.

Failure Modes

Under Tensile Load

- In the SCRIMP specimens with biaxial fabrics, the fibers in the outer ply pulled apart while in the SCRIMP specimens with quadraxial fabrics sheared of at fibers that were oreinted at 45^0.
- In the pultruded specimens, the outer ply pulled apart leaving the core intact. The failure was initiated at the interface of outer ply and core (matrix) due to the differential strain developed in outer ply and core in pultruded specimens.

Under Bending Loads

- Failure modes in SCRIMP specimens under bending were more of delamination type, while the failure mode in pultruded specimens were more of ductile failure.
- Failure modes in pultruded specimens were less catastrophic compared to SCRIMP specimens

Under Shear Loads

- As the shear increased, cracks formed at the interface of laminates (rovings and fabric), i.e., the rovings split apart from the fabrics. From this we can conclude that the matrix (between rovings and fabric) first underwent cracking, leading interlaminar shear failure.

Others

- Composite with 3-D stitched fabrics exhibited 30% more strength and 20% more stiffness than 2-D stitched fabrics
- Ultimate strength of composite with 3-D stitched fabrics were 95% more than that of conventional material (steel)
- Good correlation between experimental and theoretical results with respect to stiffness and strength has been noted.

CHAPTER 5

DEVELOPMENT OF SECOND GENERATION FRP BRIDGE DECK

5.1 Introduction

Bridge deck deterioration has been recognized by highway agencies to be one of the most complex problems of the infrastructure. Fiber-reinforced polymer (FRP) composites have been acknowledged as one of the advanced materials for the repair and replacement of bridge decks. First generation FRP bridge deck (Figure 5.1) was used to build Laurel Lick bridge and Wick Wire Run bridge. In the sections 5.1.1 and 5.1.2. of this chapter, profile of first generation FRP bridge deck component and stiffness of the FRP bridge deck are discussed. The optimization of first generation FRP bridge deck leading to second generation FRP bridge deck component with respect to weight and fiber architecture is discussed in section 5.2. In the second generation FRP bridge deck component the thickness of the component is being reduced to have an overall decrease in unit weight of component. The fiber volume fraction has been increased to improve bending stiffness of the second generation FRP bridge deck component.

5.1 Details of First Generation FRP Bridge Deck Component

5.1.1 Profile/Shape of First Generation FRP Bridge Deck Component

Non-corrosive FRP composite materials have been used to develop FRP composite bridge deck component that have high strength to weight ratio and stiffness to weight ratio, and good fatigue resistance (Gangarao et.al., 1999). The first generation FRP bridge deck component cross-section is shown in Figure 5.1. Based on previous experience with other FRP structural shapes such as I-beams and box beams, it was established that a cross-section made of full-depth hexagons and half-depth trapezoids would enhance the structural performance. The height of the FRP bridge deck component was constrained to 8 inches to replace conventional concrete deck. The length and thickness of flange and web of FRP double trapezoid and hexagon components are given in Table 5.1.

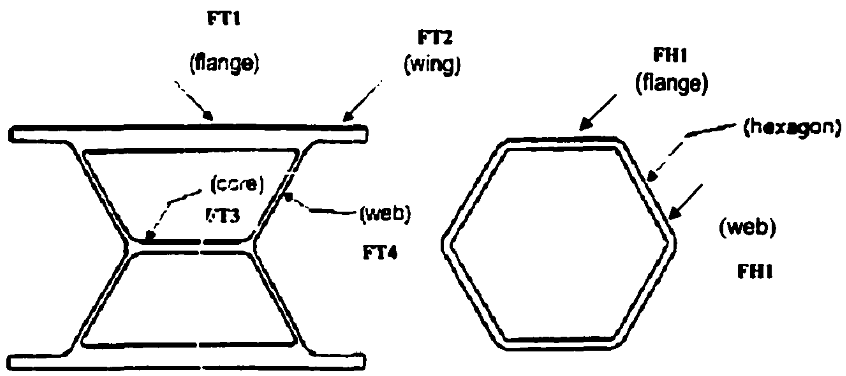

Figure 5.1 Cross Section of First Generation FRP Bridge Deck Component

Component	Part	Length (in)	Thickness (in)
Double-Trapezoid	Flange (FT1)	8	0.75
	Wing (FT2)	2	0.438
	Core (FT3)	4	0.375
	Web (FT4)	4	0.228
Hexagon	Flange (FH1)	4	0.3125
	Web (FH1)	4	0.3125

Table 5.1 Dimensions of Each Component in First Generation FRP Bridge Deck Component

The fiber architecture consists of E-glass fibers in the form of multi-axial 2-D stitched fabrics, continuous rovings, and chopped strand mats with vinyl ester resin as the matrix. Fiber architecture for the first generation bridge deck component is shown in Figure 5.2. The pultruded first generation FRP composite deck component weighs about 22 lbs/ft^2.

5.1.2 Stiffness of First Generation FRP Bridge Deck Component

The bending stiffness of first generation FRP bridge deck component was computed both experimentally and theoretically (Vedam, 1997). Three point static bending tests were conducted on double-trapezoid and hexagonal components, in the longitudinal direction for three different spans (60 inches, 84 inches, and 108 inches) to study stiffness variation. The specimens were subjected to two types of loading: patch load of 20 inches x 10 inches, and strip load using a 6 inch wide plate. The patch load represents the approximate dimension of wheel distribution of an AASHTO standard truck. Experimental stiffness in the longitudinal direction was obtained from the load versus deflection plot. Theoretical stiffness in the longitudinal direction was predicted using the approximate classical lamination theory (CLT). The cross-section was sub-divided into individual parts (preferably rectangular) for ease of computation. The stiffness of each component was determined and then added using the principal of "parallel axis theorem" to obtain the stiffness of the section as a whole. The bending stiffness of the first generation FRP bridge deck component was found to be 8.44E+08 lbs-in^2/ft.

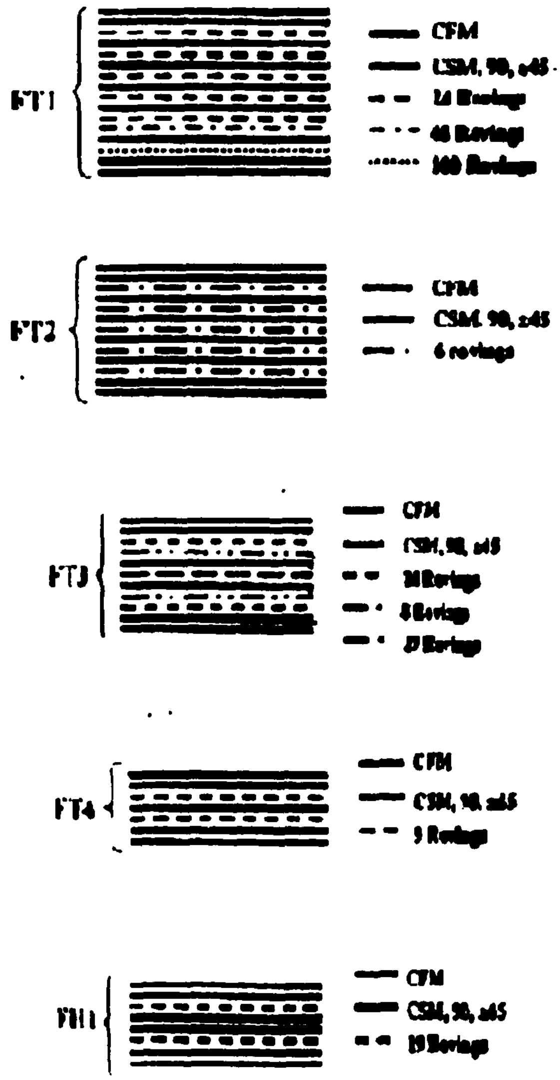

Figure 5.2 Fiber Architecture for First Generation FRP Bridge Deck Component

5.2 Second Generation FRP Bridge Deck Component

5.2.1 Introduction

The pultruded composite decks present a challenge to the composites industry and bridge engineers in terms of producing a durable product at competitive prices. In addition, the product has to resist HS 25 and HS 30 truck loads and harsh environments during its service life. The failure in the present FRP bridge deck component (first generation FRP bridge deck component) was initiated due to delamination of fabric in the wing (Figure 5.3) of the double-trapezoid component, at the junction of hexagon and double-trapezoid component on the bottom side. This kind of failure is a result of issues dealing with fiber architecture and the manufacturing process, i.e., 1) uneven curing, 2) high pullout speed and 3) improper wet-out.

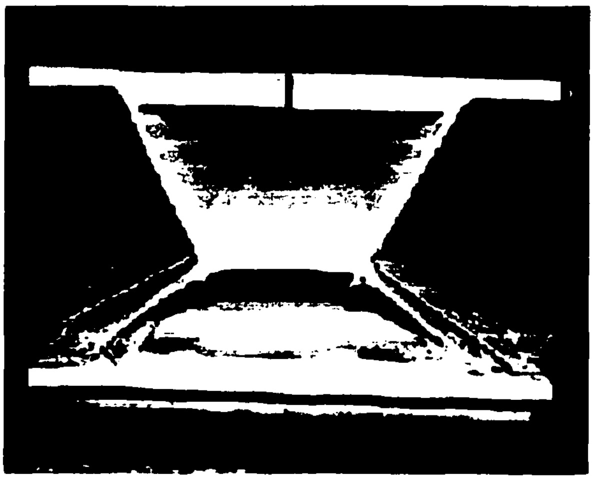

Figure 5.3 Cross-Section of Failed Double-Trapezoid Component (First Generation FRP Bridge Deck Component)

5.2.2 Profile/Shape of Second Generation FRP Bridge Deck Component

The Constructed Facilities Center at West Virginia University, in co-operation with Creative Pultrusions Inc., proposed various cross-sections for the second generation FRP bridge deck component. The various proposed cross-sections for a second generation FRP bridge deck component are shown in Figures 5.4 through 5.5. The Figures reveal that the proposed cross-sections for second generation FRP bridge deck component, no longer comprise double-trapezoid and hexagon components separately. The two components have been combined into a single component with the primary goal to reduce the weight of FRP composite deck component while satisfying the demands of original stiffness (first generation bridge deck component), highway bridges loads and durability under harsh environments. In addition, labor and material costs will be reduced along with improvements in the quality of end product.

Figure 5.4 (a) reveals that a small opening in the hexagon component was proposed. This small opening may lead to improper curing of the composite part. To overcome the above deficiency, a larger opening (Figure 5.4 b) was proposed for proper circulation of heat thereby leading to better curing of the composite part. Other advantage of this profile over previous shapes is the symmetry in the shape which leads to ease in production. But the disadvantages of this profile are in terms of tolerances, stress concentration due to local distortion at the web, and damage to web while lifting or assembling. Due to these limitations, CFC-WVU and Creative Pultrusions Inc., developed a new cross-section as shown in Figure 5.5. Small nodules and indentations are provided in the flanges to help pressurize the adhesive at the glue line. Probability of damage during lifting or assembling the component is less compared to the previous cross-sections. The cross-section shown in Figure 5.5 was considered to be the final cross-section for second generation FRP bridge deck component.

In the first generation FRP bridge deck component, the length of adhesive used to bond the components was 24 inches while the adhesive length used in the second generation FRP bridge deck component (Figure 5.5) is only 4 inches. Thus, a reduction of about 83% in the volume of adhesive is achieved. The fiber architecture for the second generation FRP bridge deck is shown in Figure 5.6. Top and bottom flanges of the component are built with rovings and bi-axial fabrics (40 oz biaxial with 0.75 oz chopped mat). In 40 oz of bi-axial fabrics, 24 oz is oriented at 0^0 and 16 oz is oriented at 90^0 to improve bending stiffness of the component. The web of the component is built with rovings and triaxial fabrics (40 oz of triaxial with 0.75 oz chopped mat). In 40 oz of triaxial fabrics, 24 oz is oriented at $\pm45^0$ and 16 oz is oriented at 90^0 to have better shear resistance. The overlap length for fabrics is maintained at 1 to 1.5". The voids at corners are provided with rovings and the component is built up with new fiber architecture. This optimized second generation FRP bridge deck component has a self- weight of 19.5 lbs/ft^2. Thus, there is a reduction of about 11% in weight of second generation FRP bridge deck component when compared to first generation FRP bridge deck component. Reduction in weight of the deck and reduction in the length of adhesive line in the second generation bridge deck component reduces the overall cost of the bridge deck.

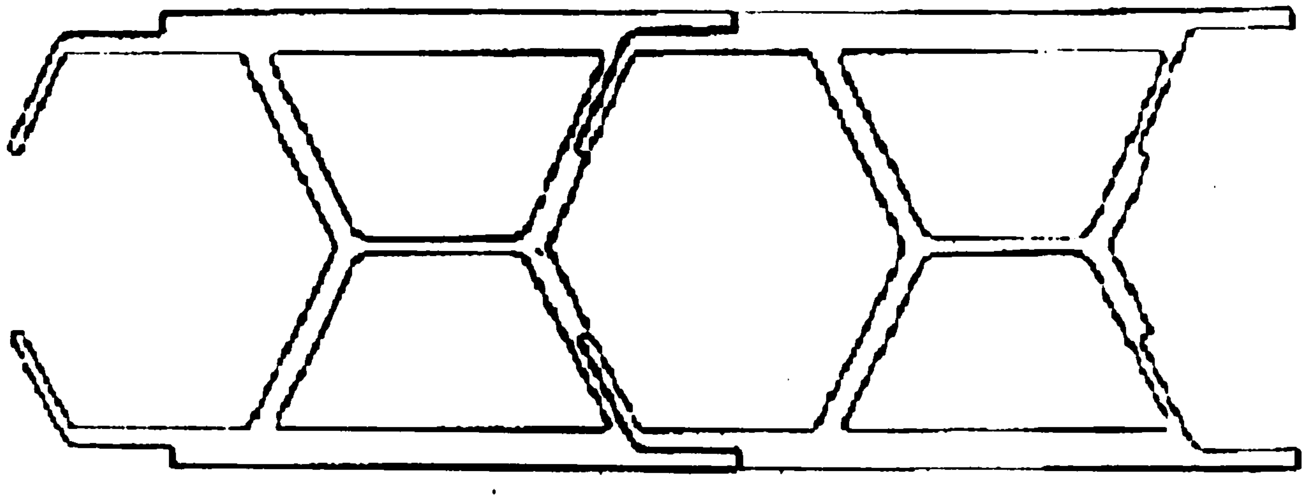

Figure 5.4 (a) First Proposal for Cross-Section of Second Generation FRP Bridge Deck Component

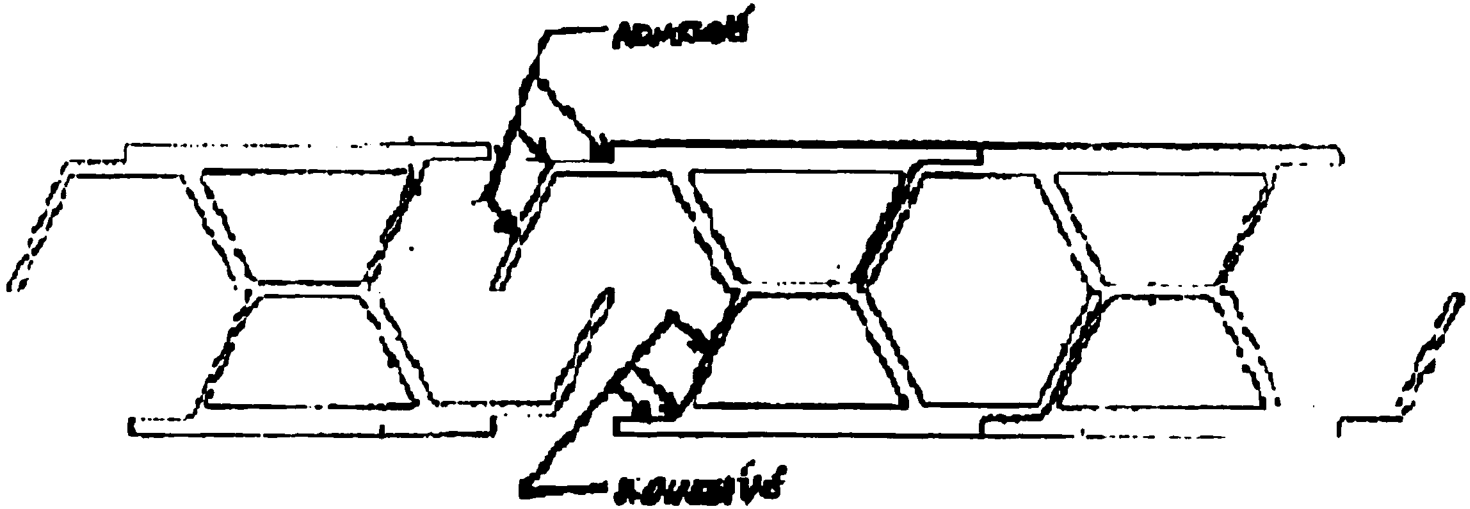

Figure 5.4 (b) Second Proposal for Cross-Section of Second Generation FRP Bridge Deck Component

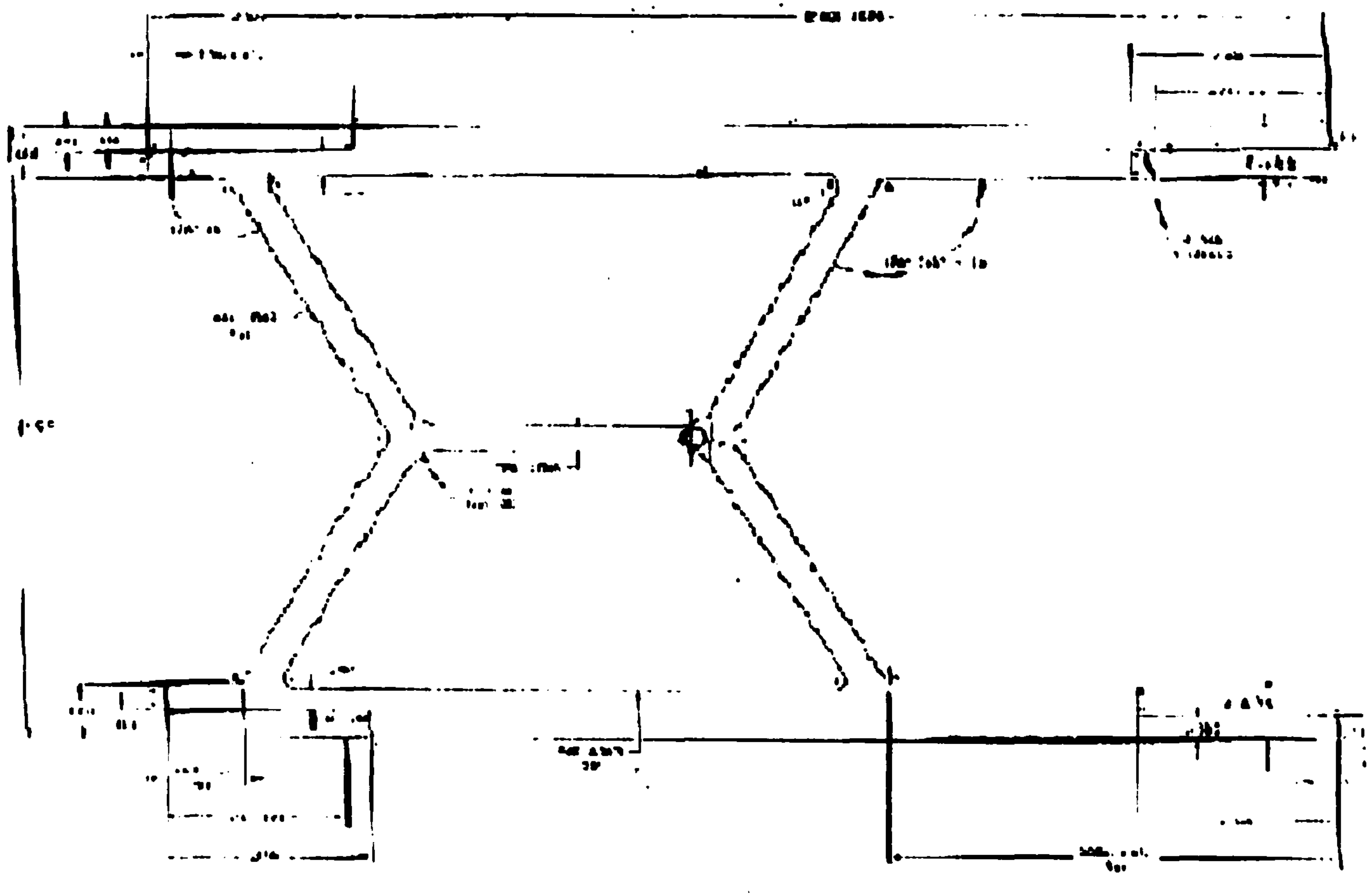

Figure 5.5 Final Proposal for Cross-Section of Second Generation FRP Bridge Deck Component

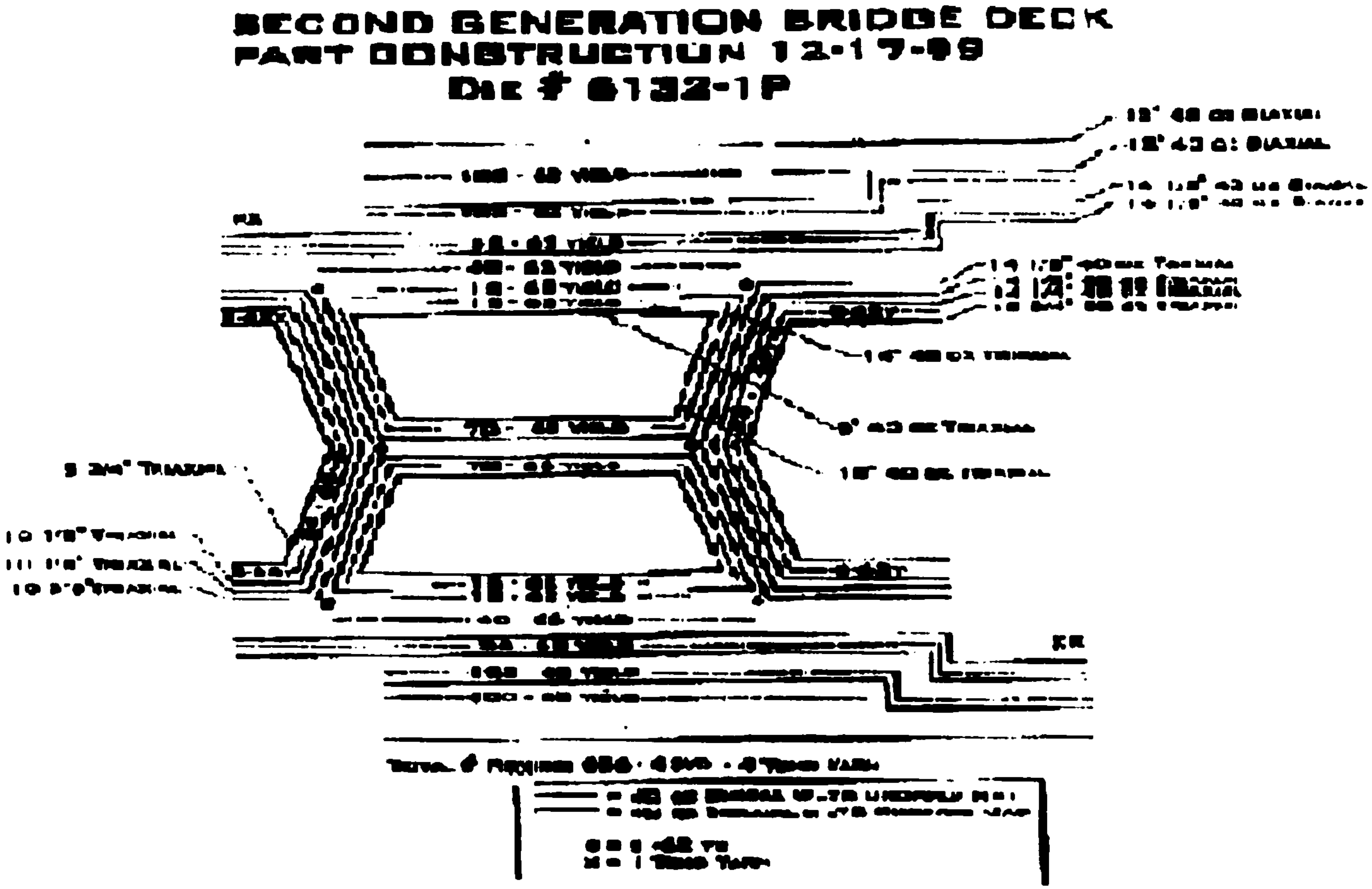

Figure 5.6 Fiber Architecture of Second Generation FRP Bridge Deck Component

5.3 Testing of Second Generation FRP Bridge Deck Component in Longitudinal Direction

The Second generation FRP bridge deck component was tested under static loads to study the bending response of the component. Three point bending test was conducted for a patch load (10" x 20") with simply supported conditions. The patch load represents the approximate dimensions of wheel load distribution of an highway truck, being used for designing bridges, as recommended by AASHTO highway bridge design specifications. Strain gages and dial gages were mounted at mid-span to measure strain and deflections. The load versus deflection curve and load versus strain curve are shown for the first and second generation FRP bridge deck component are shown in figure 5.7 and figure 5.8 respectively.

The stiffness of second generation FRP bridge deck component was found to be 8.28E+08 lbs-in^2/foot width while the stiffness of first generation FRP bridge deck component was found to be 8.44E+08 lbs-in^2/foot. The ultimate stress of first generation FRP bridge deck was 10 ksi while the ultimate stress of second generation FRP bridge deck was found to be about 30 ksi (Table 5.2). The second generation FRP bridge deck with reduced weight, was able to resist about twice the load of first generation FRP bridge deck component.

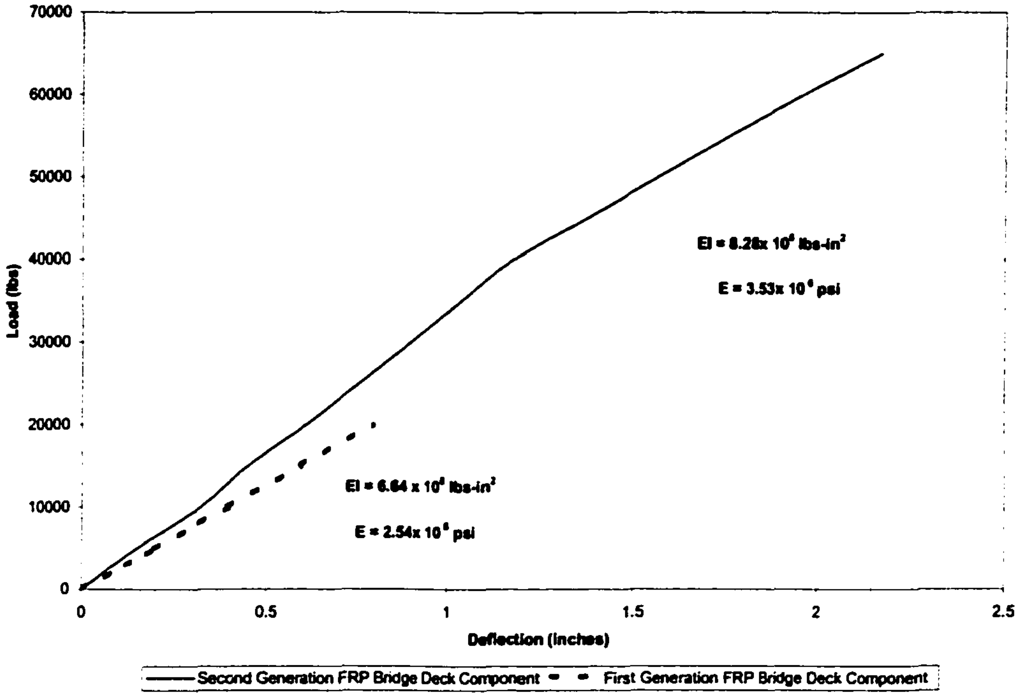

Figure 5.7 Comparison of Load Versus Deflection Curve for FRP Bridge Deck Components

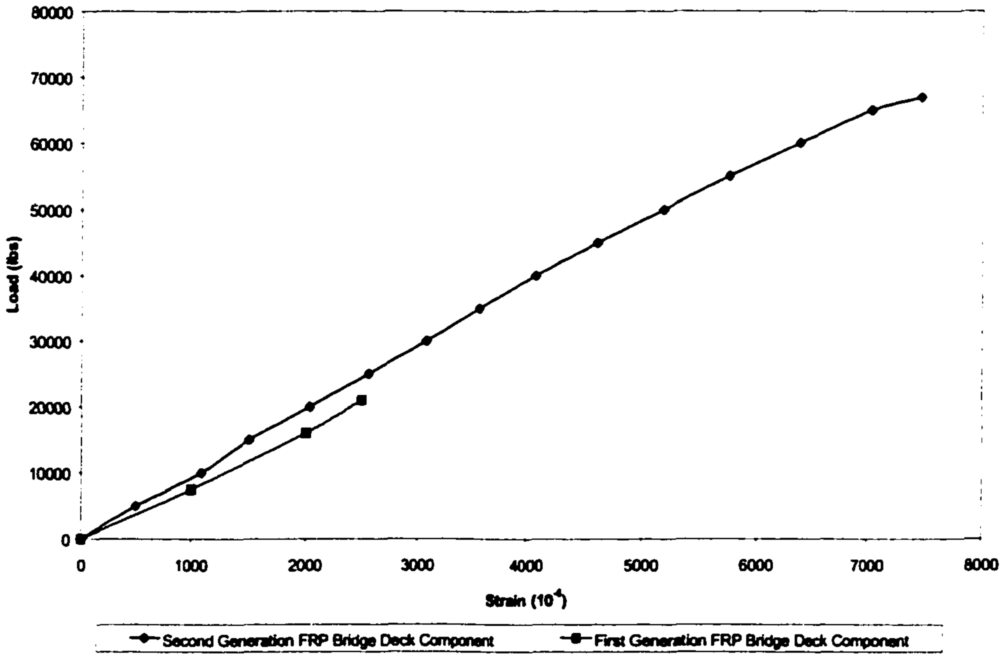

Figure 5.8 Comparison of Load Versus Strain Curve for FRP Bridge Deck Components

Bridge Deck Component	Span (feet)	Ultimate Load (kips)	Ultimate Stress (ksi)
First Generation	7	67	30.8
Second Generation	9	32	10.3

Tabel 5.2 Comparison of Ultimate Load and Stress in FRP Bridge Deck Components

5.4 Theoretical Analysis of Second Generation FRP Bridge Deck Component

A theoretical analysis (Appendix B) has been carried out to predict the stiffness of the component for the cross-section shown in Figure 5.6 Approximation Classical Lamination Theory (ACLT) has been used to find theoretical stiffness of FRP bridge deck component. The theoretical analyses involves the following steps:

- Collection of material properties of E-glass fibers, and vinyl ester resin (such as elastic modulus, shear modulus and Poisson's ratio).
- Determination of fiber volume fraction.
- Evaluation of elastic modulus of composite laminae.
- Evaluation of in-plane stiffness [A], bending-extension coupling stiffness [B] and bending stiffness [D]
- Computation of component stiffness employing the principles of parallel axis theorem.

Step-by-step approach of theoretical computations of bending stiffness of the second generation FRP bridge deck is given in Appendix B.

5.5 Theoretical Comparison of Stiffness (Bending and Shear) in First Generation and Second Generation FRP Bridge Deck Components

Comparison of stiffness (bending and shear) of first and second generation FRP bridge deck components is shown in Table 5.2. With reduced weight (11 % lower) and modified fiber architecture, the bending stiffness of the second generation FRP bridge deck component is almost same as the bending stiffness of the first generation bridge deck component. The shear stiffness of second generation FRP bridge deck component is 1.4 times the shear stiffness of first generation FRP bridge deck because the web in the second generation FRP bridge deck component is built with more rovings compared to the web in the first generation FRP bridge deck component.

Bridge Deck Component	**Bending Stiffness ($lbs\text{-}in^2/ft$)**	**Shear Stiffness (lbs/ft)**	**Weight (lbs/ft^2)**
First generation	8.44E+08	3.80E+06	22
Second generation	8.27E+08	5.36E+06	19.3

Table 5.3 Comparison of Bending , Shear Stiffnesses and Weight in FRP Bridge Deck Components

5.6 Buckling of FRP Structural Shapes

Most FRP shapes are thin-walled structures, i.e. depth exceeds four time the thickness (Structural Plastic Design Manual, 1984) and manufactured by pultrusion process (Qiao et.al 1999). The web thickness of such thin-walled structures must be adequate to resist in-plane shear, axial, and bending loads. Otherwise inadequate web thickness will lead to premature failure in FRP shape due to local buckling coupled with bending in the web. Hence, the web must be designed to resist combined in-plane thrust, bending and shear.

In the current section, second generation FRP bridge deck component is evaluated for local web buckling. The induced stress due to axial, bending and shear should be less than the allowable stress in the FRP wall. The failure load of a second generation FRP bridge deck component of 108" span length under three-point bending with a patch load (10" x 20") was 67 kips. The bending, axial and shear stress under failure load of 67 kips are computed as follows:

Computation of bending moment:

The failure load is 67 kips over a patch load of 20" (perpendicular to traffic direction) x 10" (parallel to traffic direction) as shown in the Figure 5.7.

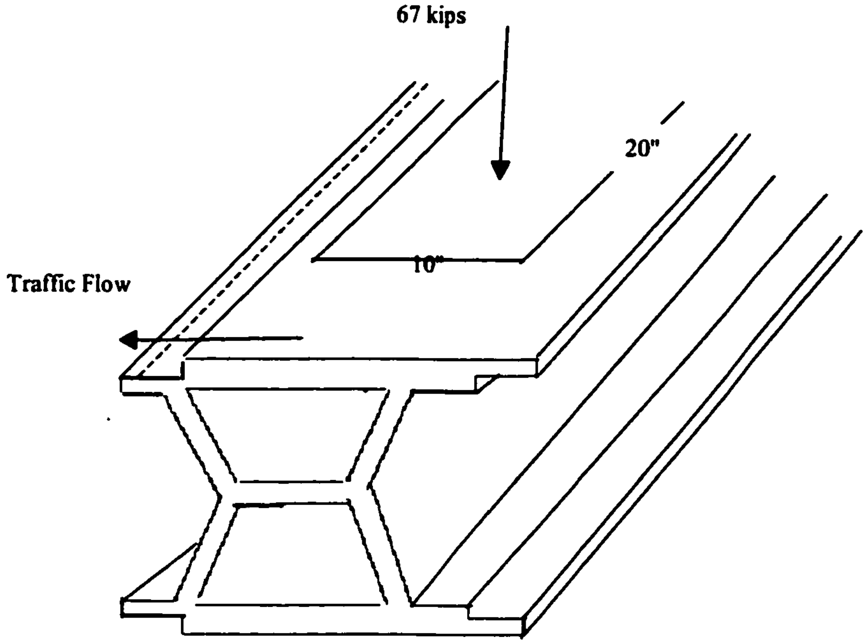

Figure 5.7 Patch load on FRP Bridge Deck Component

Assuming the load is effective over a length of 24" (20" + 2" of additional load distribution length on each side of the load point), along the direction perpendicular to traffic,

Load acting along the FRP deck component length (parallel to traffic) is:

$$W = \frac{67}{24} = 2.79 kips$$

Hence, total load acting along the FRP deck component length over a width of one inch (along the direction perpendicular to traffic) is 2.79 kips (Figure 5.8)

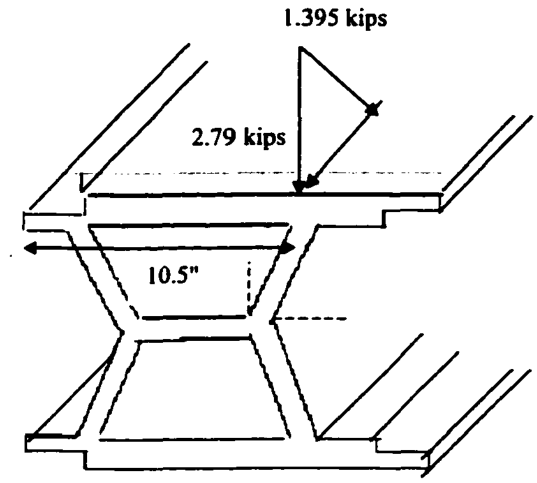

Figure 5.8 Loads Acting on the Web of Second Generation FRP Bridge Deck Component

Load acting per unit length = $\frac{W}{L} = \frac{2.79}{8} \approx 0.35 kip/in$ (where L = 8" is the distance between two webs)

Assuming fixed boundary conditions between web and flange, bending moment acting at the flange-web junction = $\frac{wL^2}{12} = \frac{(0.35 \times 8 \times 8)}{12} = 1.87 kip-in$

The bending moment acting at the web-flange junction is distributed in proportion to flange and web stiffness.

Therefore, total bending moment acting on the web is

$$M = \left(\frac{E_w}{E_f + E_w}\right) \times 1.87$$

$E_f = 1.73 \times 10^6$ psi;

$Ew = 2.62 \times 10^6$ psi (Appendix C)

Therefore,

$$M = \frac{2.62 \times 10^6}{1.73 \times 10^6 + 2.62 \times 10^6} \times 1.87 = 1.126 kips - in$$

Computation of axial and shear load:

Reaction on the web = $\frac{W}{2} = \frac{2.79}{2} = 1.395 kips$

Resolving the force 1.395 kips into force components parallel and perpendicular to the web, the parallel and perpendicular force components are:

Axial load on web (parallel component) = 1.395 x cos30^0 = 1.208 kips

Shear load on web (perpendicular component) = 1.395 x sin30^0 = 0.697 kips

The goal is to check the adequacy of web thickness (t_w = 0.4") of second generation FRP bridge deck component to resist shear, axial, and bending loads.

Hence, the following checks are carried out.

Check for bending stress:

Induced bending stress < Critical bending stress

Induced bending stress $= \sigma_{ib} = \frac{Mc}{I}$

Where, M = Bending moment acting on the web = 1.126 kip-in

c = thickness of web/2 = $\frac{0.4}{2} = 0.2in$

I = Moment of inertia = $\frac{bt_w^3}{12} = \frac{1 \times 0.4^3}{12} = 0.0053in^4$

Induced bending stress = $\frac{1.126 \times 1000 \times 0.2}{0.0053} = 42{,}490 psi$

Critical bending stress $= \sigma_{cb} = \varepsilon_b E_w$

Where ε_b is bending strain = 18,000 to 23,000 microstrain (Based on experimental test results)

E_w is bending stiffness of web = 2.62 x 10^6 psi (Based on fiber volume fraction of 25% ~ 30% in the transverse direction)

Therefore , $\sigma_{cb} = 18000 \times 10^{-6} \times 2.62 \times 10^{-6} = 47{,}160\ psi$

Induced bending stress < Critical bending stress (safe)

Check for shear stress:

Induced shear stress < Critical shear stress

Induced shear stress = $\tau_i = \frac{1.5V}{bt_w}$ (for a rectangular section)

Where V is shear load = 0.697 kips (as computed above)

Induced shear stress $= \tau_i = \frac{1.5 \times 0.697 \times 1000}{1 \times 0.4} = 2{,}614 psi$

Critical shear stress $= \tau_c = \varepsilon_s G_w$

Where ε_s is the shear strain

G_w is shear modulus = 0.849e+06 (Appendix B)

The ultimate shear strain is about 20,000 microstrain, (Wen, 1999), but the strain does not increase linearly, i.e., the shear stress versus shear strain curve for a GFRP composite sample is nonlinear. Hence taking the average strain value of about 10000 mircrostrain,

Critical shear stress = $\tau_c = 10000 \times 10^{-6} \times 0.849 \times 10^{-6} = 8{,}490 psi$

Induced shear stress < Critical shear stress (safe)

Check for axial stress:

Induced axial stress < Critical axial stress

Induced axial stress $= \sigma_{ia} = \dfrac{P}{A}$

Where, P = axial load = 1.208 kips (as computed above)

A = cross sectional area of the web = 0.4 in^2

Induced axial stress $= \sigma_{ia} = \dfrac{1.208 \times 1000}{0.4} = 3{,}020 psi$

Critical axial stress = $\sigma_{ca} = \dfrac{k\pi^2 E_w}{12(1-\nu^2)}\left(\dfrac{t_w}{a}\right)^2$ (Structural Plastic Design Manual, 1984)

Where $\nu = 0.35$

a = depth of web = d_w = 3.87 in

k ranges from 1.0 to 1.5

Assuming pinned ends, k = 1.5

Therefore, critical stress $= \sigma_{ca} = \dfrac{1.5 \times \pi^2 \times 2.62 \times 10^{-6}}{12(1-0.35^2)} \times \left(\dfrac{0.4}{3.87}\right)^2 = 39{,}351 psi$

Induced axial stress < Critical axial stress (safe)

Interaction equation check:

Assuming the interaction equation for combined bending, shear and axial are same as that for steel:

$$\left(\frac{\sigma_{ib}}{\sigma_{cb}}\right)^2 + \left(\frac{\tau_i}{\tau_c}\right)^2 + \left(\frac{\sigma_{ia}}{\sigma_{ca}}\right) \leq 1 \qquad \text{(Johnston, 1976)}$$

$$\left(\frac{42490}{47160}\right)^2 + \left(\frac{2614}{8490}\right)^2 + \left(\frac{3020}{39351}\right) = 0.98 < 1$$

Hence, the web is safe to resist local buckling, under 67 kips load for the proposed fiber architecture. It should be noted that the interaction equations are well established for steel structures. Since we do not have enough experimental data for the combined effect of axial, bending and shear stresses on composite structures, the interaction equation for composite in the current design is considered to be same as that of steel.

5.7 Conclusions

- Theoretical stiffness of second generation FRP bridge deck component has been predicted by Approximate Classical Lamination Theory (ACLT).
- The weight of second generation FRP bridge deck component has been reduced by 11% compared to first generation FRP bridge deck component.
- Adhesive bond length of second generation FRP bridge deck component has been reduced by 83% compared to first generation FRP bridge deck.
- The overall cost of second generation FRP bridge deck component has been reduced because of weight reduction and bond length reduction.
- Modified fiber architecture has enhanced the structural properties of the deck component.
- The shear stiffness of the second generation FRP bridge deck component is 1.4 times that of first generation deck component.

- Second generation FRP bridge deck component is safe against local buckling in the web for an ultimate load of 67 kips.

CHAPTER 6

SUMMARY, CONCLUSIONS AND RECOMMENDATIONS

The following sections describes the summary, conclusion and recommendations on the current work.

6.1 Summary

3-D stitched fabrics were produced by machine stitching and were used to manufacture laminate composites. Composites with 3-D stitched fabrics, having different fiber architecture, stitch density, stitch material and manufacturing process (SCRIMP and pultrusion) were fabricated and examined. Tension, bending and short-beam shear tests were carried out on composites reinforced with 3-D stitched fabrics at coupon level to compute laminate properties. Strength and stiffness of composites with respect to manufacturing process (SCRIMP and pultrusion), fiber architecture, stitch material and stitch density were evaluated. With respect to manufacturing process, pultruded specimens were stiffer and stronger than SCRIMP specimens because during manufacturing process, SCRIMP specimens undergo low curing temperature, improper wet-out improper resin absorption. With respect to stitch density, specimens with stitch density 7 and 3.5 had more or less same strength. Failure modes of SCRIMP and pultruded specimens under tension, bending and shear loads were also observed. Under bending loads, pultruded specimens failed less catastrophically than SCRIMP specimens.

Laminae properties were also computed based on the rule of mixtures, and Halpin-Tsai equations were incorporated into Classical Lamination Theory (CLT) to compute the laminate properties. The experimental results were about 20% less than theoretical results, which may be due to handling errors while conducting the experiments.

The structural properties of composites with 3-D stitched fabrics were compared with that of 2-D stitched fabrics. There was about 30% ~ 40% enhancement in the structural property (strength) of composites with 3-D stitched fabrics compared to that of 2-D fabrics.

The existing FRP bridge deck component (first generation FRP bridge deck component) was optimized with respect to fiber architecture and weight resulting in second generation FRP bridge deck component. Global stiffness of the second generation FRP bridge deck component was computed both experimentally (three point bending test) and theoretically (Approximate Classical Lamination Theory (ACLT)) and compared with that of first generation FRP bridge deck component. The stiffness of second generation FRP bridge deck component with reduced weight, was approximately same as that first generation FRP bridge deck component.

6.2 Conclusions

The structural properties of composites with 3-D stitched fabrics are greatly affected by fiber architecture, stitch density, stitch material, and manufacturing process which are discussed in the current section. The failure modes of composite with 3-D stitched fabrics are also established.

Effect of Fiber Architecture

- Composites with bi-axial fabrics were approximately 30 ~ 40% stronger than composites with quadraxial fabrics because there was less contribution from $\pm 45^0$ oriented fibers, in quadraxial fabrics, towards the overall strength of composite.
- There was no significant difference in strength and stiffness of composites that had two layers of biaxial/quadraxial fabrics compared when to the properties of four layers of biaxial/quadraxial fabrics. This was attributed to 100% increase in thickness and load resistance, in composites with four layers of biaxial/quadraxial fabrics over composites with two layers of bi-axial/quadraxial fabrics.

Effect of Stitch Material and Stitch Density

- The ultimate bending stresses of specimens that were stitched at Johnston Industries Inc., and WVU, were only 60% of the specimens stitched at Johnston Industries Inc.. This was attributed to high stress concentrations due to needle punch in specimens that were further stitched at WVU.
- There was no significant increase in strength for specimens with a stitch density of 7 from those with a stitch density of 3.5. The specimens with a stitch density of 7, were stitched with alternate of glass and yarn, while the specimens with a stitch density of 3.5 were stitched only with glass which eventually indicated that there was no significant contribution of strength from the yarn thread.

Effect of Manufacturing Process

- Strength and stiffness of SCRIMP specimens were 50% of pultruded specimens because of major drawbacks in SCRIMP process such as lack of resin absorption, improper wet-out, and low curing temperature.
- Pultruded specimens from Creative Pultrusions Inc., were about 20% lower in strength than specimens from Reichhold Industries Inc. This may be attributed to low curing temperature, inadequate wet-out at Creative Pultrusions Inc.

Failure Modes

- Failure in pultruded specimens was less catastrophic than failure in SCRIMP specimens.
- Failure was initiated at the interface of outer ply and core (i.e. matrix) due to differential strain developed in outer ply and core in the pultruded specimens.
- Under bending loads, SCRIMP specimens were observed to fail approximately at 20000 microstrain and the failure was mostly of delamination type.

Composites with 3-D Stitched Fabrics Versus 2-D Stitched Fabrics

- Composite with 3-D stitched fabrics had about 30% ~ 40% property enhancement (strength) over composites with 2-D stitched fabrics.
- Ultimate stress of composite with 3-D stitched fabrics (75 ~80 ksi) were 95% more than that of conventional material (steel) (40 ksi).

Comparison Between Theoretical and Experimental results

- Classical Lamination Theory (CLT) was used to compute laminate properties at coupon level. There was good correlation between theoretical and experimental test results.
- Theoretical results (tensile modulus, bending modulus and ultimate stress) were about 20% higher than experimental test results.

Second Generation FRP Bridge Deck Component

- Modified fiber architecture enhanced the structural properties at component level in second generation FRP bridge deck component.
- The weight of second generation FRP bridge deck component reduced by 11% compared to first generation FRP bridge deck component.
- The volume of adhesive used in second generation FRP bridge deck component reduced to 83% compared to first generation FRP bridge deck component.
- Approximate Classical Lamination Theory (ACLT) was used to compute bending stiffness in second generation FRP bridge deck component. The stiffness of second generation FRP bridge deck component was almost same as that first generation FRP bridge deck component.
- The web of second generation FRP bridge deck module was found to be safe against local buckling. The web was checked for a combined effect of bending, in-plane shear and axial load.

6.3 Recommendations

- In composite with 3-D stitched fabrics, the failure was initiated at the interface of outer ply and core, due to differential strain. The differential strain was attributed to mismatch in stiffness between the core and outer plies. Hence, fiber architecture for the composite with 3-D fabrics may be improved by maintaining same stiffness between core and outer plies.
- Bi-axial, Tri-axial and rovings were used in the flanges and webs of second generation FRP bridge deck component. The fiber architecture in the flanges and webs can further be improved by stitching all fabrics (bi-axial, tri-axial and rovings) through-the thickness direction. The stitching of fabrics can be done on-line, before the fabrics/fibers pass into the die in pultrusion process or the fabrics can be stapled with plastic staples using a stapler gun.
- The second generation FRP bridge deck component can be further optimized with respect to thickness and fiber architecture provided on-line stitching is adopted. Further the second generation FRP bridge deck module has to be tested under fatigue loads.
- Pultruding three components together as one piece will reduce production and installation costs and will enhance properties further as the number of joints are reduced.
- All conventional failure stress theories (maximum stress theory, Tsai-Hill failure theory, Tsai-Wu failure theory etc) were developed based on uni-directional fibers, which is not applicable to predict failure in composites with bi-axial or tri-axial fabrics. Hence, a new failure theory has to be developed based on fabrics.

BIBLIOGRAPHY

Adnaur, S. and Yen P. Tsao (1994) "Stitch Bonded Textile Structural Composites," 26th International SAMPE Technical Conference, October 17-20, pp 25 - 35.

Antonia Miravete (1999), "3-D Textile Reinforcements in Composite Materials," Woodhead Publishing Limited, pp 1- 40.

ASTM D 3039/3039 M -95, "Standard Test Method for Tensile Properties of Polymer Matrix Composite Materials," pp 114 - 123.

ASTM D 2344- 84, "Standard Test Method for Apparent Interlaminar Shear Strength of Parallel Fiber Composites by Short-Beam Method," pp 15 - 17.

ASTM D 790 -86, "Standard Test Method for Flexural Properties of Unreinforced and Reinforced Plastics and Electrical Materials," pp 296 - 305.

Barbero, E.J. (1998), " Introduction to Composite Materials Design," Taylor & Francis Inc.

Bathegate R.G., Wang, C.H., Feiyi Pang (1997), "Effects Of Temperature On the Creep Behaviour Of Woven and Stitched Composites," Composite Structures Proceedings, 9th

International Conference on Composite Structures, September, Vol. 38, No.1-4, pp 435 - 445.

Cholakara, M.T., Jang, B.Z., and Wang, C.Z. (1989), "Deformation and Failure Mechanisms in 3-D composites," In Proceedings of 34th Int. SAMPE Conf. pp 2153-2160

Chung, W.C., (1987), "Fracture Behavior in Multidimensional Fiber Reinforced Composties," Ph.D Dissertation, Auburn University, AL.

Doyle, J.R. (1991), "Behavior of Bolt and Adhesive Connections in Fiber Reinforced Members," M.S Thesis, Department of Civil and Environmental Engineering, West Virginia University, Morgantown, WV 26506, USA.

GangaRao, H.V.S., Sotiropoulos, S.N. (1993), "Review of Connectors for FRP Members," Research Report CFC-93-152, Constructed Facilities Center, West Virginia University, Morgantown, WV 26506, USA, pp 31

GangaRao, H.V.S et.al. (1999), "Development of Glass Fiber Reinforced Polymer Composite Bridge Deck," SAMPE Journal, Vol.35, No.4, pp 12 - 24.

Hinrichs., PalmerR.et.al. (Personal correspondence) "Mechanical Property Evaluations of Stitched/RFI Composites," NASA Langley Research Center (IABSE), pp 1- 20.

Israel H., Bannister, Michael K. (1993), "Tensile Properties of Thin Stitched Carbon/Epoxy Composites," Proceedings of the 5th Australian Aeronautical Conference, September 13-15, Vol.1, No. 93, pp 213 - 218.

James M. Whitney (1987), " Structural Analysis of Laminated Anisotropic Plates," Technomic Publishing Co. Inc.

John L. Clarke (1996), " Structural Design of Polymer Composite," EUROCOMP Design Code and Handbook, E & FN Spon Publishing Co.

Johnston B.G., (1976). " Guide to Stability Design Criteria for Metal Structures," Structural Stability Research Council, 3rd Edition, Wiley, New York, pp.198.

Jones R.M., (1975), "Mechanics of Composite Materials," Hemisphere Publishing Co.

Kim R.Y. (1983), "Proceedings of 28th National SAMPE Symposium," Vol. 28, Azusa, CA, pp. 200-209.

Lopez-Anido, R. (1995), "Analysis and Design of Orthotropic Plates Stiffened by Laminated Beams for Bridge Superstructures," Ph.D. Dissertation submitted in partial fulfillment of degree of Doctor of Philosophy, Department of Civil and Environmental Engineering, West Virginia University, Morgantown, WV 26506, USA.

Mouritz. A.P., Gallagher. J. Goodwin.A.A. (1997), "Flexural Strength And Interlaminar Shear Strength Of Stitched GRP Laminates Following Repeated Impacts," Composites Science and Technology, Vol. 57, No. 5, pp 509 - 522.

Nagraj, V. (1994), "Static and Fatigue Response of Pultruded FRP Beams Without and With Splice Connections," M.S. Thesis, Department of Civil and Environmental Engineering, West Virginia University, Morgantown, WV 26506, USA.

Nikki Overby (1998), M.S. Thesis, Department of Civil and Environmental Engineering, West Virginia University, Morgantown, WV 26506, USA.

Quio P., Davalos J.F., Barberi E.J., Troutman D. (1999), "Step-by-Step Engineering Equations for FRP Structural Beams, ICE'99, Cincinnati, OH, pp. 10-12.

Sonti S.S., and Barbero, E.J. (1992), "Stress Analysis of Pultruded FRP Structural Shapes," Report CFC-92-TR138. Constructed Facilities Center, West Virginia University Morgantown, WV 26506, USA.

Sonti S.S. (1997), "Evaluation of Joint Efficiency and Performance of Multi-Cellular Deck Panel," M.S Thesis, Department of Civil and Environmental Engineering, West Virginia University, Morgantown, WV 26506, USA.

Sotiropoulos, S.N. (1991), "Static Response of Bridge Superstructures Made of FRP Reinforced Plastic, M.S. Thesis, Department of Civil and Environmental Engineering, West Virginia University, Morgantown, WV 26506, USA.

Sotiropoulos, S.N. (1995), "Performance of FRP Component and Connection for Bridge Deck Systems," Ph.D. Dessertation, Department of Civil and Environmental Engineering, West Virginia University, Morgantown, WV 26506, USA.

"Structural Plastics Design Manual", (1984), American Society of Civil Engineers, NewYork.

Vedam, V.R. (1997), "Characterization of Composite Material Bridge," M.S. Thesis, Department of Civil and Environmental Engineering, West Virginia University, Morgantown, WV 26506, USA.

Wen (1999), "Compressive Strength Prediction for Composite Unmanned Aerial Vehicles," M.S. Thesis, Department of Civil and Environmental Engineering, West Virginia University, Morgantown, WV 26506, USA. pp108 - 110.

Wu, E. and Wang, J., (1994), "Behavior of Stitched Laminates Under In-Plane Tensile and Transverse Impact Loading," Journal Of Composite Materials, Vol. 29, No. 17.

APPENDIX A

THEORETICAL PREDICTION OF STIFFNESS IN 3-D COMPOSITE LAMINATES

Composite with 3-D stitched fabrics have fiber architecture as shown in Fig A.1

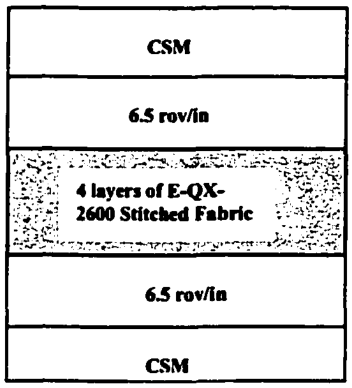

Figure A.1 Fiber Architecture of 3-D Composite Laminate

The composite with 3-D stitched fabrics is analyzed using micromechanics and macromechanics principles. Classical Lamination Theory (CLT) is used to evaluate axial and bending stiffness of composite laminate. The stitched fabric in 3-D composite is considered like an equivalent isotropic material. (Refer step 6). The following equations are used for computing the axial and bending stiffness of composite laminate.

Step 1: Compute Material Properties

The material properties include modulus of elasticity, shear modulus and density of fiber and matrix. These properties are usually given by the manufacturer. From the above properties, one can compute Poisson's ratio for fiber and matrix. In the current problem, the material properties are considered as follows:

Modulus of elasticity of fiber = E_f (psi) = 1.05E+07

Modulus of elasticity of Matrix = E_m (psi) = 7.34e+05

Shear modulus of fiber = G_f (psi) = 4.18e+06

Poisson's ratio of fiber = $\nu_f = \frac{E_f}{2G_f} - 1 = 0.26$ Poisson's ratio of matrix = $\nu_m = \frac{E_m}{2G_m} - 1 = 0.55$

Step 2: Compute Fiber Volume Fraction

Fiber volume fraction (V_f) for each laminae present in the composite is calculated. The 3-D composite consist of CSM (Chopped Strand Mat), rovings and 3-D stitched fabric (E-QX-2600 5). Stitched fabric has four layer of 26 oz/yd^2 stitched through the thickness direction. Each of 26 oz/yd^2 mat has 6.5 oz/yd^2 at 0^0 , 6.5 oz/yd^2 at 45^0, 6.5 oz/yd^2 at 90^0, and 6.5 oz/yd^2 at-45^0.

For Rovings

$$\mathrm{v}_f = \frac{n\pi D^2}{4bt}$$

Where

n= number of rovings

b = width of laminae (in)

t= thickness of roving layer (in)

D = Diameter of fiber = $\sqrt{\frac{1}{\rho_f \mathrm{Y} 9\pi}}$

ρ_f is density of fiber (lb/in^3) and

Y = yield

For CSM and Fabric

$$v_f = \frac{W_f}{\rho_f L_v}$$

Where

W_f = Weight of fiber (lb)

L_v = Volume of 1ft x 1ft of lamina

Step 3: Evaluate Lamina Properties

Stiffness properties of laminae are computed by rule of mixture, which relates the properties of fabric and matrix to the unit composite ply.

For Fabric and Rovings

Longitudinal Modulus (psi): $E_{11} = E_f V_f + E_m(1 - V_f)$ (A.1)

Poisson's Ratio : $\nu_{12} = \nu_f V_f + \nu_m(1 - V_m)$ $\nu_{21} = \frac{\nu_{12} E_{22}}{E_{11}}$ (A 2)

Transverse Modulus (psi): $E_{22} = \frac{E_f E_m}{E_f V_m + E_m V_f}$ (A 3)

Shear Modulus (psi): $G_{12} = \frac{G_f G_m}{G_f V_m + G_m V_f}$ (A. 4)

For CSM (Chopped Strand Mat)

Elastic Modulus of CSM (psi): $$E_{ran} = \frac{3}{8}E_{11} + \frac{5}{8}E_{22} \qquad \text{(A.5)}$$

Shear Modulus of CSM (psi): $$G_{ran} = \frac{1}{8}E_{11} + \frac{1}{4}E_{22} \qquad \text{(A.6)}$$

Poisson's Ratio of CSM (psi): $$\nu_{ran} = \left(\frac{E_{ran}}{2G_{ran}}\right) - 1 \qquad \text{(A.7)}$$

Step 4: Calculate In-Plane Reduced Stiffness Matrix (Q)

For Rovings and Fabric

$$Q_{11} = \frac{E_{11}}{\delta}$$

$$Q_{12} = \frac{\nu_{12}E_{22}}{\delta}$$

$$Q_{22} = \frac{E_{22}}{\delta}$$

$$Q_{66} = G_{12}$$

$$\delta = 1 - \nu_{12}\nu_{21} \qquad \text{(A.8)}$$

For CSM (Chopped Strand Mat)

$$Q_{11} = Q_{22} = \frac{E_{ran}}{\delta}$$

$$Q_{12} = \frac{\nu_{ran}E_{ran}}{\delta}$$

$$Q_{66} = G_{ran} \qquad \text{(A.9)}$$

Step 5: Calculate Transformed Reduced Stiffness Matrix $[\bar{Q}]$

$$\bar{Q}_{11} = Q_{11}\cos^4\theta + 2(Q_{12} + 2Q_{66})\sin^2\theta\cos^2\theta + Q_{22}\sin^4\theta$$

$$\bar{Q}_{12} = (Q_{11} + Q_{22} - 4Q_{66})\sin^2\theta\cos^2\theta + Q_{12}(\sin^4\theta + \cos^4\theta)$$

$$\bar{Q}_{22} = Q_{11}\sin^4\theta + 2(Q_{12} + 2Q_{66})\sin^2\theta\cos^2\theta + Q_{22}\cos^4\theta$$

$$\bar{Q}_{16} = (Q_{11} - Q_{12} - 2Q_{66})\sin\theta\cos^3\theta + (Q_{12} - Q_{22} + 2Q_{66})\sin^3\theta\cos\theta$$

$$\bar{Q}_{26} = (Q_{11} - Q_{12} - 2Q_{66})\sin\theta^3\cos\theta + (Q_{12} - Q_{22} + 2Q_{66})\sin\theta\cos^3\theta$$

$$\bar{Q}_{66} = (Q_{11} + Q_{22} - 2Q_{12} - 2Q_{66})\sin^2\theta\cos^2\theta + Q_{66}(\sin^4\theta + \cos^4\theta)$$

(A.10)

For CSM and rovings and $[\bar{Q}]$ matrix is same as [Q] matrix. The stitched fabric (104 oz consist of fibers oriented in 0^0, 45^0, 90^0 and -45^0. Therefore transformed reduced stiffness matrices is to be found for the fibers oriented in 0^0, 45^0, 90^0 and -45^0.

Step 6: Compute the Final $[\bar{Q}]$ Matrix

Here the final $[\bar{Q}]$ remains same for CSM and Rovings as computed in step 5. The stitched fabric (ie 104 oz/yd^2) has totally 26 oz/yd^2 at 0^0, 26 oz/yd^2 at 45^0, 26 oz/yd^2 at 90^0, and 26 oz/yd^2 at -45^0. As we already know the $[\bar{Q}]$ for the 0^0, 45^0, 90^0, and -45^0 separately as computed in step 5, for the stitched fabric, the contribution of each fiber orientation to the final $[\bar{Q}]$ is proportional to its weight. Therefore final $[\bar{Q}]$ matrix for stitched fabric will be:

$$[\bar{Q}]_{\text{stitched fabric}} = 1/4\{[\bar{Q}]_0 + [\bar{Q}]_{45} + [\bar{Q}]_{90} + [\bar{Q}]_{-45}\} \quad \text{(A.11)}$$

Here the stitched fabric is now no more treated like an orthotropic layer, but it is considered like an isotropic layer.

Step 7: Compute the Stiffness Matrix

Laminate properties can be computed using extensional stiffness matrix [A], coupling stiffness matrix [B], and bending stiffness matrix [D]. The [A] matrix, [B] matix, and [D] matrix are developed by incorporating the lamina properties into the lamination theory. The stiffness are calculated as follows:

$$A_{ij} = \sum_{n=1}^{N} \left(Q_{ij}\right) t_n$$

$$D_{ij} = \sum_{n=1}^{N} \left(Q_{ij}\right)_n \cdot \left(t_n . z_n^2 + \frac{t_n^3}{12}\right)$$

$$B_{ij} = \sum_{n=1}^{N} \left(Q_{ij}\right)_n . t_n . z_n \qquad \text{(A.13)}$$

Step 8: Compute Laminate Modulus

Tension Modulus

$$E_x^t = \frac{A_{11}A_{22} - A_{12}^2}{tA_{22}} \qquad \text{(A.14)}$$

Bending Modulus

$$E_x^b = \frac{12\left(D_{11}D_{22} - D_{22}^2\right)}{t^3 D_{22}} \qquad \text{(A.15)}$$

Step 9: Compute Axial Stiffness and Bending Stiffness

Axial Stiffness = $E_x^t A$

Bending Stiffness = $E_x^b I$

Where,

A = cross sectional area of the composite laminate

And I = Moment of Inertia of the composite laminate

The computation of axial and bending modulus of 3-D stitched laminate as per the above procedure using a spread sheet program is shown in the next section.

Computation of Laminate Moduli for E-QX-2600 5 (Pultruded)					
Micromechanic and Macromechanic Approach					
Section	**Rectangular strip**				
Dimension	**1" x 0.25"**				
Fiber Architecture					
1 oz of CSM					
62Y of 6.5 rov/in.					
E-QX-2600 5					
62Y of 6.5 rov/in.					
1 oz of CSM					
Step 1					
Computation of Material Properties					
E_{fiber}	E_{matrix}	G_{fiber}	G_{matrix}	ν_{fiber}	ν_{matrix}
(psi)	**(psi)**	**(psi)**	**(psi)**		
1.05E+07	7.34E+05	4.18E+06	2.37E+05	0.26	0.55
Step 2					
Computation of Fiber Volume Fraction (V_f) of CSM					
Thk of lamina	**Wt. Of Fabric**	**Wt. Of Fabric**	**Wt.of 1ft^2**	**Density of**	
(in.)	**(oz/yd2)**	**(oz/ft2)**	**(lb)**	**(lb/in3)**	
0.015	9	1.000	0.063	0.092	
Volume of	**Volume of**	**Fiber Volume**	**Matrix Volume**		
fiber	**composite**	**fraction (Vf)**	**fraction (Vm)**		
0.679	2.16	0.31	0.69		
Computation of Fiber Volume Fraction (V_f) of Fabric					
Thk of lamina	**Wt. Of Fabric**	**Wt. Of Fabric**	**Wt.of 1ft^2**	**Density of**	
(in.)	**(oz/yd2)**	**(oz/ft2)**	**(lb)**	**(lb/in3)**	
0.107	104	11.556	0.722	0.092	
Volume of	**Volume of**	**Fiber Volume**	**Matrix Volume**		
fiber	**composite**	**fraction**	**fraction**		
7.850	15.408	0.51	0.49		

Computation of Fiber Volume Fraction (V_f) of Rovings					
Rovings	**thickness**	**Yield**	**diameter**	**width**	
	(in)	**yards**	**(in)**	**(in)**	
62Y of 6.5 rov/in.	0.054	62	0.079	1	
bundles	**Fiber Volume**	**Matrix Volume**			
(no:)	**Fraction (V_f)**	**Fraction (V_m)**			
6.5	0.59	0.41			
Step 3					
Evaluation of Laminae Properties					
Fiber	E_{11}	E_{22}	G_{12}	v_{12}	v_{21}
1 oz of csm	3.81E+06	1.04E+06			
104 oz of fabric	5.71E+06	1.40E+06	4.56E+05	0.399	0.098
62Y of 6.5 rov/in.	6.46E+06	1.61E+06	5.30E+05	0.377	0.094
Fiber	E_{11}	E_{22}	G_{12}	v_{12}	v_{21}
1 oz of csm	2.08E+06	2.08E+06	7.35E+05	0.412	0.412
104 oz of fabric	5.71E+06	1.40E+06	4.56E+05	0.399	0.098
62Y of 6.5 rov/in.	6.46E+06	1.61E+06	5.30E+05	0.377	0.094
Step 4					
Caluculation of In-Plane Reduced Stiffness Matrix					
Fiber Architecture	δ				
1 oz of CSM	0.830				
62Y of 6.5 rov/in.	0.964				
104 oz of fabric	0.961				
62Y of 6.5 rov/in.	0.964				
1 oz of CSM	0.830				
Fiber Architecture	Q_{11}	Q_{12}	Q_{21}	Q_{22}	Q_{66}
1 oz of CSM	2.50E+06	1.03E+06	1.03E+06	2.50E+06	7.35E+05
62Y of 6.5 rov/in.	6.70E+06	6.31E+05	6.31E+05	1.67E+06	5.30E+05
104 oz of fabric	5.94E+06	5.80E+05	5.80E+05	1.45E+06	4.56E+05
62Y of 6.5 rov/in.	6.70E+06	6.31E+05	6.31E+05	1.67E+06	5.30E+05
1 oz of CSM	2.50E+06	1.03E+06	1.03E+06	2.50E+06	7.35E+05

Step 5				
Calculation of Transformed Reduced Stiffness Matrix				
Fiber Architecture	**Orient. of fabric (degrees)**	**Orient. of fabric (Radians)**		
1 oz of CSM	0	0.00		
62Y of 6.5 rov/in.	0	0.00		
104 oz of fabric has fibers oriented in 0^0, 45^0, 90^0, and -45^0				
	0	0.00		
	45	0.79		
	90	1.57		
	-45	-0.79		
Fiber Architecture	Q_{b11}	Q_{b12}	Q_{b21}	
1 oz of CSM	2.50E+06	1.03E+06	1.03E+06	
62Y of 6.5 rov/in.	6.70E+06	6.31E+05	6.31E+05	
104 oz of fabric has fibers oriented in 0^0, 45^0, 90^0, and -45^0				
0	5.94E+06	5.80E+05	5.80E+05	
45	2.59E+06	1.68E+06	1.68E+06	
90	1.45E+06	5.80E+05	5.80E+05	
-45	2.59E+06	1.68E+06	1.68E+06	
Fiber Architecture	Q_{b22}	Q_{b16}	Q_{b26}	Q_{b66}
1 oz of CSM	2.50E+06	0.00E+00	0.00E+00	7.35E+05
62Y of 6.5 rov/in.	1.67E+06	0.00E+00	0.00E+00	5.30E+05
104 oz of fabric has fibers oriented in 0^0, 45^0, 90^0, and -45^0				
0	1.45E+06	0.00E+00	0.00E+00	4.56E+05
45	2.59E+06	1.12E+06	1.12E+06	1.56E+06
90	5.94E+06	2.50E-12	2.73E-10	4.56E+05
-45	2.59E+06	-1.12E+06	-1.12E+06	1.56E+06

Step 6					
Computation of Final Trasformed Stiffness Matrix					
1/4(Q_b of 0^0 + Q_b of 45^0 + Q_b of 90^0 + Q_b of -45^0)					
Fiber Architecture	**Q_{b11}**	**Q_{b12}**	**Q_{b21}**		
1 oz of CSM	2.50E+06	1.03E+06	1.03E+06		
62Y of 6.5 rov/in.	6.70E+06	6.31E+05	6.31E+05		
104 oz of fabric	3.15E+06	1.13E+06	1.13E+06		
62Y of 6.5 rov/in.	6.70E+06	6.31E+05	6.31E+05		
1 oz of CSM	2.50E+06	1.03E+06	1.03E+06		
	2.15E+07	**4.45E+06**	**4.45E+06**		
Fiber Architecture	**Q_{b22}**	**Q_{b16}**	**Q_{b26}**	**Q_{b66}**	
1 oz of CSM	2.50E+06	0.00E+00	0.00E+00	7.35E+05	
62Y of 6.5 rov/in.	1.67E+06	0.00E+00	0.00E+00	5.30E+05	
104 oz of fabric	3.15E+06	0.00E+00	5.82E-11	1.01E+06	
62Y of 6.5 rov/in.	1.67E+06	0.00E+00	0.00E+00	5.30E+05	
1 oz of CSM	2.50E+06	0.00E+00	0.00E+00	7.35E+05	
	1.15E+07	**0.00E+00**	**5.82E-11**	**3.54E+06**	
Step 7					
Computation of Stiffness Matrix					
Distance from mid-surface of lamiante to each laminae (z)					
Fiber Architecture	**z (in)**				
1 oz of CSM	-0.1150				
62Y of 6.5 rov/in.	-0.0805				
104 oz fabric	0.000				
62Y of 6.5 rov/in.	0.0805				
1 oz of CSM	0.1150				
Computation of extensional stiffness					
Fiber architecture	**Thk.of lamiane**	**A_{11}**	**A_{12}**	**A_{21}**	
	(in)	**(lbs/in)**	**(lbs/in)**	**(lbs/in)**	
1 oz of CSM	0.015	3.75E+04	1.54E+04	1.54E+04	
62Y of 6.5 rov/in.	0.054	3.62E+05	3.41E+04	3.41E+04	
104 oz fabric	0.107	3.37E+05	1.21E+05	1.21E+05	
62Y of 6.5 rov/in.	0.054	3.62E+05	3.41E+04	3.41E+04	
1 oz of CSM	0.015	3.75E+04	1.54E+04	1.54E+04	
		1.13E+06	**2.20E+05**	**2.20E+05**	

Fiber architecture	A_{22}	A_{16}	A_{26}	A_{66}	
	(lbs/in)	(lbs/in)	(lbs/in)	(lbs/in)	
1 oz of CSM	3.75E+04	0.00E+00	0.00E+00	1.10E+04	
62Y of 6.5 rov/in.	9.04E+04	0.00E+00	0.00E+00	2.86E+04	
104 oz of fabric	3.37E+05	0.00E+00	6.23E-12	1.08E+05	
62Y of 6.5 rov/in.	9.04E+04	0.00E+00	0.00E+00	2.86E+04	
1 oz of CSM	3.75E+04	0.00E+00	0.00E+00	1.10E+04	
	5.92E+05	**0.00E+00**	**6.23E-12**	**1.87E+05**	
Computation of bending-extension coupling stiffness					
Fiber architecture	**Thk.of lamiane**	**Z**	B_{11}	B_{12}	B_{21}
	(in)	(in)	(lbs)	(lbs)	(lbs)
1 oz of CSM	0.015	-0.1150	-4.31E+03	-1.78E+03	-1.78E+03
62Y of 6.5 rov/in.	0.054	-0.0805	-2.91E+04	-2.74E+03	-2.74E+03
104 oz fabric	0.112	0.0000	0.00E+00	0.00E+00	0.00E+00
62Y of 6.5 rov/in.	0.054	0.0805	2.91E+04	2.74E+03	2.74E+03
1 oz of CSM	0.015	0.1150	4.31E+03	1.78E+03	1.78E+03
			0.00E+00	**0.00E+00**	**0.00E+00**
Fiber architecture	B_{22}	B_{16}	B_{26}	B_{66}	
	(lbs)	(lbs)	(lbs)	(lbs)	
1 oz of CSM	-4.31E+03	0.00E+00	0.00E+00	-1.27E+03	
62Y of 6.5 rov/in.	-7.27E+03	0.00E+00	0.00E+00	-2.30E+03	
104 oz fabric	0.00E+00	0.00E+00	0.00E+00	0.00E+00	
62Y of 6.5 rov/in.	7.27E+03	0.00E+00	0.00E+00	2.30E+03	
1 oz of CSM	4.31E+03	0.00E+00	0.00E+00	1.27E+03	
	0.00E+00	**0.00E+00**	**0.00E+00**	**0.00E+00**	

Computation of bending-extension coupling stiffness					
Fiber architecture	Thk.of lamiane	Z	D_{11}	D_{12}	D_{21}
	(in)	(in)	(lbs-in)	(lbs-in)	(lbs-in)
1 oz of CSM	0.015	-0.1150	4.97E+02	2.04E+02	2.04E+02
62Y of 6.5 rov/in.	0.054	-0.0805	2.43E+03	2.29E+02	2.29E+02
104 oz fabric	0.112	0.000	3.68E+02	1.32E+02	1.32E+02
62Y of 6.5 rov/in.	0.054	0.0805	2.43E+03	2.29E+02	2.29E+02
1 oz of CSM	0.015	0.1150	4.97E+02	2.04E+02	2.04E+02
			6.22E+03	**9.99E+02**	**9.99E+02**
Fiber architecture	D_{22}	D_{16}	D_{26}	D_{66}	
	(lbs-in)	(lbs-in)	(lbs-in)	(lbs-in)	
1 oz of CSM	4.97E+02	0.00E+00	0.00E+00	1.46E+02	
62Y of 6.5 rov/in.	6.08E+02	0.00E+00	0.00E+00	1.92E+02	
104 oz fabric	3.68E+02	0.00E+00	6.81E-15	1.18E+02	
62Y of 6.5 rov/in.	6.08E+02	0.00E+00	0.00E+00	1.92E+02	
1 oz of CSM	4.97E+02	0.00E+00	0.00E+00	1.46E+02	
	2.58E+03	**0.00E+00**	**6.81E-15**	**7.95E+02**	
Step 8					
Computation of in-plane moduli of laminate (E_x^t)					
$E_x^t = [(A_{11}A_{22})-A^2_{12}]/(tA_{22})$	**4.21E+06**				
Computation of bending moduli of laminate (Ex^b)					
$Ex^b = [12(D_{11}D_{22}-D_{12}^2)]/(t^3D_{22})$	**4.48E+06**				
Computation of shear moduli of laminate (G_{xy})					
$Gxy = 12D_{66}/t3$	**6.49E+05**				
Shear Strength	**6.49E+03**				
(assuming shear strain of 0.01)					

APPENDIX B

THEORETICAL PREDICTION OF STIFFNESS IN SECOND GENERATION FRP BRIDGE DECK COMPONENT

The analytical evaluation of the bending stiffness using the approximate classical lamination theory (ACLT) involves the following steps. In the approximate classical lamination theory, modulus of laminate along the fiber direction is being modified. The cross-section is divided into individual parts (preferably rectangular) for the ease of computation (Figure B-1). The stiffness of each part is determined and then added, using the principle of "parallel axis theorem" to obtain the stiffness of the section as a whole.

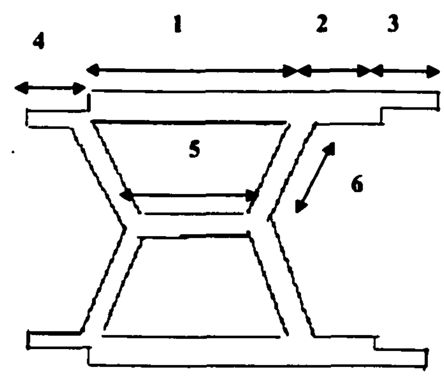

Figure B.1 Cross-Section of Second Generation FRP Bridge Deck Component with Sub Divided Parts

Step 1: Compute Material Properties

The material properties include modulus of elasticity, shear modulus and density of fiber and matrix. These properties are usually given by the manufacturer. From the above properties one can compute the Poisson's ratio for fiber and matrix. In the current problem the material properties are considered as follows:

Modulus of elasticity of fiber = $\mathbf{E_f}$ (psi) = 1.05E+07

Modulus of elasticity of Matrix = E_m (psi) = 7.34e+05

Shear modulus of fiber = G_f (psi) = 4.18e+06

Poisson's ratio of fiber $= \nu_f = \dfrac{E_f}{2G_f} - 1 = 0.26$

Poisson's ratio of matrix $= \nu_m = \dfrac{E_m}{2G_m} - 1 = 0.55$

STEP 2: Determine Thickness of Each component

Each component (flange or web) is built typically with unidirectional fibers (rovings), randomly oriented fibers (chopped strand mat) and fabrics or a combination of fibers and fabrics. Composite thickness of each ply in the laminate depends on the weight of fibers/fabrics. On an average, for example, 40 oz/yd^2 of fabric yields through pultrusion a composite of about 0.05 inch thickness, and 3 rovings/inch can result in a composite of about 0.03 inch thickness. Accuracy of thickness (typically given by the manufacturer) depends on the manufacturing process.

Step 3: Compute Fiber Volume Fraction

Each individual component is built of rovings and biaxial/triaxial fabrics. Based on the thickness and weight of fabric of each ply in the component, fiber volume fraction is computed as follows:

For Rovings

$$V_f = \frac{n\pi D^2}{4bt}$$

Where,

n= number of rovings

b = width of laminae (in)

t= thickness of roving layer (in)

ρ_f is density of fiber (lb/in^3)

Y = yield

For CSM and Fabric

$$V_f = \frac{W_f}{\rho_f L_v}$$

Where,

W_f = Weight of fiber (lb)

L_v = Volume of 1ft x 1ft of lamina

Step 4: Evaluate Laminate Properties

The stiffness properties of laminate are computed by rule of mixture, which relates the properties of fabric and matrix to the unit composite ply.

For Fabric and Rovings

Longitudinal Modulus (psi): $E_{11} = E_f V_f + E_m(1 - V_f)$ (B.1)

Poisson's Ratio: $\nu_{12} = \nu_f V_f + \nu_m(1 - V_m)$ (B.2)

$$\nu_{21} = \frac{\nu_{12} E_{22}}{E_{11}} \quad (B.3)$$

Transverse Modulus (psi): $$E_{22} = \frac{E_f E_m}{E_f V_m + E_m V_f} \quad \text{(B.4)}$$

Shear Modulus (psi): $$G_{12} = \frac{G_f G_m}{G_f V_m + G_m V_f} \quad \text{(B.5)}$$

For CSM (Chopped Strand Mat)

Elastic Modulus of CSM (psi): $$E_{ran} = \frac{3}{8} E_{11} + \frac{5}{8} E_{22} \quad \text{(B.6)}$$

Shear Modulus of CSM (psi): $$G_{ran} = \frac{1}{8} E_{11} + \frac{1}{4} E_{22} \quad \text{(B.7)}$$

Poisson's Ratio of CSM (psi): $$\nu_{ran} = \left(\frac{E_{ran}}{2G_{ran}} \right) - 1 \quad \text{(B.8)}$$

STEP 5: Compute Ex

Modulus of lamina in the direction of bending (along the fiber direction) is determined by

$$E_x \approx E_{11} \cos^4(\theta) \quad \text{(Nagaraj, 1994)} \quad \text{(B.9)}$$

where θ is the angle of fiber orientation with respect to bending direction. The global and material coordinate systems are represented in Figure B2.

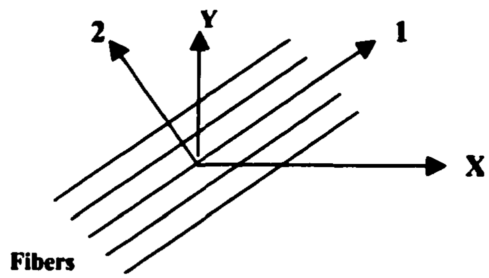

Note: X, Y are Global axes
1, 2 are Local axes

Figure B.2 Local and Global Coordinate Systems

For 40 oz biaxial/triaxial with 0.75 oz CSM stitched mat, E_x is computed individualy for CSM, 0^0, 90^0 and $\pm 45^0$ and the E_x of the stitched mat is computed by distritbuting the contribution of stiffness of each layer in weight ratio. E_x for stitched mat is computed as follows

40 oz biaxial fabric with CSM = $6.75/46.75(E_x CSM) + 24/46.75(E_x 0^0) + 16/46.75(E_x 90^0)$

40 oz triaxial fabric with CSM = $6.75/46.75(E_x CSM) + 12/46.75(E_x 45^0) + 12/46.75(E_x {-45}^0) + 16/46.75(E_x 90^0)$

STEP 6: Compute In-plane Stiffness [A]

$$A_f = A_w = b\sum_{k=1}^{N}(E_x)_k t_k \qquad \text{(B.10)}$$

Where,

$(E_x)_k = E_x$ in k^{th} layer, where 'x' corresponds to global axis
t_k = thickness of the k^{th} layer (in)
b = width of laminate (in)

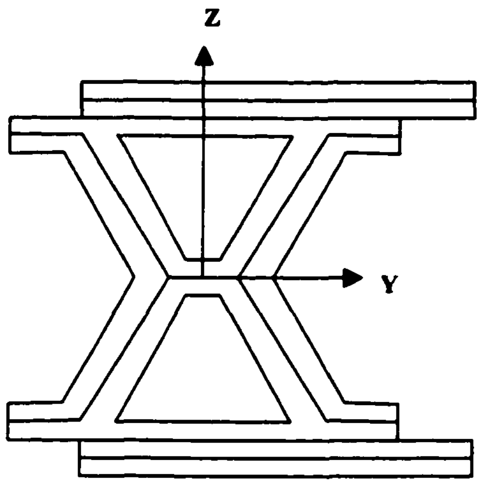

Figure B.3 Cross Section of Second Generation FRP Bridge Deck Component with 'k' Layers

STEP 7: Compute Extensional-Bending Coupling Stiffness [B]

$$B \approx b\sum_{k=1}^{N}(E_x)_k t_k Z_k \qquad \text{(B.11)}$$

Where 'Z_k' is distance of mid-surface of k^{th} lamina from the centroid of the section.

STEP 8: Compute Flange and Web Bending Stiffness

For flange, (Nagraj, 1994):

$$D_f \approx b\sum_{k=1}^{N}(E_x)_k\left[t_k Z_k^2 + \frac{t_k^3}{12}\right] \qquad \text{(B.12)}$$

For web (Lopez, 1995):

$$D_w \approx b\sum_{k=1}^{N}(E_x)_k\left[\left(\frac{t_k^3}{12}+t_k Z_k^2\right)\cos^2(\phi)+\left(\frac{b^2 t_k}{12}\right)\sin^2(\phi)\right] \qquad \text{(B.13)}$$

Where, 'ϕ ' is angle of the component with respect to the horizontal; 'f' refers to flange and 'w' refers to web.

STEP 9: Compute Global Bending Stiffeness (EI) in X direction

$$EI \approx \sum_{f=1}^{n}\left[D_f + A_f e_f^2\right] + \sum_{w=1}^{m}\left[D_w + A_w e_w^2\right] \qquad \text{(B.14)}$$

Where,

n = number of flanges

m = number of webs

e_f = eccentricity of a flange or web from the mid-surface of component

STEP 10: Compute Global Shear Stiffness (GA) in XY plane

$$GA = d\sum_{k=1}^{N}(G_x)_k t_k \qquad \text{(B.15)}$$

Where,

$(G_x) \approx E_{11}\sin^2\theta\cos^2\theta + G_{12}(\sin^2\theta - \cos^2\theta)^2$

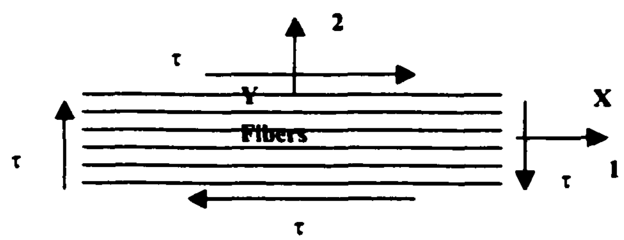

Figure B.4 Representation of G_{12} (X and Y refer to global axes; 1 and 2 refer to local axes)

$(G_x)_k$ = shear in kth layer (psi)

t_k = thickness of kth layer (in)

d = depth of the laminate (in)

The global shear stiffness formula (Equation B.15) yields approximate value up to fiber orientation of 45^0. The shear stiffness in reality is higher than the calculated value as E_{22} effect (Transverse Modulus) is not accounted for in Equation B.15. We suggest using Classical Lamination Theory (CLT) to compute accurate shear stiffness.

The bending and shear stiffness of second generation FRP bridge deck component as per the above procedure using a spread sheet program is presented in the next section.

24 oz of 0 and 16 oz Of 90					
ANALYSIS OF THE SECOND GENERATION OF COMPONENT					
Approximate Classical Lamination Theory					
Computation of Bending Stiffness					
Step 1					
Material Properties					
Elastic constants for E-glass fabric and Matrix					
E_{fiber}	E_{matrix}	G_{fiber}	G_{matrix}	v_{fiber}	v_{matrix}
(psi)	**(psi)**	**(psi)**	**(psi)**		
1.05E+07	7.34E+05	4.18E+06	2.37E+05	0.256	0.549
Step 2					
Fiber Architecture					
Section	**Dimension**				
1	**6.435" x 0.601"**				
Fiber Architecture	**Thickness**				
40 oz Biaxial with 0.75 OC	0.055				
10.38 rov/in - 62 Y (66.79)	0.104				
40 oz Biaxial with 0.75 OC	0.055				
8.5 rov/in - 62 Y (54.69)	0.085				
40 oz Biaxial with 0.75 OC	0.055				
2.48 rov/in - 62Y (15.96)	0.025				
40 oz Biaxial with 0.75 OC	0.055				
5.16 rov/in - 62 Y (33.20)	0.052				
3 rov/in - 62 Y (19.3)	0.03				
3 rov/in - 62 Y (19.3)	0.03				
40 oz Triaxial with 0.75 OC	0.055				
Total thickness of Section 1	**0.601**				
Step 3					
Computation of Fiber Volume Fraction (V_f) of 40 oz of fabric (bi-axial)					
40 oz of fabric has 24 oz at 0^0 and 16 oz at 90^0					
Thk of lamina	**Wt. Of Fabric**	**Wt. Of Fabric**	**Wt.of 1ft² Comp.**	**Density of fiber**	
(in.)	**(oz/yd2)**	**(oz/ft2)**	**(lb)**	**(lb/in3)**	
0.0282	24	2.667	0.167	0.092	
0.0188	16	1.778	0.111	0.092	
Volume of	**Volume of**	**Fiber Volume**	**Matrix Volume**		
fiber	**composite**	**fraction (Vf)**	**fraction (Vm)**		
1.812	4.0608	0.45	0.55		
1.208	2.7072	0.45	0.55		
Computation of Fiber Volume Fraction (V_f) of 40 oz of fabric (triaxial)					
40 oz of fabric has 12 oz at 45^0 12 oz at -45^0 and 16 oz at 90^0					
Thk of lamina	**Wt. Of Fabric**	**Wt. Of Fabric**	**Wt.of 1ft² Comp.**	**Density of fiber**	
(in.)	**(oz/yd2)**	**(oz/ft2)**	**(lb)**	**(lb/in3)**	
0.0141	12	1.333	0.083	0.092	
0.0141	12	1.333	0.083	0.092	
0.0188	16	1.778	0.111	0.092	

Volume of fiber	**Volume of composite**	**Fiber Volume fraction (Vf)**	**Matrix Volume fraction (Vm)**		
0.906	2.0304	0.45	0.55		
0.906	2.0304	0.45	0.55		
1.208	2.7072	0.45	0.55		
Computation of Fiber Volume Fraction (V_f) of 0.75 oz of fabric					
Thk of lamina (in.)	**Wt. Of Fabric (oz/yd2)**	**Wt. Of Fabric (oz/ft2)**	**Wt.of 1ft^2 (lb)**	**Density of (lb/in3)**	
0.008	6.75	0.750	0.047	0.092	
Volume of fiber	**Volume of composite**	**Fiber Volume fraction**	**Matrix Volume fraction**		
0.510	1.152	0.44	0.56		
Computation of Fiber Volume Fraction (V_f) of Rovings					
Rovings	**thickness (in)**	**Yield yards**	**Dia.of rov. (in)**	**Width (in)**	
62Y - 66.79 bundles	0.104	62	0.079	6.435	
62Y - 54.69 bundles	0.085	62	0.079	6.435	
62Y - 15.9 bundles	0.025	62	0.079	6.435	
62Y - 33.20 bundles	0.052	62	0.079	6.435	
62Y - 19.3 bundles	0.030	62	0.079	6.435	
62Y - 19.3 bundles	0.030	62	0.079	6.435	
bundles (no:)	**Fiber Volume Fraction (V_f)**	**Matrix Volume Fraction (V_m)**			
66.79	0.49	0.51			
54.69	0.49	0.51			
15.96	0.49	0.51			
33.2	0.49	0.51			
19.3	0.49	0.51			
19.3	0.49	0.51			
Step 4					
Computation of Laminae Properties					
Ply	**E_{11}**	**E_{22}**	**G_{12}**	**ν_{12}**	**ν_{21}**
0.75 oz CSM	5.05E+06	1.25E+06			
40 oz Biaxial					
0^0	5.09E+06	1.25E+06	4.09E+05	0.418	0.103
90^0	5.09E+06	1.25E+06	4.09E+05	0.418	0.103
40 oz Triaxial					
45^0	5.09E+06	1.25E+06	4.09E+05	0.418	0.103
$\_45^0$	5.09E+06	1.25E+06	4.09E+05	0.418	0.103
90^0	5.09E+06	1.25E+06	4.09E+05	0.418	0.103
62Y - 66.79 bundles	5.48E+06	1.34E+06	4.38E+05	0.406	0.099
62Y - 54.69 bundles	5.49E+06	1.34E+06	4.38E+05	0.406	0.099
62Y - 15.9 bundles	5.52E+06	1.35E+06	4.41E+05	0.405	0.099
62Y - 33.2 bundles	5.48E+06	1.34E+06	4.38E+05	0.406	0.099
62Y - 19.3 bundles	5.49E+06	1.34E+06	4.38E+05	0.406	0.099
62Y - 19.3 bundles	5.49E+06	·1.34E+06	4.38E+05	0.406	0.099
For 0.75 oz of CSM	2.67E+06	2.67E+06	9.43E+05	0.417	0.417

Step 5					
Computation of E_x					
Ply	**Ornt. of fibers**	**Ornt. of fibers**	**$E_x = E_{11} Cos^4 0$**		
	(in degrees)	**(in radians)**	**(psi)**		
0.75 oz of CSM	0	0.00	2.67E+06		
40 oz Biaxial					
0	0	0.00	5.09E+06		
90	90	1.57	7.17E-59		
40 oz Biaxial with CSM					
CSM and 0/90 **(the stiffness is distributed in the weight ratios)**			**3.00E+06**		
40 oz Triaxial					
45	45	0.79	1.27E+06		
-45	-45	-0.79	1.27E+06		
90	90	1.57	7.17E-59		
40 oz Triaxial with CSM					
CSM and 45/-45/90 **(the stiffness is distributed in the weight ratios)**			**1.04E+06**		
62Y - 66.79 bundles	0	0.00	5.48E+06		
62Y - 54.69 bundles	0	0.00	5.49E+06		
62Y - 15.9 bundles	0	0.00	5.52E+06		
62Y - 33.2 bundles	0	0.00	5.48E+06		
62Y - 19.3 bundles	0	0.00	5.49E+06		
62Y - 19.3 bundles	0	0.00	5.49E+06		
Step 6					
Computation of Axial Stiffness					
Fiber	**Width of lamina**	**Thk. of lamina**	**E_x**	**A_f**	
	(in)	**(in)**	**(psi)**	**(lbs)**	
40 oz Biaxial with 0.75 CSM	6.435	0.055	3.00E+06	1.06E+06	
10.38 rov/in - 62 Y (66.79)	6.435	0.104	5.48E+06	3.67E+06	
40 oz Biaxial with 0.75 CSM	6.435	0.055	3.00E+06	1.06E+06	
8.5 rov/in - 62 Y (54.69)	6.435	0.085	5.49E+06	3.00E+06	
40 oz Biaxial with 0.75 CSM	6.435	0.055	3.00E+06	1.06E+06	
2.48 rov/in - 62Y (15.96)	6.435	0.025	5.52E+06	8.88E+05	
40 oz Biaxial with 0.75 CSM	6.435	0.055	3.00E+06	1.06E+06	
5.16 rov/in - 62 Y (33.20)	6.435	0.052	5.48E+06	1.83E+06	
3 rov/in - 62 Y (19.3)	6.435	0.03	5.49E+06	1.06E+06	
3 rov/in - 62 Y (19.3)	6.435	0.03	5.49E+06	1.06E+06	
40 oz Triaxial with 0.75 CSM	6.435	0.055	1.04E+06	3.68E+05	
		0.601		**1.61E+07**	
Step 7					
Computation of Extensional Bending Coupling Stiffness					
Fiber	**Width of lamina**	**Thk. of lamina**	**Z**	**E_x**	**B_f**
	(in)	**(in)**	**(in)**	**(psi)**	**(lbs-in)**
40 oz Biaxial with 0.75 CSM	6.435	0.055	-0.273	3.00E+06	-2.90E+05
10.38 rov/in - 62 Y (66.79)	6.435	0.104	-0.194	5.48E+06	-7.10E+05
40 oz Biaxial with 0.75 CSM	6.435	0.055	-0.114	3.00E+06	-1.21E+05
8.5 rov/in - 62 Y (54.69)	6.435	0.085	-0.044	5.49E+06	-1.32E+05
40 oz Biaxial with 0.75 CSM	6.435	0.055	0.026	3.00E+06	2.76E+04
2.48 rov/in - 62Y (15.96)	6.435	0.025	0.066	5.52E+06	5.86E+04
40 oz Biaxial with 0.75 CSM	6.435	0.055	0.106	3.00E+06	1.13E+05
5.16 rov/in - 62 Y (33.20)	6.435	0.052	0.160	5.48E+06	2.93E+05
3 rov/in - 62 Y (19.3)	6.435	0.03	0.201	5.49E+06	2.12E+05
3 rov/in - 62 Y (19.3)	6.435	0.03	0.231	5.49E+06	2.44E+05
40 oz Triaxial with 0.75 CSM	6.435	0.055	0.273	1.04E+06	1.00E+05
		0.601			**-2.04E+05**

Step 8					
Computation of Bending Stiffness					
Ply	Width of lamina	Thk. Of lamina	Z	E_x	D_f
	(in)	(in)	(in)	(psi)	(lbs-in^2)
40 oz Biaxial with 0.75 CSM	6.435	0.055	-0.273	3.00E+06	7.94E+04
10.38 rov/in - 62 Y (66.79)	6.435	0.104	-0.194	5.48E+06	1.41E+05
40 oz Biaxial with 0.75 CSM	6.435	0.055	-0.114	3.00E+06	1.41E+04
8.5 rov/in - 62 Y (54.69)	6.435	0.085	-0.044	5.49E+06	7.62E+03
40 oz Biaxial with 0.75 CSM	6.435	0.055	0.026	3.00E+06	9.85E+02
2.48 rov/in - 62Y (15.96)	6.435	0.025	0.066	5.52E+06	3.91E+03
40 oz Biaxial with 0.75 CSM	6.435	0.055	0.106	3.00E+06	1.22E+04
5.16 rov/in - 62 Y (33.20)	6.435	0.052	0.160	5.48E+06	4.71E+04
3 rov/in - 62 Y (19.3)	6.435	0.03	0.201	5.49E+06	4.27E+04
3 rov/in - 62 Y (19.3)	6.435	0.03	0.231	5.49E+06	5.64E+04
40 oz Triaxial with 0.75 CSM	6.435	0.055	0.273	1.04E+06	2.75E+04
					4.32E+05
Bending Stiffness of Section 1	$D_f + A_f e_o^2$	2.21E+08			

ANALYSIS OF THE SECOND GENERATION OF COMPONENT

Approximate Classical Lamination Theory

Computation of Bending Stiffness

Step 1

Material Properties

Elastic constants for E-glass fabric and Matrix

E_{fiber} (psi)	E_{matrix} (psi)	G_{fiber} (psi)	G_{matrix} (psi)	v_{fiber}	v_{matrix}
1.05E+07	7.34E+05	4.18E+06	2.37E+05	0.256	0.549

Step 2

Fiber Architecture

Section	Dimension
2	3.065" x 0.688"

Fiber Architecture	Thickness
40 oz Biaxial with 0.75 OC	0.055
10.38 rov/in - 62 Y (31.81)	0.104
40 oz Biaxial with 0.75 OC	0.055
8.5 rov/in - 62 Y (26.05)	0.085
40 oz Biaxial with 0.75 OC	0.055
2.48 rov/in - 62Y (7.60)	0.025
40 oz Biaxial with 0.75 OC	0.055
40 oz Triaxial with 0.75 OC	0.055
40 oz Triaxial with 0.75 OC	0.055
40 oz Triaxial with 0.75 OC	0.055
2.94 rov/in - 62 Y (9)	0.029
40 oz Triaxial with 0.75 OC	0.055
	0.683

Step 3

Computation of Fiber Volume Fraction (V_f) of 40 oz of fabric (bi-axial)

40 oz of fabric has 24 oz at 0^0 and 16 oz at 90^0

Thk of lamina (in.)	Wt. Of Fabric (oz/yd2)	Wt. Of Fabric (oz/ft2)	Wt.of 1ft² Comp. (lb)	Density of fiber (lb/in3)
0.0282	24	2.667	0.167	0.092
0.0188	16	1.778	0.111	0.092

Volume of fiber	Volume of composite	Fiber Volume fraction (Vf)	Matrix Volume fraction (Vm)
1.812	4.0608	0.45	0.55
1.208	2.7072	0.45	0.55

Computation of Fiber Volume Fraction (V_f) of 40 oz of fabric (triaxial)

40 oz of fabric has 12 oz at 45^0 12 oz at -45^0 and 16 oz at 90^0

Thk of lamina (in.)	Wt. Of Fabric (oz/yd2)	Wt. Of Fabric (oz/ft2)	Wt.of 1ft² Comp. (lb)	Density of fiber (lb/in3)
0.0141	12	1.333	0.083	0.092
0.0141	12	1.333	0.083	0.092
0.0188	16	1.778	0.111	0.092

Volume of fiber	**Volume of composite**	**Fiber Volume fraction (Vf)**	**Matrix Volume fraction (Vm)**		
0.906	2.0304	0.45	0.55		
0.906	2.0304	0.45	0.55		
1.208	2.7072	0.45	0.55		
Computation of Fiber Volume Fraction (V_f) of 0.75 oz of fabric					
Thk of lamina (in.)	**Wt. Of Fabric (oz/yd2)**	**Wt. Of Fabric (oz/ft2)**	**Wt.of 1ft^2 (lb)**	**Density of (lb/in3)**	
0.008	6.75	0.750	0.047	0.092	
Volume of fiber	**Volume of composite**	**Fiber Volume fraction**	**Matrix Volume fraction**		
0.510	1.152	0.44	0.56		
Computation of Fiber Volume Fraction (V_f) of Rovings					
Rovings	**thickness (in)**	**Yield yards**	**Dia.of rov. (in)**	**Width (in)**	
62Y - 31.81 bundles	0.104	62	0.079	3.065	
62Y - 26.05 bundles	0.085	62	0.079	3.065	
62Y - 7.6 bundles	0.025	62	0.079	3.065	
62Y - 9 bundles	0.029	62	0.079	3.065	
bundles (no:)	**Fiber Volume Fraction (V_f)**	**Matrix Volume Fraction (V_m)**			
31.81	0.49	0.51			
26.05	0.49	0.51			
7.6	0.49	0.51			
9	0.49	0.51			
Step 4					
Computation of Laminae Properties					
Ply	**E_{11}**	**E_{22}**	**G_{12}**	**v_{12}**	**v_{21}**
0.75 oz OC	5.05E+06	1.25E+06			
40 oz Biaxial					
0^0	5.09E+06	3.12E+06	1.12E+06	0.418	0.256
90^0	5.09E+06	1.25E+06	4.09E+05	0.418	0.103
40 oz Triaxial					
45^0	5.09E+06	1.25E+06	4.09E+05	0.418	0.103
-45^0	5.09E+06	1.25E+06	4.09E+05	0.418	0.103
90^0	5.09E+06	1.25E+06	4.09E+05	0.418	0.103
62Y - 31.81 bundles	5.48E+06	1.34E+06	4.38E+05	0.406	0.099
62Y - 26.05 bundles	5.49E+06	1.34E+06	4.38E+05	0.406	0.099
62Y - 7.6 bundles	5.52E+06	1.35E+06	4.41E+05	0.405	0.099
62Y - 9 bundles	5.55E+06	1.36E+06	4.43E+05	0.404	0.099
For 0.75 oz of OC	2.67E+06	2.67E+06	9.43E+05	0.417	0.417

Step 5					
Computation of E_x					
Ply	**Ornt. of fibers**	**Ornt. of fibers**	**$E_x = E_{11}Cos^4\theta$**		
	(in degrees)	**(in radians)**	**(psi)**		
0.75 oz of OC	0	0.00	2.67E+06		
40 oz Biaxial					
0	0	0.00	5.09E+06		
90	90	1.57	7.17E-59		
40 oz Biaxial with OC					
OC and 0/90 **(the stiffness is distributed in the weight ratios)**			**3.00E+06**		
40 oz Triaxial					
45	45	0.79	1.27E+06		
-45	-45	-0.79	1.27E+06		
90	90	1.57	7.17E-59		
40 oz Triaxial with OC					
OC and 45/-45/90 **(the stiffness is distributed in the weight ratios)**			**1.04E+06**		
62Y - 31.81 bundles	0	0.00	5.48E+06		
62Y - 26.05 bundles	0	0.00	5.49E+06		
62Y - 7.6 bundles	0	0.00	5.52E+06		
62Y - 9 bundles	0	0.00	5.55E+06		
Step 6					
Computation of Axial Stiffness					
Ply	**Width of lamina**	**Thk. of lamina**	**E_x**	**A_f**	
	(in)	**(in)**	**(psi)**	**(lbs)**	
40 oz Biaxial with 0.75 OC	3.065	0.055	3.00E+06	5.06E+05	
10.38 rov/in - 62 Y (31.81)	3.065	0.104	5.48E+06	1.75E+06	
40 oz Biaxial with 0.75 OC	3.065	0.055	3.00E+06	5.06E+05	
8.5 rov/in - 62 Y (26.05)	3.065	0.085	5.49E+06	1.43E+06	
40 oz Biaxial with 0.75 OC	3.065	0.055	3.00E+06	5.06E+05	
2.48 rov/in - 62Y (7.60)	3.065	0.025	5.52E+06	4.23E+05	
40 oz Biaxial with 0.75 OC	3.065	0.055	3.00E+06	5.06E+05	
40 oz Triaxial with 0.75 OC	3.065	0.055	1.04E+06	1.75E+05	
40 oz Triaxial with 0.75 OC	3.065	0.055	1.04E+06	1.75E+05	
40 oz Triaxial with 0.75 OC	3.065	0.055	1.04E+06	1.75E+05	
2.94 rov/in - 62 Y (9)	3.065	0.029	5.55E+06	4.93E+05	
40 oz Triaxial with 0.75 OC	3.065	0.055	1.04E+06	1.75E+05	
				6.82E+06	
Step 7					
Computation of Extensional Bending Coupling Stiffness					
Ply	**Width of lamina**	**Thk. of lamina**	**Z**	**E_x**	**B_f**
	(in)	**(in)**	**(in)**	**(psi)**	**(lbs-in)**
40 oz Biaxial with 0.75 OC	3.065	0.055	-0.314	3.00E+06	-1.59E+05
10.38 rov/in - 62 Y (31.81)	3.065	0.104	-0.235	5.48E+06	-4.10E+05
40 oz Biaxial with 0.75 OC	3.065	0.055	-0.155	3.00E+06	-7.84E+04
8.5 rov/in - 62 Y (26.05)	3.065	0.085	-0.085	5.49E+06	-1.22E+05
40 oz Biaxial with 0.75 OC	3.065	0.055	-0.015	3.00E+06	-7.58E+03
2.48 rov/in - 62Y (7.60)	3.065	0.025	0.025	5.52E+06	1.06E+04
40 oz Biaxial with 0.75 OC	3.065	0.055	0.065	3.00E+06	3.29E+04
40 oz Triaxial with 0.75 OC	3.065	0.055	0.120	1.04E+06	2.10E+04
40 oz Triaxial with 0.75 OC	3.065	0.055	0.175	1.04E+06	3.07E+04
40 oz Triaxial with 0.75 OC	3.065	0.055	0.230	1.04E+06	4.03E+04
2.94 rov/in - 62 Y (9)	3.065	0.029	0.272	5.55E+06	1.34E+05
40 oz Triaxial with 0.75 OC	3.065	0.055	0.314	1.04E+06	5.50E+04
		0.683			**-4.51E+05**

Step 8					
Computation of Bending Stiffness					
Ply	Width of lamina	Thk. Of lamina	Z	E_x	D_f
	(in)	(in)	(in)	(psi)	(lbs-in^2)
40 oz Biaxial with 0.75 OC	3.065	0.055	-0.314	3.00E+06	5.00E+04
10.38 rov/in - 62 Y (31.81)	3.065	0.104	-0.235	5.48E+06	9.76E+04
40 oz Biaxial with 0.75 OC	3.065	0.055	-0.155	3.00E+06	1.23E+04
8.5 rov/in - 62 Y (26.05)	3.065	0.085	-0.085	5.49E+06	1.12E+04
40 oz Biaxial with 0.75 OC	3.065	0.055	-0.015	3.00E+06	2.41E+02
2.48 rov/in - 62Y (7.60)	3.065	0.025	0.025	5.52E+06	2.86E+02
40 oz Biaxial with 0.75 OC	3.065	0.055	0.065	3.00E+06	2.26E+03
40 oz Triaxial with 0.75 OC	3.065	0.055	0.120	1.04E+06	2.57E+03
40 oz Triaxial with 0.75 OC	3.065	0.055	0.175	1.04E+06	5.41E+03
40 oz Triaxial with 0.75 OC	3.065	0.055	0.230	1.04E+06	9.31E+03
2.94 rov/in - 62 Y (9)	3.065	0.029	0.272	5.55E+06	3.65E+04
40 oz Triaxial with 0.75 OC	3.065	0.055	0.314	1.04E+06	1.73E+04
		0.683			**2.45E+05**
Step 9					
Bending Stiffness of Section 2	$D_f + A_f e_o^2$	**9.15E+07**			

ANALYSIS OF THE SECOND GENERATION OF COMPONENT					
Approximate Classical Lamination Theory					
Computation of Bending Stiffness					
Step1					
Material Properties					
Elastic constants for E-glass fabric and Matrix					
E_{fiber}	E_{matrix}	G_{fiber}	G_{matrix}	v_{fiber}	v_{matrix}
(psi)	(psi)	(psi)	(psi)		
1.05E+07	7.34E+05	4.18E+06	2.37E+05	0.256	0.549
Step 2					
Fiber Architecture					
Section	**Dimension**				
3	2.5" x 0.33"				
Fiber Architecture	**Thickness**				
40 oz Biaxial with 0.75 OC	0.055				
40 oz Biaxial with 0.75 OC	0.055				
8.5 rov/in - 62 Y (21.25)	0.085				
40 oz Biaxial with 0.75 OC	0.055				
2.48 rov/in - 62 Y (6.2)	0.025				
40 oz Biaxial with 0.75 OC	0.055				
Total thickness of Section 3	**0.33**				
Step 3					
Computation of Fiber Volume Fraction (V_f) of 40 oz of fabric (bi-axial)					
40 oz of fabric has 24 oz at 0^0 and 16 oz at 90^0					
Thk of lamina	**Wt. Of Fabric**	**Wt. Of Fabric**	**Wt.of 1ft² Comp.**	**Density of fiber**	
(in.)	**(oz/yd2)**	**(oz/ft2)**	**(lb)**	**(lb/in3)**	
0.0282	24	2.667	0.167	0.092	
0.0188	16	1.778	0.111	0.092	
Volume of	**Volume of**	**Fiber Volume**	**Matrix Volume**		
fiber	**composite**	**fraction (Vf)**	**fraction (Vm)**		
1.812	4.0608	0.45	0.55		
1.208	2.7072	0.45	0.55		
Computation of Fiber Volume Fraction (V_f) of 40 oz of fabric (triaxial)					
40 oz of fabric has 12 oz at 45^0 12 oz at -45^0 and 16 oz at 90^0					
Thk of lamina	**Wt. Of Fabric**	**Wt. Of Fabric**	**Wt.of 1ft² Comp.**	**Density of fiber**	
(in.)	**(oz/yd2)**	**(oz/ft2)**	**(lb)**	**(lb/in3)**	
0.0141	12	1.333	0.083	0.092	
0.0141	12	1.333	0.083	0.092	
0.0188	16	1.778	0.111	0.092	
Volume of	**Volume of**	**Fiber Volume**	**Matrix Volume**		
fiber	**composite**	**fraction (Vf)**	**fraction (Vm)**		
0.906	2.0304	0.45	0.55		
0.906	2.0304	0.45	0.55		
1.208	2.7072	0.45	0.55		

Computation of Fiber Volume Fraction (V_f) of 0.75 oz of fabric					
Thk of lamina	**Wt. Of Fabric**	**Wt. Of Fabric**	**Wt.of 1ft^2**	**Density of**	
(in.)	**(oz/yd2)**	**(oz/ft2)**	**(lb)**	**(lb/in3)**	
0.008	6.75	0.750	0.047	0.092	
Volume of	**Volume of**	**Fiber Volume**	**Matrix Volume**		
fiber	**composite**	**fraction**	**fraction**		
0.510	1.152	0.44	0.56		
Computation of Fiber Volume Fraction (V_f) of Rovings					
Rovings	**thickness**	**Yield**	**Dia.of rov.**	**Width**	
	(in)	**yards**	**(in)**	**(in)**	
62Y - 21.25 bundles	0.085	62	0.079	2.5	
62Y - 6.2 bundles	0.025	62	0.079	2.5	
bundles	**Fiber Volume**	**Matrix Volume**			
(no:)	**Fraction (V_f)**	**Fraction (V_m)**			
21.25	0.49	0.51			
6.2	0.49	0.51			
Step 4					
Computation of Laminae Properties					
Ply	E_{11}	E_{22}	G_{12}	v_{12}	v_{21}
0.75 oz OC	5.05E+06	1.25E+06			
40 oz Biaxial					
0^0	5.09E+06	1.25E+06	4.09E+05	0.418	0.103
90^0	5.09E+06	1.25E+06	4.09E+05	0.418	0.103
40 oz Triaxial					
45^0	5.09E+06	1.25E+06	4.09E+05	0.418	0.103
$\_45^0$	5.09E+06	1.25E+06	4.09E+05	0.418	0.103
90^0	5.09E+06	1.25E+06	4.09E+05	0.418	0.103
62Y - 21.25 bundles	5.49E+06	1.34E+06	4.38E+05	0.406	0.099
62Y - 6.2 bundles	5.52E+06	1.35E+06	4.41E+05	0.405	0.099
For 0.75 oz of OC	2.67E+06	2.67E+06	9.43E+05	0.417	0.417
Step 5					
Computation of E_x					
Ply	**Ornt. of fibers**	**Ornt. of fibers**	$E_x = E_{11} Cos^4 0$		
	(in degrees)	**(in radians)**	**(psi)**		
0.75 oz of OC	0	0.00	2.67E+06		
40 oz Biaxial					
0	0	0.00	5.09E+06		
90	90	1.57	7.17E-59		
40 oz Biaxial with OC					
OC and 0/90 **(the stiffness is distributed in the weight ratios)**			**3.00E+06**		
40 oz Triaxial					
45	45	0.79	1.27E+06		
-45	-45	-0.79	1.27E+06		
90	90	1.57	7.17E-59		
40 oz Triaxial with OC					
OC and 45/-45/90 **(the stiffness is distributed in the weight ratios)**			**1.04E+06**		
62Y - 21.25 bundles	0	0.00	5.49E+06		
62Y - 6.2 bundles	0	0.00	5.52E+06		

Step 6					
Computation of Axial Stiffness					
Ply	**Width of lamina**	**Thk. of lamina**	**E_x**	**A_f**	
	(in)	**(in)**	**(psi)**	**(lbs)**	
40 oz Biaxial with 0.75 OC	2.5	0.055	3.00E+06	4.12E+05	
40 oz Biaxial with 0.75 OC	2.5	0.055	3.00E+06	4.12E+05	
8.5 rov/in - 62 Y (21.25)	2.5	0.085	5.49E+06	1.17E+06	
40 oz Biaxial with 0.75 OC	2.5	0.055	3.00E+06	4.13E+05	
2.48 rov/in - 62 Y (6.2)	2.5	0.025	5.52E+06	3.45E+05	
40 oz Biaxial with 0.75 OC	2.5	0.055	3.00E+06	4.13E+05	
		0.33		**3.16E+06**	
Step 7					
Computation of Extensional Bending Coupling Stiffness					
Ply	**Width of lamina**	**Thk. of lamina**	**Z**	**E_x**	**B_f**
	(in)	**(in)**	**(in)**	**(psi)**	**(lbs-in)**
40 oz Biaxial with 0.75 OC	2.5	0.055	-0.138	3.00E+06	-5.67E+04
40 oz Biaxial with 0.75 OC	2.5	0.055	-0.083	3.00E+06	-3.40E+04
8.5 rov/in - 62 Y (21.25)	2.5	0.085	-0.013	5.49E+06	-1.46E+04
40 oz Biaxial with 0.75 OC	2.5	0.055	0.058	3.00E+06	2.37E+04
2.48 rov/in - 62 Y (6.2)	2.5	0.025	0.098	5.52E+06	3.36E+04
40 oz Biaxial with 0.75 OC	2.5	0.055	0.138	3.00E+06	5.67E+04
					8.75E+03
Step 8					
Computation of Bending Stiffness					
Ply	**Width of lamina**	**Thk. Of lamina**	**Z**	**E_x**	**D_f**
	(in)	**(in)**	**(in)**	**(psi)**	**(lbs-in^2)**
40 oz Biaxial with 0.75 OC	2.5	0.055	-0.138	3.00E+06	7.90E+03
40 oz Biaxial with 0.75 OC	2.5	0.055	-0.083	3.00E+06	2.91E+03
8.5 rov/in - 62 Y (21.25)	2.5	0.085	-0.013	5.49E+06	8.85E+02
40 oz Biaxial with 0.75 OC	2.5	0.055	0.058	3.00E+06	1.47E+03
2.48 rov/in - 62 Y (6.2)	2.5	0.025	0.098	5.52E+06	3.30E+03
40 oz Biaxial with 0.75 OC	2.5	0.055	0.138	3.00E+06	7.90E+03
		0.33			**2.44E+04**
Step 9					
Bending Stiffness of Section 3	$D_f + A_f e_o^2$	**4.65E+07**			

ANALYSIS OF THE SECOND GENERATION OF COMPONENT

Approximate Classical Lamination Theory

Computation of Bending Stiffness

Step 1

Material Properties

Elastic constants for E-glass fabric and Matrix

E_{fiber}	E_{matrix}	G_{fiber}	G_{matrix}	ν_{fiber}	ν_{matrix}
(psi)	(psi)	(psi)	(psi)		
1.05E+07	7.34E+05	4.18E+06	2.37E+05	0.256	0.549

Step 2

Fiber Architecture

Section	Dimension
4	2.5" x 0.36"

Fiber Architecture	Thickness
40 oz Biaxial with 0.75 OC	0.055
2.48 rov/in - 62 Y (6.2)	0.016
40 oz Biaxial with 0.75 OC	0.055
40 oz Triaxial with 0.75 OC	0.055
40 oz Triaxial with 0.75 OC	0.055
40 oz Triaxial with 0.75 OC	0.055
2.1 rov/in - 62Y (2)	0.014
40 oz Triaxial with 0.75 OC	0.055
	0.360

Step 3

Computation of Fiber Volume Fraction (V_f) of 40 oz of fabric (bi-axial)

40 oz of fabric has 24 oz at 0^0 and 16 oz at 90^0

Thk of lamina	Wt. Of Fabric	Wt. Of Fabric	Wt.of 1ft² Comp.	Density of fiber
(in.)	(oz/yd2)	(oz/ft2)	(lb)	(lb/in3)
0.0282	24	2.667	0.167	0.092
0.0188	16	1.778	0.111	0.092

Volume of fiber	Volume of composite	Fiber Volume fraction (Vf)	Matrix Volume fraction (Vm)
1.812	4.0608	0.45	0.55
1.208	2.7072	0.45	0.55

Computation of Fiber Volume Fraction (V_f) of 40 oz of fabric (triaxial)

40 oz of fabric has 12 oz at 45^0 12 oz at -45^0 and 16 oz at 90^0

Thk of lamina	Wt. Of Fabric	Wt. Of Fabric	Wt.of 1ft² Comp.	Density of fiber
(in.)	(oz/yd2)	(oz/ft2)	(lb)	(lb/in3)
0.0141	12	1.333	0.083	0.092
0.0141	12	1.333	0.083	0.092
0.0188	16	1.778	0.111	0.092

Volume of fiber	Volume of composite	Fiber Volume fraction (Vf)	Matrix Volume fraction (Vm)
0.906	2.0304	0.45	0.55
0.906	2.0304	0.45	0.55
1.208	2.7072	0.45	0.55

Computation of Fiber Volume Fraction (V_f) of 0.75 oz of fabric					
Thk of lamina	**Wt. Of Fabric**	**Wt. Of Fabric**	**Wt.of 1ft^2**	**Density of**	
(in.)	**(oz/yd2)**	**(oz/ft2)**	**(lb)**	**(lb/in3)**	
0.008	6.75	0.750	0.047	0.092	
Volume of	**Volume of**	**Fiber Volume**	**Matrix Volume**		
fiber	**composite**	**fraction**	**fraction**		
0.510	1.152	0.44	0.56		
Computation of Fiber Volume Fraction (V_f) of Rovings					
Rovings	**thickness**	**Yield**	**Dia.of rov.**	**Width**	
	(in)	**yards**	**(in)**	**(in)**	
62Y - 6.2 bundles	0.016	62	0.079	2.5	
62Y - 2 bundles	0.014	62	0.079	0.95	
bundles	**Fiber Volume**	**Matrix Volume**			
(no:)	**Fraction (V_f)**	**Fraction (V_m)**			
6.2	0.75	0.25			
2	0.73	0.27			
Step 4					
Computation of Laminae Properties					
Ply	**E_{11}**	**E_{22}**	**G_{12}**	**v_{12}**	**v_{21}**
0.75 oz OC	5.05E+06	1.25E+06			
40 oz Biaxial					
0^0	5.09E+06	1.25E+06	4.09E+05	0.418	0.103
90^0	5.09E+06	1.25E+06	4.09E+05	0.418	0.103
40 oz Triaxial					
45^0	5.09E+06	1.25E+06	4.09E+05	0.418	0.103
-45^0	5.09E+06	1.25E+06	4.09E+05	0.418	0.103
90^0	5.09E+06	1.25E+06	4.09E+05	0.418	0.103
62Y - 6.2 bundles	8.11E+06	2.46E+06	8.23E+05	0.328	0.100
62Y - 2 bundles	7.89E+06	2.30E+06	7.66E+05	0.334	0.098
For 0.75 oz of OC	2.67E+06	2.67E+06	9.43E+05	0.417	0.417
Step 5					
Computation of E_x					
Ply	**Ornt. of fibers**	**Ornt. of fibers**	**$E_x = E_{11} Cos^4 \theta$**		
	(in degrees)	**(in radians)**	**(psi)**		
0.75 oz of OC	0	0.00	2.67E+06		
40 oz Biaxial					
0	0	0.00	5.09E+06		
90	90	1.57	7.17E-59		
40 oz Biaxial with OC					
OC and 0/90 **(the stiffness is distributed in the weight ratios)**			**3.00E+06**		
40 oz Triaxial					
45	45	0.79	1.27E+06		
-45	-45	-0.79	1.27E+06		
90	90	1.57	7.17E-59		
40 oz Triaxial with OC					
OC and 45/-45/90 **(the stiffness is distributed in the weight ratios)**			**1.04E+06**		
62Y - 6.2 bundles	0	0.00	8.11E+06		
62Y - 2 bundles	0	0.00	7.89E+06		

Step 6					
Computation of Axial Stiffness					
Ply	**Width of lamina**	**Thk. of lamina**	**E_x**	**A_f**	
	(in)	**(in)**	**(psi)**	**(lbs)**	
40 oz Biaxial with 0.75 OC	2.5	0.055	3.00E+06	4.12E+05	
2.48 rov/in - 62 Y (6.2)	2.5	0.016	8.11E+06	3.24E+05	
40 oz Biaxial with 0.75 OC	2.5	0.055	3.00E+06	4.12E+05	
40 oz Triaxial with 0.75 OC	2.5	0.055	1.04E+06	1.43E+05	
40 oz Triaxial with 0.75 OC	2.5	0.055	1.04E+06	1.43E+05	
40 oz Triaxial with 0.75 OC	2.5	0.055	1.04E+06	1.43E+05	
2.1 rov/in - 62Y (2)	2.5	0.014	7.89E+06	2.76E+05	
40 oz Triaxial with 0.75 OC	2.5	0.055	1.04E+06	1.43E+05	
		0.36		**2.00E+06**	
Step 7					
Computation of Extensional Bending Coupling Stiffness					
Ply	**Width of lamina**	**Thk. of lamina**	**Z**	**E_x**	**B_f**
	(in)	**(in)**	**(in)**	**(psi)**	**(lbs-in)**
40 oz Biaxial with 0.75 OC	2.5	0.055	-0.153	3.00E+06	-6.31E+04
2.48 rov/in - 62 Y (6.2)	2.5	0.016	-0.117	8.11E+06	-3.79E+04
40 oz Biaxial with 0.75 OC	2.5	0.055	-0.082	3.00E+06	-3.36E+04
40 oz Triaxial with 0.75 OC	2.5	0.055	-0.027	1.04E+06	-3.79E+03
40 oz Triaxial with 0.75 OC	2.5	0.055	0.029	1.04E+06	4.15E+03
40 oz Triaxial with 0.75 OC	2.5	0.055	0.084	1.04E+06	1.19E+04
2.1 rov/in - 62Y (2)	2.5	0.014	0.118	7.89E+06	3.26E+04
40 oz Triaxial with 0.75 OC	2.5	0.055	0.153	1.04E+06	2.19E+04
		0.36			**-6.79E+04**
Step 8					
Computation of Bending Stiffness					
Ply	**Width of lamina**	**Thk. Of lamina**	**Z**	**E_x**	**D_f**
	(in)	**(in)**	**(in)**	**(psi)**	**(lbs-in^2)**
40 oz Biaxial with 0.75 OC	2.5	0.055	-0.153	3.00E+06	9.76E+03
2.48 rov/in - 62 Y (6.2)	2.5	0.016	-0.117	8.11E+06	4.45E+03
40 oz Biaxial with 0.75 OC	2.5	0.055	-0.0815	3.00E+06	2.84E+03
40 oz Triaxial with 0.75 OC	2.5	0.055	-0.0265	1.04E+06	1.36E+02
40 oz Triaxial with 0.75 OC	2.5	0.055	0.029	1.04E+06	1.56E+02
40 oz Triaxial with 0.75 OC	2.5	0.055	0.0835	1.04E+06	1.03E+03
2.1 rov/in - 62Y (2)	2.5	0.014	0.118	7.89E+06	3.85E+03
40 oz Triaxial with 0.75 OC	2.5	0.055	0.153	1.04E+06	3.38E+03
					2.56E+04
Step 9					
Bending Stiffness of Section 4	$D_f + A_f e_o^2$	**2.43E+07**			

ANALYSIS OF THE SECOND GENERATION OF COMPONENT					
Approximate Classical Lamination Theory					
Computation of Bending Stiffness					
Step1					
Material Properties					
Elastic constants for E-glass fabric and Matrix					
E_{fiber}	E_{matrix}	G_{fiber}	G_{matrix}	v_{fiber}	v_{matrix}
(psi)	(psi)	(psi)	(psi)		
1.05E+07	7.34E+05	4.18E+06	2.37E+05	0.256	0.549
Step 2					
Fiber Architecture					
Section	**Dimension**				
5	3.6" x 0.33"				
Fiber Architecture	**Thickness**				
40 oz Triaxial with 0.75 OC	0.055				
5.8 rov/in (18.59)	0.057				
40 oz Triaxial with 0.75 OC	0.055				
40 oz Triaxial with 0.75 OC	0.055				
5.8 rov/in (18.59)	0.057				
40 oz Triaxial with 0.75 OC	0.055				
	0.334				
Step 3					
Computation of Fiber Volume Fraction (V_f) of 40 oz of fabric (bi-axial)					
40 oz of fabric has 24 oz at 0^0 and 16 oz at 90^0					
Thk of lamina	**Wt. Of Fabric**	**Wt. Of Fabric**	**Wt.of 1ft^2 Comp.**	**Density of fiber**	
(in.)	**(oz/yd2)**	**(oz/ft2)**	**(lb)**	**(lb/in3)**	
0.0282	24	2.667	0.167	0.092	
0.0188	16	1.778	0.111	0.092	
Volume of fiber	**Volume of composite**	**Fiber Volume fraction (Vf)**	**Matrix Volume fraction (Vm)**		
1.812	4.0608	0.45	0.55		
1.208	2.7072	0.45	0.55		
Computation of Fiber Volume Fraction (V_f) of 40 oz of fabric (triaxial)					
40 oz of fabric has 12 oz at 45^0 12 oz at -45^0 and 16 oz at 90^0					
Thk of lamina	**Wt. Of Fabric**	**Wt. Of Fabric**	**Wt.of 1ft^2 Comp.**	**Density of fiber**	
(in.)	**(oz/yd2)**	**(oz/ft2)**	**(lb)**	**(lb/in3)**	
0.0141	12	1.333	0.083	0.092	
0.0141	12	1.333	0.083	0.092	
0.0188	16	1.778	0.111	0.092	
Volume of fiber	**Volume of composite**	**Fiber Volume fraction (Vf)**	**Matrix Volume fraction (Vm)**		
0.906	2.0304	0.45	0.55		
0.906	2.0304	0.45	0.55		
1.208	2.7072	0.45	0.55		
Computation of Fiber Volume Fraction (V_f) of 0.75 oz of fabric					
Thk of lamina	**Wt. Of Fabric**	**Wt. Of Fabric**	**Wt.of 1ft^2**	**Density of**	
(in.)	**(oz/yd2)**	**(oz/ft2)**	**(lb)**	**(lb/in3)**	
0.008	6.75	0.750	0.047	0.092	

Volume of fiber	**Volume of composite**	**Fiber Volume fraction**	**Matrix Volume fraction**		
0.510	1.152	0.44	0.56		
Computation of Fiber Volume Fraction (V_f) of Rovings					
Rovings	**thickness (in)**	**Yield yards**	**Dia.of rov. (in)**	**Width (in)**	
62Y - 18.59 bundles	0.057	62	0.079	3.21	
62Y - 18.59 bundles	0.057	62	0.079	3.21	
bundles (no:)	**Fiber Volume Fraction (V_f)**	**Matrix Volume Fraction (V_m)**			
18.59	0.49	0.51			
18.59	0.49	0.51			
Step 4					
Computation of Laminae Properties					
Ply	E_{11}	E_{22}	G_{12}	ν_{12}	ν_{21}
0.75 oz OC	5.05E+06	1.25E+06			
40 oz Biaxial					
0^0	5.09E+06	1.25E+06	4.09E+05	0.418	0.103
90^0	5.09E+06	1.25E+06	4.09E+05	0.418	0.103
40 oz Triaxial					
45^0	5.09E+06	1.25E+06	4.09E+05	0.418	0.103
-45^0	5.09E+06	1.25E+06	4.09E+05	0.418	0.103
90^0	5.09E+06	1.25E+06	4.09E+05	0.418	0.103
62Y - 18.59 bundles	5.57E+06	1.36E+06	4.44E+05	0.404	0.099
62Y - 18.59 bundles	5.57E+06	1.36E+06	4.44E+05	0.404	0.099
For 0.75 oz of OC	2.67E+06	2.67E+06	9.43E+05	0.417	0.417
Step 5					
Computation of E_x					
Ply	**Ornt. of fibers (in degrees)**	**Ornt. of fibers (in radians)**	$E_x = E_{11}\cos^4\theta$ **(psi)**		
0.75 oz of OC	0	0.00	2.67E+06		
40 oz Biaxial					
0	0	0.00	5.09E+06		
90	90	1.57	7.17E-59		
40 oz Biaxial with OC					
OC and 0/90 **(the stiffness is distributed in the weight ratios)**			**3.00E+06**		
40 oz Triaxial					
45	45	0.79	1.27E+06		
-45	-45	-0.79	1.27E+06		
90	90	1.57	7.17E-59		
40 oz Triaxial with OC					
OC and 45/-45/90 **(the stiffness is distributed in the weight ratios)**			**1.04E+06**		
62Y - 18.59 bundles	0	0.00	5.57E+06		
62Y - 18.59 bundles	0	0.00	5.57E+06		
Step 6					
Computation of Axial Stiffness					
Ply	**Width of lamina (in)**	**Thk. of lamina (in)**	E_x **(psi)**	A_f **(lbs)**	
40 oz Triaxial with 0.75 OC	3.21	0.055	1.04E+06	1.84E+05	
5.8 rov/in (18.59)	3.21	0.057	5.57E+06	1.02E+06	
40 oz Triaxial with 0.75 OC	3.21	0.055	1.04E+06	1.84E+05	

40 oz Triaxial with 0.75 OC	3.21	0.055	1.04E+06	1.84E+05	
5.8 rov/in (18.59)	3.21	0.057	5.57E+06	1.02E+06	
40 oz Triaxial with 0.75 OC	3.21	0.055	1.04E+06	1.84E+05	
				2.77E+06	
Step 7					
Computation of Extensional Bending Coupling Stiffness					
Ply	**Width of lamina**	**Thk. of lamina**	**Z**	**E_x**	**B_f**
	(in)	**(in)**	**(in)**	**(psi)**	**(lbs-in)**
40 oz Biaxial with 0.75 OC	3.21	0.055	-0.139	1.04E+06	-2.55E+04
5.8 rov/in (18.59)	3.21	0.057	-0.084	5.57E+06	-8.55E+04
40 oz Triaxial with 0.75 OC	3.21	0.055	-0.027	1.04E+06	-4.96E+03
40 oz Triaxial with 0.75 OC	3.21	0.055	0.027	1.04E+06	4.96E+03
5.8 rov/in (18.59)	3.21	0.057	0.084	5.57E+06	8.55E+04
40 oz Triaxial with 0.75 OC	3.21	0.055	0.139	1.04E+06	2.55E+04
					0.00E+00
Step 8					
Computation of Bending Stiffness					
Ply	**Width of lamina**	**Thk. Of lamina**	**Z**	**E_x**	**D_f**
	(in)	**(in)**	**(in)**	**(psi)**	**(lbs-in^2)**
40 oz Triaxial with 0.75 OC	3.21	0.055	-0.139	1.04E+06	3.59E+03
5.8 rov/in (18.59)	3.21	0.057	-0.084	5.57E+06	7.46E+03
40 oz Triaxial with 0.75 OC	3.21	0.055	-0.027	1.04E+06	1.80E+02
40 oz Triaxial with 0.75 OC	3.21	0.055	0.027	1.04E+06	1.80E+02
5.8 rov/in (18.59)	3.21	0.057	0.084	5.57E+06	7.46E+03
40 oz Triaxial with 0.75 OC	3.21	0.055	0.139	1.04E+06	3.59E+03
					2.25E+04
Step 9					
Bending Stiffness of Section 5	$D_f + Ae_o^2$	**2.25E+04**			

ANALYSIS OF THE SECOND GENERATION OF COMPONENT

Approximate Classical Lamination Theory

Computation of Bending Stiffness

Step1
Material Properties
Elastic constants for E-glass fabric and Matrix

E_{fiber} (psi)	E_{matrix} (psi)	G_{fiber} (psi)	G_{matrix} (psi)	v_{fiber}	v_{matrix}
1.05E+07	7.34E+05	4.18E+06	2.37E+05	0.256	0.549

Step 2
Fiber Architecture

Section	Dimension
6	3.87" x 0.419"

Fiber Architecture	Thickness
40 oz Triaxial with 0.75 OC	0.055
5.8 rov/in (22.4)	0.058
40 oz Triaxial with 0.75 OC	0.055
40 oz Triaxial with 0.75 OC	0.055
40 oz Triaxial with 0.75 OC	0.055
40 oz Triaxial with 0.75 OC	0.055
3.1 rov/in (11.9)	0.031
40 oz Triaxial with 0.75 OC	0.055
	0.419

Step 3
Computation of Fiber Volume Fraction (V_f) of 40 oz of fabric (bi-axial)
40 oz of fabric has 24 oz at 0^0 and 16 oz at 90^0

Thk of lamina (in.)	Wt. Of Fabric (oz/yd2)	Wt. Of Fabric (oz/ft2)	Vt.of 1ft^2 Com (lb)	Density of fiber (lb/in3)
0.0282	24	2.667	0.167	0.092
0.0188	16	1.778	0.111	0.092

Volume of fiber	Volume of composite	Fiber Volume fraction (Vf)	Matrix Volume fraction (Vm)
1.812	4.0608	0.45	0.55
1.208	2.7072	0.45	0.55

Computation of Fiber Volume Fraction (V_f) of 40 oz of fabric (triaxial)
40 oz of fabric has 12 oz at 45^0 12 oz at -45^0 and 16 oz at 90^0

Thk of lamina (in.)	Wt. Of Fabric (oz/yd2)	Wt. Of Fabric (oz/ft2)	Vt.of 1ft^2 Com (lb)	Density of fiber (lb/in3)
0.0141	12	1.333	0.083	0.092
0.0141	12	1.333	0.083	0.092
0.0188	16	1.778	0.111	0.092

Volume of fiber	Volume of composite	Fiber Volume fraction (Vf)	Matrix Volume fraction (Vm)
0.906	2.0304	0.45	0.55
0.906	2.0304	0.45	0.55
1.208	2.7072	0.45	0.55

Computation of Fiber Volume Fraction (V_f) of 0.75 oz of fabric

Thk of lamina (in.)	Wt. Of Fabric (oz/yd2)	Wt. Of Fabric (oz/ft2)	Wt.of 1ft^2 (lb)	Density of (lb/in3)
0.008	6.75	0.750	0.047	0.092

Volume of fiber	Volume of composite	Fiber Volume fraction	Matrix Volume fraction
0.510	1.152	0.44	0.56

Computation of Fiber Volume Fraction (V_f) of Rovings

Rovings	thickness (in)	Yield yards	Dia.of rov. (in)	Width (in)
62Y - 22.4 bundles	0.058	62	0.079	3.87
62Y - 11.9 bundles	0.031	62	0.079	3.87

bundles (no:)	Fiber Volume Fraction (V_f)	Matrix Volume Fraction (V_m)
22.4	0.49	0.51
11.9	0.48	0.52

Step 4

Computation of Laminae Properties

Ply	E_{11}	E_{22}	G_{12}	ν_{12}	ν_{21}
0.75 oz OC	5.05E+06	1.25E+06			
40 oz Biaxial					
0^0	5.09E+06	1.25E+06	4.09E+05	0.418	0.103
90^0	5.09E+06	1.25E+06	4.09E+05	0.418	0.103
40 oz Triaxial					
45^0	5.09E+06	1.25E+06	4.09E+05	0.418	0.103
-45^0	5.09E+06	1.25E+06	4.09E+05	0.418	0.103
90^0	5.09E+06	1.25E+06	4.09E+05	0.418	0.103
62Y - 22.4 bundles	5.48E+06	1.34E+06	4.38E+05	0.406	0.099
62Y - 11.9 bundles	5.45E+06	1.33E+06	4.35E+05	0.132	0.032
For 0.75 oz of OC	2.67E+06	2.67E+06	9.43E+05	0.417	0.417

Step 5

Computation of E_x

Ply	Ornt. of fibers (in degrees)	Ornt. of fibers (in radians)	$E_x = E_{11}Cos^4\theta$ (psi)	$G_x = E_{11}sin^2\theta\ cos^2\theta + G_{12}(sin^2\theta - cos^2\theta)^2$ (psi)
0.75 oz of OC	0	0.00	2.67E+06	9.43E+05
40 oz Triaxial				
45	45	0.79	1.27E+06	1.27E+06
-45	-45	-0.79	1.27E+06	1.27E+06
90	90	1.57	7.17E-59	4.09E+05
40 oz Triaxial with OC				
OC and 45/-45/90 **(the stiffness is distributed in the weight**			**1.04E+06**	**9.30E+05**
62Y - 22.4bundles	0	0.00	5.48E+06	4.38E+05
62Y - 11.9 bundles	0	0.00	5.45E+06	4.35E+05

Step 6					
Computation of Axial Stiffness					
Ply	**Width of lamina**	**Thk. of lamina**	**E_x**	**A_f**	
	(in)	**(in)**	**(psi)**	**(lbs)**	
40 oz Triaxial with 0.75 OC	3.87	0.055	1.04E+06	2.21E+05	
5.8 rov/in (22.4)	3.87	0.058	5.48E+06	1.23E+06	
40 oz Triaxial with 0.75 OC	3.87	0.055	1.04E+06	2.21E+05	
40 oz Triaxial with 0.75 OC	3.87	0.055	1.04E+06	2.21E+05	
40 oz Triaxial with 0.75 OC	3.87	0.055	1.04E+06	2.21E+05	
40 oz Triaxial with 0.75 OC	3.87	0.055	1.04E+06	2.21E+05	
3.1 rov/in (11.9)	3.87	0.031	5.45E+06	6.54E+05	
40 oz Triaxial with 0.75 OC	3.87	0.055	1.04E+06	2.21E+05	
				3.21E+06	
Step 7					
Computation of Extensional Bending Coupling Stiffness					
Ply	**Width of lamina**	**Thk. of lamina**	**Z**	**E_x**	**B_f**
	(in)	**(in)**	**(in)**	**(psi)**	**(lbs-in)**
40 oz Triaxial with 0.75 OC	3.87	0.055	-0.182	1.04E+06	-4.03E+04
5.8 rov/in (22.4)	3.87	0.058	-0.125	5.48E+06	-1.54E+05
40 oz Triaxial with 0.75 OC	3.87	0.055	-0.069	1.04E+06	-1.53E+04
40 oz Triaxial with 0.75 OC	3.87	0.055	-0.014	1.04E+06	-3.10E+03
40 oz Triaxial with 0.75 OC	3.87	0.055	0.041	1.04E+06	9.07E+03
40 oz Triaxial with 0.75 OC	3.87	0.055	0.096	1.04E+06	2.12E+04
3.1 rov/in (11.9)	3.87	0.031	0.139	5.45E+06	9.09E+04
40 oz Triaxial with 0.75 OC	3.87	0.055	0.182	1.04E+06	4.03E+04
					-5.09E+04
Step 8					
Computation of Bending Stiffness					
Ply	**Width of lamina**	**Thk. Of lamina**	**Z**	**E_x**	**D_f**
	(in)	**(in)**	**(in)**	**(psi)**	**(lbs-in^2)**
40 oz Triaxial with 0.75 OC	3.87	0.055	-0.182	1.04E+06	2.09E+05
5.8 rov/in (22.4)	3.87	0.058	-0.125	5.48E+06	1.16E+06
40 oz Triaxial with 0.75 OC	3.87	0.055	-0.069	1.04E+06	2.07E+05
40 oz Triaxial with 0.75 OC	3.87	0.055	-0.014	1.04E+06	2.07E+05
40 oz Triaxial with 0.75 OC	3.87	0.055	0.041	1.04E+06	2.07E+05
40 oz Triaxial with 0.75 OC	3.87	0.055	0.096	1.04E+06	2.08E+05
3.1 rov/in (11.9)	3.87	0.031	0.139	5.45E+06	6.15E+05
40 oz Triaxial with 0.75 OC	3.87	0.055	0.182	1.04E+06	2.09E+05
					3.02E+06
Step 9					
Bending Stiffness of Sectio	$D_f + A_f e_o^2$	**1.50E+07**			
Computation of Shear Stiffness					
Ply	**Width of lamina**	**Thk. of lamina**	**G_x**	**G_w**	
	(in)	**(in)**	**(psi)**	**(lbs)**	
40 oz Triaxial with 0.75 OC	3.87	0.055	9.30E+05	1.98E+05	
5.8 rov/in (22.4)	3.87	0.058	4.38E+05	9.82E+04	
40 oz Triaxial with 0.75 OC	3.87	0.055	9.30E+05	1.98E+05	
40 oz Triaxial with 0.75 OC	3.87	0.055	9.30E+05	1.98E+05	
40 oz Triaxial with 0.75 OC	3.87	0.055	9.30E+05	1.98E+05	
40 oz Triaxial with 0.75 OC	3.87	0.055	9.30E+05	1.98E+05	
3.1 rov/in (11.9)	3.87	0.031	4.35E+05	5.22E+04	
40 oz Triaxial with 0.75 OC	3.87	0.055	9.30E+05	1.98E+05	
				1.34E+06	

Computation of Bending Stiffness Of The Component					
Section	A	D	NO:	EI for each sectioi	Net EI
	(lbs)	(lbs-in^2)		(lbs-in^2)	(lbs-in^2)
1	1.61E+07	4.32E+05	2	2.21E+08	4.42E+08
2	6.82E+06	2.45E+05	2	9.15E+07	1.83E+08
3	3.16E+06	2.44E+04	2	4.65E+07	9.30E+07
4	2.00E+06	2.56E+04	2	2.44E+07	4.89E+07
5	2.77E+06	2.25E+04	1	2.25E+04	2.25E+04
6	3.21E+06	3.02E+06	4	1.51E+07	6.02E+07
					8.27E+08
Bending Stiffness of the component			8.27E+08		
Computation of Shear Stiffness of the Component					
Section	G_w	No:	Net G_w		
6	1.34E+06	4	5.36E+06		
Shear Stiffness of the component			5.36E+06		

APPENDIX C

To evaluate local buckling of web, stiffness values of web and flange are requried.
This appendix show the computation of the stiffness values for web and flange.
The steps are carried out in the same way as shown in Appendix B

Computation of stiffness in the web

Micromechanic and Macromechanic Approach

Step1

Material Properties

Elastic constants for E-glass fabric and Matrix

E_{fiber} (psi)	E_{matrix} (psi)	G_{fiber} (psi)	G_{matrix} (psi)	v_{fiber}	v_{matrix}
1.05E+07	7.34E+05	4.18E+06	2.37E+05	0.256	0.549

Step 2

Fiber Architecture

Section	Dimension
6	3.87" x 0.419"

Fiber Architecture	Thickness
40 oz Triaxial with 0.75 OC	0.055
5.8 rov/in (22.4)	0.058
40 oz Triaxial with 0.75 OC	0.055
40 oz Triaxial with 0.75 OC	0.055
40 oz Triaxial with 0.75 OC	0.055
40 oz Triaxial with 0.75 OC	0.055
3.1 rov/in (11.9)	0.031
40 oz Triaxial with 0.75 OC	0.055
	0.419

Step 3

Computation of Fiber Volume Fraction (V_f) of 40 oz of fabric (triaxial)

40 oz of fabric has 12 oz at 45⁰ 12 oz at -45⁰ and 16 oz at 90⁰

Thk of lamina (in.)	Wt. Of Fabric (oz/yd2)	Wt. Of Fabric (oz/ft2)	Wt.of 1ft² Com (lb)	density of fiber (lb/in3)
0.0141	12	1.333	0.083	0.092
0.0141	12	1.333	0.083	0.092
0.0188	16	1.778	0.111	0.092

Volume of fiber	Volume of composite	Fiber Volume fraction (Vf)	Matrix Volume fraction (Vm)
0.906	2.0304	0.45	0.55
0.906	2.0304	0.45	0.55
1.208	2.7072	0.45	0.55

Computation of Fiber Volume Fraction (V_f) of 0.75 oz of fabric

Thk of lamina (in.)	Wt. Of Fabric (oz/yd2)	Wt. Of Fabric (oz/ft2)	Wt.of 1ft² (lb)	Density of (lb/in3)
0.008	6.75	0.750	0.047	0.092

Volume of fiber	Volume of composite	Fiber Volume fraction	Matrix Volume fraction
0.510	1.152	0.44	0.56

Computation of Fiber Volume Fraction (V_f) of Rovings					
Rovings	**thickness**	**Yield**	**Dia.of rov.**	**Width**	
	(in)	**yards**	**(in)**	**(in)**	
62Y - 22.4 bundles	0.058	62	0.079	3.87	
62Y - 11.9 bundles	0.031	62	0.079	3.87	
bundles	**Fiber Volume**	**latrix Volume**			
(no:)	**Fraction (V_f)**	**Fraction (V_m)**			
22.4	0.49	0.51			
11.9	0.48	0.52			
Step 4					
Computation of Laminae Properties					
Ply	**E_{11}**	**E_{22}**	**G_{12}**	**v_{12}**	**v_{21}**
0.75 oz OC	5.05E+06	1.25E+06			
40 oz Triaxial					
45^0	5.09E+06	1.25E+06	4.09E+05	0.418	0.103
$\_45^0$	5.09E+06	1.25E+06	4.09E+05	0.418	0.103
90^0	5.09E+06	1.25E+06	4.09E+05	0.418	0.103
62Y - 22.4 bundles	5.48E+06	1.34E+06	4.38E+05	0.406	0.099
62Y - 11.9 bundles	5.45E+06	1.33E+06	4.35E+05	0.407	0.100
For 0.75 oz of OC	2.67E+06	2.67E+06	9.43E+05	0.417	0.417
Ply	**E_{11}**	**E_{22}**	**G_{12}**	**v_{12}**	**v_{21}**
0.75 oz OC	2.67E+06	2.67E+06	9.43E+05	0.417	0.417
40 oz Triaxial					
45^0	5.09E+06	1.25E+06	4.09E+05	0.418	0.103
$\_45^0$	5.09E+06	1.25E+06	4.09E+05	0.418	0.103
90^0	5.09E+06	1.25E+06	4.09E+05	0.418	0.103
62Y - 22.4 bundles	5.48E+06	1.34E+06	4.38E+05	0.406	0.099
62Y - 11.9 bundles	5.45E+06	1.33E+06	4.35E+05	0.407	0.100
Step 5					
Caluculation of In-Plane Reduced Stiffness Matrix					
Ply	**δ**				
0.75 oz OC	0.826				
40 oz Triaxial					
45^0	0.957				
$\_45^0$	0.957				
90^0	0.957				
62Y - 22.4 bundles	0.960				
62Y - 23.9 bundles	0.959				
Fiber Architecture	**Q_{11}**	**Q_{12}**	**Q_{21}**	**Q_{22}**	**Q_{66}**
0.75 oz OC	3.24E+06	1.35E+06	1.35E+06	3.24E+06	9.43E+05
40 oz Triaxial					
45^0	5.32E+06	5.48E+05	5.48E+05	1.31E+06	4.09E+05
$\_45^0$	5.32E+06	5.48E+05	5.48E+05	1.31E+06	4.09E+05
90^0	5.32E+06	5.48E+05	5.48E+05	1.31E+06	4.09E+05
62Y - 22.4 bundles	5.71E+06	5.67E+05	5.67E+05	1.40E+06	4.38E+05
62Y -11.9 bundles	5.68E+06	5.66E+05	5.66E+05	1.39E+06	4.35E+05

Step 5					
Calculation of Transformed Reduced Stiffness Matrix					
Fiber Architecture	**Orient. of fabric**	**Orient. of fabric**			
	(degrees)	**(Radians)**			
0.75 oz OC	0	0.00			
40 oz Triaxial					
45^0	45	0.79			
$\_45^0$	-45	-0.79			
90^0	90	1.57			
62Y - 22.4 bundles	0	0.00			
62Y - 11.9 bundles	0	0.00			
Fiber Architecture	Q_{b11}	Q_{b12}	Q_{b21}		
0.75 oz OC	3.24E+06	1.35E+06	1.35E+06		
40 oz Triaxial					
45^0	2.34E+06	1.52E+06	1.52E+06		
$\_45^0$	2.34E+06	1.52E+06	1.52E+06		
90^0	1.31E+06	5.48E+05	5.48E+05		
62Y - 22.4 bundles	5.71E+06	5.67E+05	5.67E+05		
62Y - 11.9 bundles	5.68E+06	5.66E+05	5.66E+05		
Fiber Architecture	Q_{b22}	Q_{b16}	Q_{b26}	Q_{b66}	
0.75 oz OC	3.24E+06	0.00E+00	0.00E+00	9.43E+05	
40 oz Triaxial					
45^0	2.34E+06	1.00E+06	1.00E+06	1.38E+06	
$\_45^0$	2.34E+06	-1.00E+06	-1.00E+06	1.38E+06	
90^0	5.32E+06	3.39E-12	2.42E-10	4.09E+05	
62Y - 22.4 bundles	1.40E+06	0.00E+00	0.00E+00	4.38E+05	
62Y - 11.9 bundles	1.39E+06	0.00E+00	0.00E+00	4.35E+05	
Step 6					
Computation of Final Trasformed Stiffness Matrix					
6.75/46.75(Q_b of OC) + 12/46.75(Q_b of $45^{0)}$ + 12/46.75(Q_b of -45^0) + 16/46.75(Q_b of 90^0)					
Fiber Architecture	Q_{b11}	Q_{b12}	Q_{b21}		
40 oz Triaxial	2.12E+06	1.16E+06	1.16E+06		
62Y - 22.4 bundles	5.71E+06	5.67E+05	5.67E+05		
62Y - 11.9 bundles	5.68E+06	5.66E+05	5.66E+05		
Fiber Architecture	Q_{b22}	Q_{b16}	Q_{b26}	Q_{b66}	
40 oz Triaxial	3.49E+06	1.16E-12	8.29E-11	9.87E+05	
62Y - 22.4 bundles	1.40E+06	0.00E+00	0.00E+00	4.38E+05	
62Y - 11.9 bundles	1.39E+06	0.00E+00	0.00E+00	4.35E+05	
Step 7					
Computation of Stiffness Matrix					
Distance from mid-surface of lamiante to each laminae (z)					
Ply	**z (in)**				
40 oz Triaxial with 0.75 OC	-0.182				
5.8 rov/in (22.4)	-0.125				
40 oz Triaxial with 0.75 OC	-0.069				
40 oz Triaxial with 0.75 OC	-0.014				
40 oz Triaxial with 0.75 OC	0.041				
40 oz Triaxial with 0.75 OC	0.096				
3.1 rov/in (11.9)	0.139				
40 oz Triaxial with 0.75 OC	0.182				

Computation of extensional stiffness					
Fiber architecture	**Thk.of lamiane**	**A_{11}**	**A_{12}**	**A_{21}**	
	(in)	**(lbs/in)**	**(lbs/in)**	**(lbs/in)**	
40 oz Triaxial with 0.75 OC	0.055	1.16E+05	6.40E+04	6.40E+04	
5.8 rov/in (22.4)	0.058	3.31E+05	3.29E+04	3.29E+04	
40 oz Triaxial with 0.75 OC	0.055	1.16E+05	6.40E+04	6.40E+04	
40 oz Triaxial with 0.75 OC	0.055	1.16E+05	6.40E+04	6.40E+04	
40 oz Triaxial with 0.75 OC	0.055	1.16E+05	6.40E+04	6.40E+04	
40 oz Triaxial with 0.75 OC	0.055	1.16E+05	6.40E+04	6.40E+04	
3.1 rov/in (11.9)	0.031	1.76E+05	1.75E+04	1.75E+04	
40 oz Triaxial with 0.75 OC	0.055	1.16E+05	6.40E+04	6.40E+04	
		1.21E+06	**4.35E+05**	**4.35E+05**	
Fiber architecture	**A_{22}**	**A_{16}**	**A_{26}**	**A_{66}**	
	(lbs/in)	**(lbs/in)**	**(lbs/in)**	**(lbs/in)**	
40 oz Triaxial with 0.75 OC	1.92E+05	6.39E-14	4.56E-12	5.43E+04	
5.8 rov/in (22.4)	8.10E+04	0.00E+00	0.00E+00	2.54E+04	
40 oz Triaxial with 0.75 OC	1.92E+05	6.39E-14	4.56E-12	5.43E+04	
40 oz Triaxial with 0.75 OC	1.92E+05	6.39E-14	4.56E-12	5.43E+04	
40 oz Triaxial with 0.75 OC	1.92E+05	6.39E-14	4.56E-12	5.43E+04	
40 oz Triaxial with 0.75 OC	1.92E+05	6.39E-14	4.56E-12	5.43E+04	
3.1 rov/in (11.9)	4.31E+04	0.00E+00	0.00E+00	1.35E+04	
40 oz Triaxial with 0.75 OC	1.92E+05	6.39E-14	4.56E-12	5.43E+04	
	1.28E+06	**3.83E-13**	**2.74E-11**	**3.64E+05**	
Computation of bending-extension coupling stiffness					
Fiber architecture	**Thk.of lamiane**	**Z**	**B_{11}**	**B_{12}**	**B_{21}**
	(in)	**(in)**	**(lbs)**	**(lbs)**	**(lbs)**
40 oz Triaxial with 0.75 OC	0.055	-0.1820	-2.12E+04	-1.17E+04	-1.17E+04
5.8 rov/in (22.4)	0.058	-0.1250	-4.14E+04	-4.11E+03	-4.11E+03
40 oz Triaxial with 0.75 OC	0.055	-0.0690	-8.04E+03	-4.42E+03	-4.42E+03
40 oz Triaxial with 0.75 OC	0.055	-0.0140	-1.63E+03	-8.97E+02	-8.97E+02
40 oz Triaxial with 0.75 OC	0.055	0.0410	4.78E+03	2.63E+03	2.63E+03
40 oz Triaxial with 0.75 OC	0.055	0.0960	1.12E+04	6.15E+03	6.15E+03
3.1 rov/in (11.9)	0.031	0.1390	2.45E+04	2.44E+03	2.44E+03
40 oz Triaxial with 0.75 OC	0.055	0.1820	2.12E+04	1.17E+04	1.17E+04
			-1.06E+04	**1.78E+03**	**1.78E+03**

Fiber architecture	B_{22}	B_{16}	B_{26}	B_{66}	
	(lbs)	(lbs)	(lbs)	(lbs)	
40 oz Triaxial with 0.75 OC	-3.49E+04	-1.16E-14	-8.30E-13	-9.88E+03	
5.8 rov/in (22.4)	-1.01E+04	0.00E+00	0.00E+00	-3.17E+03	
40 oz Triaxial with 0.75 OC	-1.32E+04	-4.41E-15	0.00E+00	-1.65E+03	
40 oz Triaxial with 0.75 OC	-1.07E+03	0.00E+00	0.00E+00	-3.37E+02	
40 oz Triaxial with 0.75 OC	3.13E+03	0.00E+00	0.00E+00	9.82E+02	
40 oz Triaxial with 0.75 OC	1.84E+04	6.13E-15	4.38E-13	5.21E+03	
3.1 rov/in (11.9)	5.99E+03	0.00E+00	0.00E+00	1.88E+03	
40 oz Triaxial with 0.75 OC	-3.49E+04	-1.16E-14	-8.30E-13	-9.88E+03	
	-6.68E+04	**-2.15E-14**	**-1.22E-12**	**-6.97E+03**	
Computation of bending-extension coupling stiffness					
Fiber architecture	**Thk.of lamiane**	**Z**	D_{11}	D_{12}	D_{21}
	(in)	(in)	(lbs-in)	(lbs-in)	(lbs-in)
40 oz Triaxial with 0.75 OC	0.055	-0.1820	3.89E+03	2.14E+03	2.14E+03
5.8 rov/in (22.4)	0.058	-0.1250	5.27E+03	5.23E+02	5.23E+02
40 oz Triaxial with 0.75 OC	0.055	-0.0690	5.84E+02	3.21E+02	3.21E+02
40 oz Triaxial with 0.75 OC	0.055	-0.0140	5.22E+01	2.87E+01	2.87E+01
40 oz Triaxial with 0.75 OC	0.055	0.0410	2.25E+02	1.24E+02	1.24E+02
40 oz Triaxial with 0.75 OC	0.055	0.0960	1.10E+03	6.06E+02	6.06E+02
3.1 rov/in (11.9)	0.031	0.1390	3.42E+03	3.40E+02	3.40E+02
40 oz Triaxial with 0.75 OC	0.055	0.1820	3.89E+03	2.14E+03	2.14E+03
			1.84E+04	**6.22E+03**	**6.22E+03**
Fiber architecture	D_{22}	D_{16}	D_{26}	D_{66}	
	(lbs-in)	(lbs-in)	(lbs-in)	(lbs-in)	
40 oz Triaxial with 0.75 OC	6.41E+03	2.13E-15	1.52E-13	1.81E+03	
5.8 rov/in (22.4)	1.29E+03	0.00E+00	0.00E+00	4.04E+02	
40 oz Triaxial with 0.75 OC	9.62E+02	3.20E-16	2.29E-14	2.72E+02	
40 oz Triaxial with 0.75 OC	8.60E+01	2.86E-17	2.04E-15	2.43E+01	
40 oz Triaxial with 0.75 OC	3.71E+02	1.24E-16	8.81E-15	1.05E+02	
40 oz Triaxial with 0.75 OC	1.82E+03	6.05E-16	4.32E-14	5.14E+02	
3.1 rov/in (11.9)	8.35E+02	0.00E+00	0.00E+00	2.62E+02	
40 oz Triaxial with 0.75 OC	6.41E+03	2.13E-15	1.52E-13	1.81E+03	
	1.82E+04	**5.34E-15**	**3.81E-13**	**5.20E+03**	
Step 8					
Computation of in-plane moduli of laminate (E_x^t)					
$E_x^t = [(A_{11}A_{22})-A^2_{12}]/(tA_{22})$	**2.53E+06**				
$E_Y^t = [(A_{11}A_{22})-A^2_{12}]/(tA_{11})$	**2.67E+06**				
$G_{xy} = A_{66}/t$	**8.70E+05**				
$nxy = A_{12}/A_{22}$	**0.341**				
Computation of bending moduli of laminate (Ex^b)					
$Ex^b = [12(D_{11}D_{22}-D_{12}^2)]/(t^3D_{22}$	**2.66E+06**				
E_Y^b =[12(D11D22-D122)]/(t3l	**2.62E+06**				
$G_{xy}^b = 12D_{66}/t^3$	**8.49E+05**				
$nxy = D_{12}/D_{22}$	**0.342**				

Computation of Stiffness in the Flange					
Micromechanic and Macromechanic Approach					
Step1					
Material Properties					
Elastic constants for E-glass fabric and Matrix					
E_{fiber}	E_{matrix}	G_{fiber}	G_{matrix}	ν_{fiber}	ν_{matrix}
(psi)	**(psi)**	**(psi)**	**(psi)**		
1.05E+07	7.34E+05	4.18E+06	2.37E+05	0.256	0.549
Step 2					
Fiber Architecture					
Section	**Dimension**				
1	**6.435" x 0.601"**				
Fiber Architecture	**Thickness**				
40 oz Biaxial with 0.75 OC	0.055				
10.38 rov/in - 62 Y (66.79)	0.104				
40 oz Biaxial with 0.75 OC	0.055				
8.5 rov/in - 62 Y (54.69)	0.085				
40 oz Biaxial with 0.75 OC	0.055				
2.48 rov/in - 62Y (15.96)	0.025				
40 oz Biaxial with 0.75 OC	0.055				
5.16 rov/in - 62 Y (33.20)	0.052				
3 rov/in - 62 Y (19.3)	0.03				
3 rov/in - 62 Y (19.3)	0.03				
40 oz Triaxial with 0.75 OC	0.055				
Total thickness of Section 1	**0.601**				
Step 3					
Computation of Fiber Volume Fraction (V_f) of 40 oz of fabric (bi-axial)					
40 oz of fabric has 24 oz at 0° and 16 oz at 90°					
Thk of lamina	**Wt. Of Fabric**	**Wt. Of Fabric**	**Wt.of 1ft² Comp**	**Density of fiber**	
(in.)	**(oz/yd2)**	**(oz/ft2)**	**(lb)**	**(lb/in3)**	
0.0282	24	2.667	0.167	0.092	
0.0188	16	1.778	0.111	0.092	
Volume of	**Volume of**	**Fiber Volume**	**Matrix Volume**		
fiber	**composite**	**fraction (Vf)**	**fraction (Vm)**		
1.812	4.0608	0.45	0.55		
1.208	2.7072	0.45	0.55		
Computation of Fiber Volume Fraction (V_f) of 40 oz of fabric (triaxial)					
40 oz of fabric has 12 oz at 45° 12 oz at -45° and 16 oz at 90°					
Thk of lamina	**Wt. Of Fabric**	**Wt. Of Fabric**	**Wt.of 1ft² Comp**	**Density of fiber**	
(in.)	**(oz/yd2)**	**(oz/ft2)**	**(lb)**	**(lb/in3)**	
0.0141	12	1.333	0.083	0.092	
0.0141	12	1.333	0.083	0.092	
0.0188	16	1.778	0.111	0.092	
Volume of	**Volume of**	**Fiber Volume**	**Matrix Volume**		
fiber	**composite**	**fraction (Vf)**	**fraction (Vm)**		
0.906	2.0304	0.45	0.55		
0.906	2.0304	0.45	0.55		
1.208	2.7072	0.45	0.55		

Computation of Fiber Volume Fraction (V_f) of 0.75 oz of fabric					
Thk of lamina	**Wt. Of Fabric**	**Wt. Of Fabric**	**Wt.of 1ft^2**	**Density of**	
(in.)	**(oz/yd2)**	**(oz/ft2)**	**(lb)**	**(lb/in3)**	
0.008	6.75	0.750	0.047	0.092	
Volume of fiber	**Volume of composite**	**Fiber Volume fraction**	**Matrix Volume fraction**		
0.510	1.152	0.44	0.56		
Computation of Fiber Volume Fraction (V_f) of Rovings					
Rovings	**thickness**	**Yield**	**Dia.of rov.**	**Width**	
	(in)	**yards**	**(in)**	**(in)**	
62Y - 66.79 bundles	0.104	62	0.079	6.435	
62Y - 54.69 bundles	0.085	62	0.079	6.435	
62Y - 15.9 bundles	0.025	62	0.079	6.435	
62Y - 33.20 bundles	0.052	62	0.079	6.435	
62Y - 19.3 bundles	0.030	62	0.079	6.435	
62Y - 19.3 bundles	0.030	62	0.079	6.435	
bundles	**Fiber Volume**	**Matrix Volume**			
(no:)	**Fraction (V_f)**	**Fraction (V_m)**			
66.79	0.49	0.51			
54.69	0.49	0.51			
15.96	0.49	0.51			
33.2	0.49	0.51			
19.3	0.49	0.51			
19.3	0.49	0.51			
Step 4					
Computation of Laminae Properties					
Ply	**E_{11}**	**E_{22}**	**G_{12}**	**v_{12}**	**v_{21}**
0.75 oz CSM	5.05E+06	1.25E+06			
40 oz Biaxial					
0^0	5.09E+06	1.25E+06	4.09E+05	0.418	0.103
90^0	5.09E+06	1.25E+06	4.09E+05	0.418	0.103
40 oz Triaxial					
45^0	5.09E+06	1.25E+06	4.09E+05	0.418	0.103
_45^0	5.09E+06	1.25E+06	4.09E+05	0.418	0.103
90^0	5.09E+06	1.25E+06	4.09E+05	0.418	0.103
62Y - 66.79 bundles	5.48E+06	1.34E+06	4.38E+05	0.406	0.099
62Y - 54.69 bundles	5.49E+06	1.34E+06	4.38E+05	0.406	0.099
62Y - 15.9 bundles	5.52E+06	1.35E+06	4.41E+05	0.405	0.099
62Y - 33.2 bundles	5.48E+06	1.34E+06	4.38E+05	0.406	0.099
62Y - 19.3 bundles	5.49E+06	1.34E+06	4.38E+05	0.406	0.099
62Y - 19.3 bundles	5.49E+06	1.34E+06	4.38E+05	0.406	0.099
For 0.75 oz of CSM	2.67E+06	2.67E+06	9.43E+05	0.417	0.417
Ply	**E_{11}**	**E_{22}**	**G_{12}**	**v_{12}**	**v_{21}**
0.75 oz OC	2.67E+06	2.67E+06	9.43E+05	0.417	0.099
40 oz Biaxial					
0^0	5.09E+06	1.25E+06	4.09E+05	0.418	0.103
90^0	5.09E+06	1.25E+06	4.09E+05	0.418	0.103

40 oz Triaxial					
45^0	5.09E+06	1.25E+06	4.09E+05	0.418	0.103
$\_45^0$	5.09E+06	1.25E+06	4.09E+05	0.418	0.103
90^0	5.09E+06	1.25E+06	4.09E+05	0.418	0.103
62Y - 66.79 bundles	5.48E+06	1.34E+06	4.38E+05	0.406	0.099
62Y - 54.69 bundles	5.49E+06	1.34E+06	4.38E+05	0.406	0.099
62Y - 15.9 bundles	5.52E+06	1.35E+06	4.41E+05	0.405	0.099
62Y - 33.2 bundles	5.48E+06	1.34E+06	4.38E+05	0.406	0.099
62Y - 19.3 bundles	5.49E+06	1.34E+06	4.38E+05	0.406	0.099
62Y - 19.3 bundles	5.49E+06	1.34E+06	4.38E+05	0.406	0.099
Step 5					
Caluculation of In-Plane Reduced Stiffness Matrix					
Ply	**δ**				
0.75 oz OC	0.959				
40 oz Biaxial					
0^0	0.957				
90^0	0.957				
40 oz Triaxial					
45^0	0.957				
$\_45^0$	0.957				
90^0	0.957				
62Y - 66.79 bundles	0.960				
62Y - 54.69 bundles	0.960				
62Y - 15.9 bundles	0.960				
62Y - 33.2 bundles	0.960				
62Y - 19.3 bundles	0.960				
62Y - 19.3 bundles	0.960				
Fiber Architecture	**Q_{11}**	**Q_{12}**	**Q_{21}**	**Q_{22}**	**Q_{66}**
0.75 oz OC	2.79E+06	1.16E+06	1.16E+06	2.79E+06	9.43E+05
40 oz Biaxial					
0^0	5.32E+06	5.48E+05	5.48E+05	1.31E+06	4.09E+05
90^0	5.32E+06	5.48E+05	5.48E+05	1.31E+06	4.09E+05
40 oz Triaxial					
45^0	5.32E+06	5.48E+05	5.48E+05	1.31E+06	4.09E+05
$\_45^0$	5.32E+06	5.48E+05	5.48E+05	1.31E+06	4.09E+05
90^0	5.32E+06	5.48E+05	5.48E+05	1.31E+06	4.09E+05
62Y - 66.79 bundles	5.71E+06	5.67E+05	5.67E+05	1.40E+06	4.38E+05
62Y - 54.69 bundles	5.72E+06	5.68E+05	5.68E+05	1.40E+06	4.38E+05
62Y - 15.9 bundles	5.75E+06	5.69E+05	5.69E+05	1.40E+06	4.41E+05
62Y - 33.2 bundles	5.71E+06	5.67E+05	5.67E+05	1.40E+06	4.38E+05
62Y - 19.3 bundles	5.72E+06	5.68E+05	5.68E+05	1.40E+06	4.38E+05
62Y - 19.3 bundles	5.72E+06	5.68E+05	5.68E+05	1.40E+06	4.38E+05
Step 5					
Calculation of Transformed Reduced Stiffness Matrix					
Fiber Architecture	**Orient. of fabric**	**Orient. of fabric**			
	(degrees)	**(Radians)**			
0.75 oz OC	0	0.00			
40 oz Biaxial					
0^0	0	0.00			
90^0	90	1.57			
40 oz Triaxial		0.00			
45^0	45	0.79			
$\_45^0$	-45	-0.79			
90^0	90	1.57			
62Y - 66.79 bundles	0	0.00			
62Y - 54.69 bundles	0	0.00			

62Y - 15.9 bundles	0	0.00			
62Y - 33.2 bundles	0	0.00			
62Y - 19.3 bundles	0	0.00			
62Y - 19.3 bundles	0	0.00			
Fiber Architecture	Q_{b11}	Q_{b12}	Q_{b21}		
0.75 oz OC	2.79E+06	1.16E+06	1.16E+06		
40 oz Biaxial					
0^0	5.32E+06	5.48E+05	5.48E+05		
90^0	1.31E+06	5.48E+05	5.48E+05		
40 oz Triaxial					
45^0	2.34E+06	1.52E+06	1.52E+06		
$\_45^0$	2.34E+06	1.52E+06	1.52E+06		
90^0	1.31E+06	5.48E+05	5.48E+05		
62Y - 66.79 bundles	5.71E+06	5.67E+05	5.67E+05		
62Y - 54.69 bundles	5.72E+06	5.68E+05	5.68E+05		
62Y - 15.9 bundles	5.75E+06	5.69E+05	5.69E+05		
62Y - 33.2 bundles	5.71E+06	5.67E+05	5.67E+05		
62Y - 19.3 bundles	5.72E+06	5.68E+05	5.68E+05		
62Y - 19.3 bundles	5.72E+06	5.68E+05	5.68E+05		
Fiber Architecture	Q_{b22}	Q_{b16}	Q_{b26}	Q_{b66}	
0.75 oz OC	2.79E+06	0.00E+00	0.00E+00	9.43E+05	
40 oz Biaxial					
0^0	1.31E+06	0.00E+00	0.00E+00	4.09E+05	
90^0	5.32E+06	3.39E-12	2.42E-10	4.09E+05	
40 oz Triaxial					
45^0	2.34E+06	1.00E+06	1.00E+06	1.38E+06	
$\_45^0$	2.34E+06	-1.00E+06	-1.00E+06	1.38E+06	
90^0	5.32E+06	3.39E-12	2.42E-10	4.09E+05	
62Y - 66.79 bundles	1.40E+06	0.00E+00	0.00E+00	4.38E+05	
62Y - 54.69 bundles	1.40E+06	0.00E+00	0.00E+00	4.38E+05	
62Y - 15.9 bundles	1.40E+06	0.00E+00	0.00E+00	4.41E+05	
62Y - 33.2 bundles	1.40E+06	0.00E+00	0.00E+00	4.38E+05	
62Y - 19.3 bundles	1.40E+06	0.00E+00	0.00E+00	4.38E+05	
62Y - 19.3 bundles	1.40E+06	0.00E+00	0.00E+00	4.38E+05	
Step 6					
Computation of Final Trasformed Stiffness Matrix					
For Biaxial = 6.75/46.75(Q_b of OC) +24/46.75(Q_b of 0^0) + 16/46.75(Q_b of 90^0)					
For Triaxial = 6.75/46.75(Q_b of OC) + 12/46.75(Q_b of $45^{0)}$ + 12/46.75(Q_b of -45^0) + 16/46.75(Q_b of 90^0)					
Fiber Architecture	Q_{b11}	Q_{b12}	Q_{b21}		
40 oz Biaxial	3.58E+06	6.37E+05	6.37E+05		
40 oz Triaxial	2.05E+06	1.14E+06	1.14E+06		
62Y - 66.79 bundles	5.71E+06	5.67E+05	5.67E+05		
62Y - 54.69 bundles	2.34E+06	5.68E+05	5.68E+05		
62Y - 15.9 bundles	1.31E+06	5.69E+05	5.69E+05		
62Y - 33.2 bundles	5.71E+06	5.67E+05	5.67E+05		
62Y - 19.3 bundles	5.72E+06	5.68E+05	5.68E+05		
62Y - 19.3 bundles	5.75E+06	5.68E+05	5.68E+05		

Fiber Architecture	Q_{b22}	Q_{b16}	Q_{b26}	Q_{b66}
40 oz Biaxial	2.90E+06	1.16E-12	8.29E-11	4.86E+05
40 oz Triaxial	3.43E+06	1.16E-12	8.29E-11	9.87E+05
62Y - 66.79 bundles	1.40E+06	0.00E+00	0.00E+00	4.38E+05
62Y - 54.69 bundles	1.40E+06	0.00E+00	0.00E+00	4.38E+05
62Y - 15.9 bundles	1.40E+06	0.00E+00	0.00E+00	4.41E+05
62Y - 33.2 bundles	1.40E+06	0.00E+00	0.00E+00	4.38E+05
62Y - 19.3 bundles	1.40E+06	0.00E+00	0.00E+00	4.38E+05
62Y - 19.3 bundles	1.40E+06	0.00E+00	0.00E+00	4.38E+05

Step 7

Computation of Stiffness Matrix

Distance from mid-surface of lamiante to each laminae (z)

Ply	z (in)
40 oz Biaxial with 0.75 OC	-0.273
10.38 rov/in - 62 Y (66.79)	-0.194
40 oz Biaxial with 0.75 OC	-0.114
8.5 rov/in - 62 Y (54.69)	-0.044
40 oz Biaxial with 0.75 OC	0.026
2.48 rov/in - 62Y (15.96)	0.066
40 oz Biaxial with 0.75 OC	0.106
5.16 rov/in - 62 Y (33.20)	0.160
3 rov/in - 62 Y (19.3)	0.201
3 rov/in - 62 Y (19.3)	0.231
40 oz Triaxial with 0.75 OC	0.273

Computation of extensional stiffness

Fiber architecture	Thk.of lamiane	A_{11}	A_{12}	A_{21}
	(in)	(lbs/in)	(lbs/in)	(lbs/in)
40 oz Biaxial with 0.75 OC	0.055	1.97E+05	3.50E+04	3.50E+04
10.38 rov/in - 62 Y (66.79)	0.104	5.94E+05	5.90E+04	5.90E+04
40 oz Biaxial with 0.75 OC	0.055	1.97E+05	3.50E+04	3.50E+04
8.5 rov/in - 62 Y (54.69)	0.085	1.99E+05	4.83E+04	4.83E+04
40 oz Biaxial with 0.75 OC	0.055	1.97E+05	3.50E+04	3.50E+04
2.48 rov/in - 62Y (15.96)	0.025	3.28E+04	1.42E+04	1.42E+04
40 oz Biaxial with 0.75 OC	0.055	1.97E+05	3.50E+04	3.50E+04
5.16 rov/in - 62 Y (33.20)	0.052	2.97E+05	2.95E+04	2.95E+04
3 rov/in - 62 Y (19.3)	0.03	1.72E+05	1.70E+04	1.70E+04
3 rov/in - 62 Y (19.3)	0.03	1.72E+05	1.70E+04	1.70E+04
40 oz Triaxial with 0.75 OC	0.055	1.13E+05	6.26E+04	6.26E+04
		2.37E+06	**3.88E+05**	**3.88E+05**

Fiber architecture	A_{22}	A_{16}	A_{26}	A_{66}
	(lbs/in)	(lbs/in)	(lbs/in)	(lbs/in)
40 oz Biaxial with 0.75 OC	1.59E+05	6.39E-14	4.56E-12	2.67E+04
10.38 rov/in - 62 Y (66.79)	1.45E+05	0.00E+00	0.00E+00	4.55E+04
40 oz Biaxial with 0.75 OC	1.59E+05	6.39E-14	4.56E-12	2.67E+04
8.5 rov/in - 62 Y (54.69)	1.19E+05	0.00E+00	0.00E+00	3.73E+04
40 oz Biaxial with 0.75 OC	1.59E+05	6.39E-14	4.56E-12	2.67E+04
2.48 rov/in - 62Y (15.96)	3.51E+04	0.00E+00	0.00E+00	1.10E+04
40 oz Biaxial with 0.75 OC	1.59E+05	6.39E-14	4.56E-12	2.67E+04
5.16 rov/in - 62 Y (33.20)	7.26E+04	0.00E+00	0.00E+00	2.28E+04
3 rov/in - 62 Y (19.3)	4.19E+04	0.00E+00	0.00E+00	1.31E+04
3 rov/in - 62 Y (19.3)	4.19E+04	0.00E+00	0.00E+00	1.31E+04
40 oz Triaxial with 0.75 OC	1.88E+05	6.39E-14	4.56E-12	5.43E+04
	1.28E+06	**3.19E-13**	**2.28E-11**	**3.04E+05**

Computation of bending-extension coupling stiffness					
Fiber architecture	Thk.of lamiane	Z	B_{11}	B_{12}	B_{21}
	(in)	(in)	(lbs)	(lbs)	(lbs)
40 oz Biaxial with 0.75 OC	0.055	-0.273	-5.38E+04	-9.56E+03	-9.56E+03
10.38 rov/in - 62 Y (66.79)	0.104	-0.194	-1.15E+05	-1.14E+04	-1.14E+04
40 oz Biaxial with 0.75 OC	0.055	-0.114	-2.25E+04	-3.99E+03	-3.99E+03
8.5 rov/in - 62 Y (54.69)	0.085	-0.044	-8.76E+03	-2.12E+03	-2.12E+03
40 oz Biaxial with 0.75 OC	0.055	0.026	5.12E+03	9.11E+02	9.11E+02
2.48 rov/in - 62Y (15.96)	0.025	0.066	2.16E+03	9.39E+02	9.39E+02
40 oz Biaxial with 0.75 OC	0.055	0.106	2.09E+04	3.71E+03	3.71E+03
5.16 rov/in - 62 Y (33.20)	0.052	0.160	4.74E+04	4.71E+03	4.71E+03
3 rov/in - 62 Y (19.3)	0.030	0.201	3.44E+04	3.41E+03	3.41E+03
3 rov/in - 62 Y (19.3)	0.030	0.231	3.98E+04	3.93E+03	3.93E+03
40 oz Triaxial with 0.75 OC	0.055	0.273	3.08E+04	1.71E+04	1.71E+04
			-1.94E+04	**7.59E+03**	**7.59E+03**

Fiber architecture	B_{22}	B_{16}	B_{26}	B_{66}
	(lbs)	(lbs)	(lbs)	(lbs)
40 oz Biaxial with 0.75 OC	-4.35E+04	-1.74E-14	-1.24E-12	-7.30E+03
10.38 rov/in - 62 Y (66.79)	-2.81E+04	0.00E+00	0.00E+00	-8.81E+03
40 oz Biaxial with 0.75 OC	-1.82E+04	-7.28E-15	-5.20E-13	-3.05E+03
8.5 rov/in - 62 Y (54.69)	-5.23E+03	0.00E+00	0.00E+00	-1.64E+03
40 oz Biaxial with 0.75 OC	4.14E+03	1.66E-15	1.19E-13	6.95E+02
2.48 rov/in - 62Y (15.96)	2.32E+03	0.00E+00	0.00E+00	7.27E+02
40 oz Biaxial with 0.75 OC	1.69E+04	6.77E-15	4.83E-13	2.84E+03
5.16 rov/in - 62 Y (33.20)	1.16E+04	0.00E+00	0.00E+00	3.63E+03
3 rov/in - 62 Y (19.3)	8.41E+03	0.00E+00	0.00E+00	2.64E+03
3 rov/in - 62 Y (19.3)	9.67E+03	0.00E+00	0.00E+00	3.03E+03
40 oz Triaxial with 0.75 OC	5.14E+04	1.74E-14	1.24E-12	1.48E+04
	9.46E+03	**1.15E-15**	**8.21E-14**	**7.57E+03**

Computation of bending-extension coupling stiffness					
Fiber architecture	Thk.of lamiane	Z	D_{11}	D_{12}	D_{21}
	(in)	(in)	(lbs-in)	(lbs-in)	(lbs-in)
40 oz Biaxial with 0.75 OC	0.055	-0.273	1.47E+04	2.62E+03	2.62E+03
10.38 rov/in - 62 Y (66.79)	0.104	-0.194	2.28E+04	2.26E+03	2.26E+03
40 oz Biaxial with 0.75 OC	0.055	-0.114	2.61E+03	4.64E+02	4.64E+02
8.5 rov/in - 62 Y (54.69)	0.085	-0.044	5.05E+02	1.22E+02	1.22E+02
40 oz Biaxial with 0.75 OC	0.055	0.026	1.83E+02	3.25E+01	3.25E+01
2.48 rov/in - 62Y (15.96)	0.025	0.066	1.44E+02	6.27E+01	6.27E+01
40 oz Biaxial with 0.75 OC	0.055	0.106	2.26E+03	4.03E+02	4.03E+02
5.16 rov/in - 62 Y (33.20)	0.052	0.160	7.62E+03	7.57E+02	7.57E+02
3 rov/in - 62 Y (19.3)	0.030	0.201	6.91E+03	6.86E+02	6.86E+02
3 rov/in - 62 Y (19.3)	0.030	0.231	9.18E+03	9.06E+02	9.06E+02
40 oz Triaxial with 0.75 OC	0.055	0.273	1.41E+04	4.78E-15	3.41E-13
			8.10E+04	**8.32E+03**	**8.32E+03**

Fiber architecture	D_{22}	D_{16}	D_{26}	D_{66}
	(lbs-in)	(lbs-in)	(lbs-in)	(lbs-in)
40 oz Biaxial with 0.75 OC	1.19E+04	4.78E-15	3.41E-13	2.00E+03
10.38 rov/in - 62 Y (66.79)	5.57E+03	0.00E+00	0.00E+00	1.75E+03
40 oz Biaxial with 0.75 OC	2.11E+03	8.47E-16	6.04E-14	3.54E+02
8.5 rov/in - 62 Y (54.69)	3.02E+02	0.00E+00	0.00E+00	9.46E+01
40 oz Biaxial with 0.75 OC	1.48E+02	5.93E-17	4.23E-15	2.48E+01
2.48 rov/in - 62Y (15.96)	1.55E+02	0.00E+00	0.00E+00	4.86E+01
40 oz Biaxial with 0.75 OC	1.83E+03	7.34E-16	5.24E-14	3.07E+02
5.16 rov/in - 62 Y (33.20)	1.86E+03	0.00E+00	0.00E+00	5.84E+02
3 rov/in - 62 Y (19.3)	1.87E+03	0.00E+00	0.00E+00	5.85E+02
3 rov/in - 62 Y (19.3)	1.87E+03	0.00E+00	0.00E+00	5.85E+02
40 oz Triaxial with 0.75 OC	4.57E+03	1.55E-15	1.11E-13	1.32E+03
	3.22E+04	**7.97E-15**	**5.69E-13**	**7.65E+03**

Step 8					
Computation of in-plane moduli of laminate (E_x^t)					
$E_x^t = [(A_{11}A_{22})-A^2_{12}]/(tA_{22})$	**3.74E+06**				
$E_Y^t = [(A_{11}A_{22})-A^2_{12}]/(tA_{11})$	**2.03E+06**				
$G_{xy} = A_{66}/t$	**5.06E+05**				
nxy = A_{12}/A_{22}	**0.303**				
Computation of bending moduli of laminate (Ex^b)					
$Ex^b = [12(D_{11}D_{22}-D_{12}^2)]/(t^3D_{22})$	**4.36E+06**				
E_Y^b =[12(D11D22-D122)]/(t3D	**1.73E+06**				
$G_{xy}^b = 12D_{66}/t^3$	**4.23E+05**				
nxy = D_{12}/D_{22}	**0.258**				